

Design Optimization of Laminated Composite Structures Using  
Explicit Finite Element Analysis

by

Krista Mika

A Thesis Presented in Partial Fulfillment  
of the Requirements for the Degree  
Master of Science

Approved November 2014 by the  
Graduate Supervisory Committee:

Subramaniam Rajan, Chair  
Narayanan Neithalath  
Barzin Mobasher

ARIZONA STATE UNIVERSITY

December 2014

## ABSTRACT

Laminated composite materials are used in aerospace, civil and mechanical structural systems due to their superior material properties compared to the constituent materials as well as in comparison to traditional materials such as metals. Laminate structures are composed of multiple orthotropic material layers bonded together to form a single performing part. As such, the layup design of the material largely influences the structural performance. Optimization techniques such as the Genetic Algorithm (GA), Differential Evolution (DE), the Method of Feasible Directions (MFD), and others can be used to determine the optimal laminate composite material layup. In this thesis, sizing, shape and topology design optimization of laminated composites is carried out. Sizing optimization, such as the layer thickness, topology optimization, such as the layer orientation and material and the number of layers present, and shape optimization of the overall composite part contribute to the design optimization process of laminates. An optimization host program written in C++ has been developed to implement the optimization methodology of both population based and numerical gradient based methods. The performance of the composite structural system is evaluated through explicit finite element analysis of shell elements carried out using LS-DYNA. Results from numerical examples demonstrate that optimization design processes can significantly improve composite part performance through implementation of optimum material layup and part shape.

To my parents and fiancé

## ACKNOWLEDGMENTS

I would like to thank my committee chair, Dr. Subramaniam Rajan, for guiding me through the research process and providing me with the opportunity to work on this project. I would also like to thank my committee members, Dr. Narayanan Neithalath and Dr. Barzin Mobasher, for serving on my committee and providing instruction on laminate composite material performance and analysis.

## TABLE OF CONTENTS

	Page
LIST OF FIGURES .....	vi
LIST OF TABLES .....	ix
NOMENCLATURE .....	xi
CHAPTER	
1. INTRODUCTION .....	1
1.1. Motivation for Research and Overview .....	1
1.2. Literature Review.....	2
1.3. Thesis Objectives .....	9
2. FINITE ELEMENT ANALYSIS IN LS-DYNA.....	10
2.1. Composite Part Analysis and Modeling in LS-DYNA.....	10
2.2. Composite Part Modeling Implications .....	13
3. COMPOSITE MATERIAL OPTIMIZATION.....	18
3.1. Optimization Theory.....	18
3.1.1. Genetic Algorithm .....	18
3.1.2. Differential Evolution .....	19
3.1.3. Method of Feasible Directions.....	19
3.2. Optimization Problem Formulation .....	20
3.2.1. Composite Material Sizing Optimization .....	22
3.2.1.1. Layer Thickness .....	23
3.2.2. Composite Material Topology Optimization .....	24
3.2.2.1. Layer Orientation .....	25
3.2.2.2. Layer Material.....	26

CHAPTER	Page
3.2.2.3. Layer Status .....	26
3.2.3. Composite Material Shape Optimization.....	27
3.3. General Solution and Algorithm.....	30
4. NUMERICAL RESULTS .....	32
4.1. Verification Tests.....	32
4.1.1. Cantilever Beam for Sizing Optimization.....	33
4.1.2. Pinned Structure for Sizing and Topology Optimization .....	39
4.1.3. Cantilever Beam for Expected Shape Optimization .....	51
4.1.3.1. Mesh Convergence Study .....	55
4.1.4. Oblique Ball Drop Demonstration.....	63
4.2. Validation Test of the COMP-OPT program.....	69
4.2.1. Optimization of a Laminate Composite Leaf Spring.....	70
4.2.2. Leaf Spring Mesh Refinement.....	83
5. CONCLUSIONS.....	86
5.1 Future Work.....	87
REFERENCES .....	89
APPENDIX A.....	94
A. DESIGN INPUT FILE FORMAT .....	94
B. DESIGN OUTPUT FILE FORMAT .....	98

## LIST OF FIGURES

Figure	Page
2.1.1 Shell Element Axis Definition .....	12
2.2.1. Model for Evaluation of Composite Finite Element Modeling .....	14
2.2.2. Finite Element Mesh for Evaluation of Composite Finite Element Modeling .....	14
2.2.3. Number of Layers Evaluations Results.....	15
2.2.4. Layer Thickness Evaluation Results .....	17
4.1.1. Initial Model for Thickness Verification .....	33
4.1.2. Element Formulation of Initial Model for Thickness Verification.....	34
4.1.3. Node 5 Location in Cantilever Beam Model .....	35
4.1.4. Element Group Definition for Test Case 1 .....	36
4.1.5. Element Group Definition for Test Case 2 .....	36
4.1.6. Element Group Definition for Test Case 3 .....	36
4.1.7. Results of Test Case 1 .....	37
4.1.8. Results of Test Case 2 .....	38
4.1.9. Results of Test Case 3 .....	38
4.1.10. Simply Supported Structure Model .....	40
4.1.11. Element Formulation for Pinned Structure Model.....	40
4.1.12. Node 115 Location In Pinned Model.....	42
4.1.13. Element Groups for Test Case 4 .....	43
4.1.14. Element Groups for Test Case 5 .....	43
4.1.15. Final Model for Test Case 4.....	44
4.1.16. Final Model for Test Case 5.....	46

Figure	Page
4.1.17. Final Model for Test Case 6.....	50
4.1.18. Final Model for Test Case 7.....	50
4.1.19. Shape Optimization Geometric Constraint Nodes.....	52
4.1.20. Possible Shape Changes for Test Case 8.....	53
4.1.21. Final Model Shape of Test Case 8.....	54
4.1.22. Final Model Thickness of Test Case 8.....	55
4.1.23. Refined Mesh from Test Case 8.....	56
4.1.24. Node 5 Deflection on Test Case 8.....	57
4.1.25. Node 5 Deflection on Refined Mesh of Test Case 8 Model.....	57
4.1.26. Grid Convergence Analysis.....	58
4.1.27. Final Model Shape for Test Case 8.1.....	60
4.1.28. Final Model Thickness for Test Case 8.1.....	60
4.1.29. Refined Test Case 8.1 Model.....	61
4.1.30. Node 5 Displacement of Mesh Refined Test Case 8.1 Model.....	62
4.1.31. Node 5 Displacement of Time Refined Test Case 8.1 Model.....	62
4.1.32. Node 112 and 116 Location on Oblique Ball Drop Composite Model.....	65
4.1.33. Impact Path of Oblique Ball Drop Demonstration.....	65
4.1.34. Element Groups for Test Case 9 and Test Case 10.....	66
4.1.35. Final Model of Test Case 9.....	68
4.1.36. Final Model of Test Case 10.....	69
4.2.1. Composite Leaf Spring Optimized Model.....	71
4.2.2. Initial Laminate Composite Leaf Spring Model.....	72

Figure	Page
4.2.3. Boundary Conditions for Laminate Composite Leaf Spring Model.....	72
4.2.4. Location of Leaf Spring Displacement Constraint .....	74
4.2.5. Location of Leaf Spring Geometric Constraint .....	75
4.2.6. Leaf Spring Shape Optimization Velocity Fields .....	75
4.2.7. Dynamic Force Imposed Upon Leaf Spring .....	76
4.2.8. Composite Leaf Spring Loading Application .....	77
4.2.9. Leaf Spring Element Group Definition.....	77
4.2.10. Optimum Leaf Spring Thickness Distribution.....	79
4.2.11. Optimum Leaf Spring Plan View Shape.....	79
4.2.12. Optimized Leaf Spring Shape Dimensions.....	80
4.2.13. 1 <sup>st</sup> Global Principal Stress Plot for Positive Peak Load .....	80
4.2.14. 1 <sup>st</sup> Global Principal Stress Plot for Negative Peak Load .....	81
4.2.15. Plot of Leaf Spring Displacement Response .....	82
4.2.16. Internal Energy of Leaf Spring Model.....	82
4.2.17. Kinetic Energy of Leaf Spring Model .....	83
4.2.18. Refined Optimum Leaf Spring Thickness Distribution .....	84
4.2.19. Refined Optimum Leaf Spring Shape Distribution .....	85

## LIST OF TABLES

Table	Page
2.2.1. Number of Layers Evaluation Results .....	15
2.2.2. Layer Thickness Evaluation Results.....	16
4.1.1. T800-F3900 Fiber/Resin Composite Material Properties (US) .....	32
4.1.2. Summary of Finite Element Model.....	34
4.1.3. Results of Layer Thickness Demonstrations.....	37
4.1.4. Summary of Finite Element Model for Pinned Structure .....	41
4.1.5. Results from Sizing and Topology Optimization .....	44
4.1.6. Details of Final Model for Test Case 4 .....	45
4.1.7. Maximum Stresses in Final Model for Test Case 4.....	45
4.1.8. Details of Final Model for Test Case 5 .....	46
4.1.9. Maximum Stresses in Final Model for Demonstration 5.....	47
4.1.10. Results from Layer Status Topology Optimization .....	49
4.1.11. Results from Shape Optimization Test Case 8 .....	54
4.1.12. Data for Grid Convergence Index Computations .....	58
4.1.13. Results from Shape Optimization of Test Case 8.1 .....	59
4.1.14. Result Comparison of Test Case 8 and Test Case 8.1 .....	61
4.1.15. Results for Oblique Ball Drop Sizing and Topology Optimization.....	67
4.1.16. Details of Final Model of Test Case 9 .....	68
4.1.17. Details of Final Model of Test Case 10 .....	69
4.2.1. T800-F3900 Fiber/Resin Composite Material Properties (Metric) .....	74
4.2.2. Optimization of Leaf Spring .....	78

Table	Page
4.2.3. Element Group Thicknesses for Optimized Leaf Spring.....	79
4.2.4. Maximum Stress in Optimized Leaf Spring .....	81
4.2.5. Stress Results for Original and Refined Leaf Spring Optimum .....	85

## NOMENCLATURE

$d_{j,o}^{allowable}$	= Allowable displacement of node $j$ in the $o$ global coordinate direction
$b$	= Allowable (minimum) geometric distance between two nodes
$\sigma_i^{allowable}$	= Allowable Principal material stresses ( $i = 1, 2, 3$ ) ( $k = 1, 2, \dots, n_m$ )
$\tau^{allowable}$	= Allowable shear stress
$\alpha_v$	= Amplitude of velocity field $v$
$\beta$	= Angle of layer orientation (positive counter clockwise) (degrees)
$n_{j,o}$	= Coordinate $o$ of node $j$
$x$	= Design variable vector
$d_{j,o}$	= Displacement of node $j$ in the $o$ global coordinate direction
$o$	= Global coordinate axis ( $o = 1, 2, 3$ )
$x^L$	= Lower limit on continuous design variables
$k$	= Material group number
$m_{p,l}$	= Material of layer $l$ in element property group $p$
$\mathbf{Q}_{3n_n \times k}$	= Matrix of velocity fields
$\mathfrak{R}_o$	= Maximum range of coordinates $x$ , $y$ , and $z$ global coordinate directions
$\tau_{\max}$	= Maximum shear stress
$n_m$	= Number of materials
$n_n$	= Number of nodes in finite element model
$n_v$	= Number of velocity field vectors
$F(x)$	= Objective function
$\beta_{p,l}$	= Orientation of layer $l$ in element property group $p$ (degrees)

$\Delta$	=	Percent allowable change from initial nodal coordinates
$\sigma_i^k$	=	Principal material stresses ( $i = 1, 2, 3$ ) ( $k = 1, 2, \dots, n_m$ )
$B_{p,l}$	=	Set of discrete orientations for layer $l$ in element property group $p$
$M_{p,l}$	=	Set of discrete materials for layer $l$ in element property group $p$
$x^{Sizing}$	=	Shape design variable vector
$x^{Shape}$	=	Sizing design variable vector
$S_{p,l}$	=	Status of layer $l$ in element property group $p$
$t_{p,l}$	=	Thickness of layer $l$ in element property group $p$
$t_p$	=	Thickness of layers in element property group $p$
$x^{Topology}$	=	Topology design variable vector
$F_r$	=	Tsai-Hill failure parameters
$x^U$	=	Upper limit on continuous design variables
$[\mathbf{G}_{initial}]_{3n_n \times 1}$	=	Vector of initial x, y, z nodal coordinates
$\mathfrak{R}_0$	=	Vector of velocity field amplitudes
$\Delta$	=	Percent allowable change from initial nodal coordinates
$\mathbf{x}_{k \times 1}$	=	Vector of velocity field magnifiers
$[\mathbf{G}_{new}]_{3n_n \times 1}$	=	Vector of current x, y, z coordinates of nodes
$a_k$	=	Velocity field magnifier of velocity field $k$

# 1. INTRODUCTION

## 1.1 Motivation for Research and Overview

Composite materials are known to be used in many fields of study. The aerospace (Altair Engineering, Inc., 2011), mechanical (Biswal, Deepak, & Bahubalendruni, 2014), and civil engineering (Bank, Gentry, Thompson, & Russell, 2003) industries are utilizing the improved material properties that laminated composite materials yield for a wide variety of structural systems. Developing algorithmic techniques to optimize the design of the laminate material layup has the potential to extend the range of application and performance of these materials. Additionally, the use of finite element analysis of laminated composite parts increases the understanding of the orthotropic material behavior. When paired with design optimization techniques, finite element analysis can be used to develop an iterative process that aids in the design of laminate materials for optimum performance.

A focus of this work is on orthotropic material behavior under dynamic loads. As a result, the composite material layup can be designed to allow a structure to perform optimally when subjected to the time-dependent loading. The design of a concrete structure to withstand a projectile impact is an example of design under dynamic loading (Daudeville & Malecot, 2011); however, the optimization processes presented is an extension of this example to the design of a laminated composite material layup. For example, the design of a composite plastic cellular phone for the impact effects of dropping the device onto a hard floor (Greenlee, 2010) or the design of composite leaf springs within commercial vehicles (Patunkar & Dolas, 2011), (Shokrieh & Rezaei,

2003) . The design optimization framework for orthotropic composite materials provides the opportunity to expand laminate composite applications and performance.

## 1.2 Literature Review

The major focus of this research is design optimization of continuous fiber laminate material parts. The laminated material is composed of multiple layers of continuous fibers held within a matrix. As a result, the layup of the composite material, the orientation of the fibers within each layer, the layer thickness, the number of layers, and layer material, directly impact the material performance.

The composite material design optimization problem formulation attempts to obtain the best performing material design given the problem constraints. Typically, the ultimate goal of the process is to minimize a chosen objective function. Commonly used objective functions include mass, volume, and maximum deflection. Other optimization problem formulations design for extremizing bending stiffness, buckling loads (Lund, 2009), or natural frequency (Muc, 2007). The problem constraints are realistic boundaries that prevent the final proposed problem solution from being impractical. For example, according to the maximum stress failure criterion, maximum principle material stresses in an orthotropic material are the largest stresses that a particular material can incur before failure (Gurdal, Haftka, & Hajela, 1999). Therefore, the optimal solution for the laminated composite material layup must result in all experienced principle material stresses to be less than the defined failure stress.

The three established optimization techniques that will be used for design optimization of laminated composite materials in this thesis are Genetic Algorithm (GA), Method of Feasible Directions (MFD), and Differential Evolution (DE). GA and DE

optimization methods are iterative and population based. Alternatively, MFD is an iterative gradient based optimization method. The design space for laminated composite material optimization problems is relatively complex. As a result, these design spaces are often multimodal (Almeida & Awruch, 2008) or non-convex (Lund & Stegmann, 2004) and cause very noisy gradient evaluations which can cause difficulty with gradient based optimization. Therefore, the population based techniques are often preferred for solving composite material layup optimization problems (Almeida & Awruch, 2008), (Muc & Gurba, 2001), (Narayana Naik, Gopalakrishnan, & Ganguli, 2008), (Soremekun, 1997), (Rao & Arvind, 2007). (Ghiasi, Pasini, & Lessard, 2009). Even so, there has been success in utilizing gradient based optimization methods for composite material design (Frecker, 2003). Typically, gradient based optimization techniques have the ability to provide quick and accurate solution convergence when numerically computed gradients can be calculated with a relative high level of accuracy (Rao S. S., 2009).

The GA technique is based on the characteristics of biological evolution and was designed for finding the optimal solutions of unconstrained optimization problems (Goldberg, 1989). The basic elements of natural genetics that the algorithm utilizes are: reproduction, crossover, and mutation (Rao S. S., 2009). These elements enable the algorithm to generate new populations of solutions to be evaluated for their fitness. The solutions with the best fitness are typically transferred to the next generation of solutions or altered in an attempt to create a better design. The reproduction process chooses good design solutions, with respect to their fitness value, to be copied; whereas crossover creates new solution strings by combining solutions within the generation (Rao S. S., 2009). Additionally, mutation implements small modifications in solution strings that

demonstrate a low probability of changing in future generations (Rao S. S., 2009). These three operations allow GA to explore the entire design space. DE (Storn & Price, 1997) similarly uses the mutation and crossover functionalities with an integrated weighted difference scheme. The weighted difference between two solutions of a population is used to provide the means to create a third solution.

Almedia and Awruch (Almeida & Awruch, 2008) recommend that the GA optimization method be used for composite optimization problems. They demonstrate the use of a modified GA optimization process and suggest that using a population based technique is beneficial. In a laminate composite layup optimization problem, the dispersion of search points reduces the likelihood that the optimizer will converge to a local optimum for the multimodal problem (Almeida & Awruch, 2008). The GA used in their demonstrations is specifically modified to execute optimization of composite material layers. The material layer orientation and material type are represented as discrete design variables that are stored as a one-digit code number. As such, there are a pair of chromosomes (one for orientation and one for material) for each laminate. A similar chromosome approach was used by Soremekun (Soremekun, 1997) in an effort to increase the performance of the GA method. Additionally, both Soremekun and Almedia and Awruch demonstrate that the optimization time can be reduced by assuming symmetric laminate layers and reducing the number of design variables.

MFD is a gradient based optimization technique (Rao S. S., 2009). The iterative design process is executed through subsequent iterations that are determined based on the usable feasible design direction. The direction is usable when a movement in the gradient direction satisfies all of the constraints and is feasible when the movement also results in

a reduction of the objective function value. Gradient based methods have been shown to perform as well or better than the population based optimization techniques previously presented. In an example optimization problem requiring the optimal placement of actuators, both GA and a quasi-Newton gradient-based method, similar to MFD, were used with success (Frecker, 2003). Gradient based methods have proven to be superior in terms of computation time and results when gradient evaluations are accurate and possible (Kathiravan & Ganguli, 2007), because moving along the largest negative gradient direction provides a reduction and convergence of the objective function at the fastest rate (Rao S. S., 2009).

Different gradient based optimization techniques, like MFD, have also been applied to composite material optimization. For example, a gradient based optimization scheme was used by Lund (Lund, 2009) to complete topology optimization of a glass/epoxy and wood-carbon/epoxy wind turbine blade in order to determine layer material and fiber orientation for compressive buckling conditions. The objective function maximized the load that would cause the blade to buckle while avoiding excessive strain of the glass/epoxy and wood-carbon/epoxy materials. Through the use of the Discrete Material Optimization method (DMO) that utilizes parameterization gradient based optimization, convergence was obtained for the problem with a successful increase in the buckling load by approximately 16%.

Three types of design options can be used with laminated composite material layup optimization problems: topology, sizing, and shape optimization. The optimization completed by Lund of the turbine blade is considered topology optimization as the optimization process was used to determine the orientation and the material of each

successive ply. Topology optimization is defined as distribution of “a given amount of material in a design domain such that an objective function is extremized” (Sigmund & Torquato, 1999). When applied to laminated composite material design, topology optimization is categorized by use of the laminated layer orientation and material type as well as the number of layers present as the problem design variables. Topology optimization is commonly completed in parallel with sizing optimization. Sizing optimization of laminate composite materials typically involves a design variable representing the thickness of a layer or ply. When used together, topology and sizing optimization design variables can completely define the composite material layup and organization. Altair Engineering (Altair Engineering, Inc., 2011) considers the sizing and topology optimization of laminated composite materials through ply orientation, thickness, and stacking sequence to be the three phases of the composite material design optimization process.

Optimization problems posed by Narayana et al. (Narayana Naik, Gopalakrishnan, & Ganguli, 2008) are examples for how topology and sizing optimization can be combined through incorporation of design variables for ply thickness, stacking sequence and the number of plies within the material. Similarly, the optimization investigations completed by Almeida and Awruch (Almeida & Awruch, 2008) utilize topology optimization with the use of discrete composite ply orientation and material stacking sequence combined with sizing optimization through incorporation of layer thickness and the number of stacked composite layers as design variables. Their optimization problems utilize the GA technique to solve multi-objective problems. As an example, a presented problem attempts to minimize the weight and the maximum

deflection of a laminate composite plate subjected to surface pressures. The objective functions of such composite plate optimization problems were evaluated through the use of finite element analysis of shell composite elements.

The incorporation of finite element analysis and optimization procedures allow for composite part optimization to be executed for certain loading conditions. The finite element results of displacement and layer stresses can be used as constraints for the optimization problem, providing realistic performance evaluations. However, because the reliability of the finite element analysis results is dependent upon the mesh density and set up, the optimization solution also has a level of mesh dependency. The optimized solution that is a result of composite material optimization is the optimal solution for the finite element model and mesh provided. Muc and Gurba (Muc & Gurba, 2001) noted that optimization of laminate composite materials depends on the finite element mesh generation describing completely the physical problem. The finite element mesh that the optimization is executed on should be fine enough to accurately predict the structural response.

Shape optimization, another optimization solution strategy that can be applied to composite structures, involves finding the optimal shape of the structure. Muc and Gurba (Muc & Gurba, 2001) provide examples of shape optimization completed for a composite plate subjected to tension. The shape optimization is executed by defining a boundary curve with Bezier spline functions. As the GA process computes new boundary curves based on the Bezier curve parameters, the finite element mesh nodes located along the original curve are replaced with nodes defining the updated boundary.

A typical approach to shape optimization is to introduce allowable moving schemes that are used to describe the final structural shape (Bendsoe, 1989). Rajan et al. (Rajan, Chin, & Gani, 1996) discusses a shape optimization procedure that simply updates the nodal locations of the entire finite element mesh undergoing shape optimization based upon a velocity field matrix and a change magnitude. This methodology requires a velocity field, or shape change, matrix that defines the nodal changes. This matrix can be obtained through a comparison of the original model shape and the resulting displaced shape of the original model from fictitious loads or specified displacements. Belegundu and Rajan (Belegundu & Rajan, 1988) utilize this concept by making the magnitude of the fictitious loads used to compute the shape change matrix design variables. Alternatively, a unit load or displacement can be applied and the optimization process utilizes an amplitude of the change multiplier as the design variable. Vaidya et al. (Vaidya, Yang, St. Ville, Nguyen, & Rajan, 2005) explain that these shape optimization concepts are non-parametric shape optimization methods that adjust the nodes in the finite element mesh directly and do not require alteration of an additional solid model.

In these approaches, the number of nodes and elements within the finite element mesh are constant throughout the optimization process. However, as a result, the finite element mesh may experience a level of mesh distortion that must be addressed manually by the designer (Vaidya, Yang, St. Ville, Nguyen, & Rajan, 2005). Geometric constraints that limit the movement of nodes within a model can be used to prevent mesh distortion. Such constraints can be implemented as a part of the design formulation where the new shape is re-adjusted prior to each function evaluation to meet the geometric constraints.

### 1.3 Thesis Objectives

The objectives of the research are as follows:

1. To develop a robust optimization problem formulation to design orthotropic composite materials for optimal performance under dynamic loading scenarios.
2. Demonstrate sizing, shape, and topology optimization of laminated composite structural systems with population and gradient based optimization methods by developing a modular computer program.

While the focus of this work involves the use of impact load and controlled displacement cases, the concept and procedure are applicable to a variety of dynamic loading types. A COMP-OPT (Composite Optimization) program written in C++ controls the program flow by using two modules: a finite element analysis program that is used during function and gradient evaluations, and an optimization toolbox that provides the optimization techniques. The finite element analysis is carried out using LS-DYNA R7.0.0 (LSTC, 2014). An optimization toolbox (Dhandapani, Jain, & Rajan, 2013) containing GA, DE and MFD methods is used to find the optimal solution. Chapter 2 contains the details of the finite element and laminate composite material model used for optimization. Chapter 3 provides extended detail on the optimization procedures and the general algorithm of the developed optimization process. Chapter 4 presents the verification tests executed to complete the algorithm development as well as a validation test through the optimal design of an automobile composite leaf spring system. Chapter 5 details the conclusions and recommendations for future improvements.

## **2. FINITE ELEMENT ANALYSIS IN LS-DYNA**

### **2.1. Composite Part Analysis and Modeling in LS-DYNA**

The optimization process presented in this work designs laminate composite parts for optimum behavior in dynamic loading situations through use of explicit finite element analysis. While, static loading situations can be evaluated with implicit finite element analysis techniques where the stiffness system of equations is solved at each time step within the model, dynamic, time-dependent loading situations require explicit finite element analysis. This is due to the nature of the dynamic loading that involves short contact times and results in stress propagation characteristics that can be captured with explicit analysis. The technique avoids the process of solving the fundamental stiffness system of equations by explicitly solving the governing differential equations with the use of the solution from the previous time step.

A fully integrated shell finite element analysis model is adopted for the purpose of laminate composite material modeling in LS-DYNA. The through thickness integration points identify the composite layer locations, similar to the LS-DYNA composite model used by Wade, Feraboli, and Osborne (Wade, Feraboli, & Osborne, 2012) and Lund (Lund, 2009). The composite material performance is evaluated based upon the stresses experienced per layer using the maximum normal stress and maximum shear stress failure criteria (Kaw, 2005). The normal stresses are reported as the principle material stresses experienced at the center of the laminate composite layer at through thickness integration points.

Composite shell part modeling in LS-DYNA can be completed in a number of different ways. Typically, the material direction for each integration point is defined

through the use of the shell part and shell integration cards (Livermore Software Technology Corporation, 2003). This method allows the orthotropic material properties and the orientation of principle material axes to be defined on a through thickness integration point basis. However, a composite modeling keyword, \*PART\_COMPOSITE, has been developed to contain the information necessary for composite material modeling within one part card. This keyword offers a simplified method to define a laminate composite layup (Chatiri, Gull, & Matzenmiller, 2009). The \*PART\_COMPOSITE keyword defines layup characteristics on an individual layer basis. For each layer, a material number representative of the layer material, the layer thickness, and the layer orientation angle is defined (Stelzmann & Hormann, 2011). Additionally, through thickness integration points are dynamically allocated to the shell elements based on the number of layers defined in the \*PART\_COMPOSITE card. The COMP-OPT program utilizes this method for laminate composite part modeling. References to layer 1 in composite layup refers to the bottom laminate layer of the model. Each increasing layer number is representative of subsequent layers above the bottom surface.

Within the COMP-OPT program, multiple \*PART\_COMPOSITE keywords can be used to define different composite layups throughout the model. Elements can be placed into groups that are assigned different part numbers correlating to their respective \*PART\_COMPOSITE card and material layup. The COMP-OPT program executes topology and sizing optimization on an element group basis. Therefore, when multiple element groups are defined within the model, the elements can be of different thicknesses

and stacking sequences. Efficient element grouping allows for material symmetry to be imposed and the potential for a further refined solution.

When using the \*PART\_COMPOSITE card, the local material axes are defined for each layer. As a result, the stress output provided from the through thickness integration points is reported in the material coordinate system. The COMP-OPT program defines the material axes based on an angle,  $\beta_{p,l}$ , for each through thickness integration point.  $\beta_{p,l}$  is defined as the angle from the primary principle material direction as defined by vector **a** in Figure 2.1.1. Vectors **a** and **b** define the principal material directions for orthotropic and anisotropic materials as aligned with the LS-DYNA AOPT = 3.0 model.

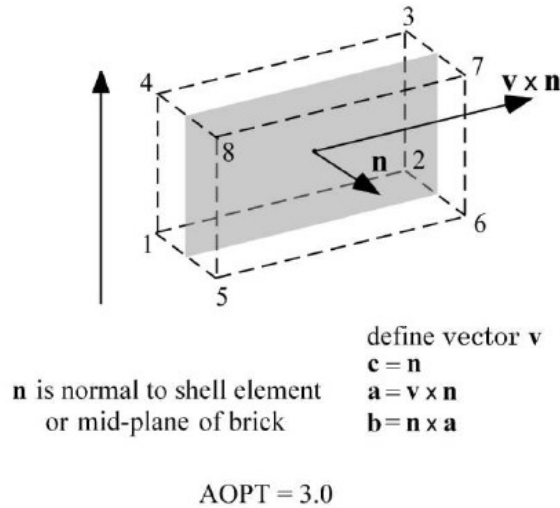


Figure 2.1.1 Shell Element Axis Definition (Graphic by Livermore Software Technology Corporation (LSTC), 2012)

The COMP-OPT program has been designed to use the composite damage material modeling card (\*MAT\_22). This orthotropic material model is used without brittle failure implications. Maximum stress theory is adopted to determine if a particular

design proposed by the COMP-OPT program is acceptable. After LS-DYNA has completed finite element analysis, the COMP-OPT program will verify if the model experiences stresses that violate this failure criterion. Strains are not evaluated for the purpose of the COMP-OPT design process as the composite damage material model is assumed to be a linear model.

## 2.2. Composite Part Modeling Implications

An exploration of the functionality of the LS-DYNA \*PART\_COMPOSITE card identifies modeling limitations with respect to the minimum number of layers that should be modeled and the maximum layer thickness that can be used. As per the \*PART\_COMPOSITE model in LS-DYNA, the number of through thickness shell integration points is dynamically allocated based on the number of layers defined. Therefore, it is expected that an increase in the number of material composite layers (resulting in an increase in the number of through thickness integration points), would provide refined performance results. Similarly, it is expected that the layer thickness, or space between through thickness integration points, would also affect the finite element analysis results. In order to demonstrate the implications of the number of layers and layer thicknesses defined in the \*PART\_COMPOSITE card, a dynamic model of a steel ball dropped upon a cantilevered composite plate is analyzed. The cantilever plate is assigned general orthotropic composite properties (Hoffarth, et al., 2014) and the steel ball is dropped vertically with an initial velocity of 100 in/s onto the plate as shown in Figure 2.2.1. The composite structure has three free edges and one side fixed from rotation and translation (Figure 2.2.1). The composite part finite element mesh used is shown in Figure 2.2.2.

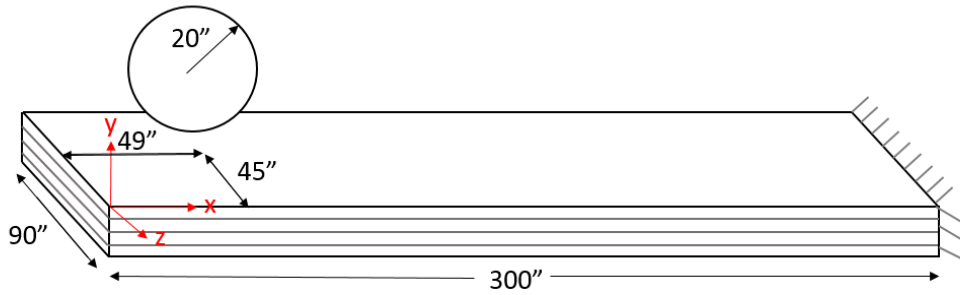


Figure 2.2.1. Model for Evaluation of Composite Finite Element Modeling



Figure 2.2.2. Finite Element Mesh for Evaluation of Composite Finite Element Modeling

Six tests demonstrate the model response with respect to the number of layers used in the composite structure. For all of the tests, the cantilevered plate has a total, uniform thickness of 2.0 inches with all composite fibers oriented parallel to the global x-axis. All layers within the composite part are assumed to be the same thickness such that the layer thicknesses increase as the number of layers in the model decrease as demonstrated in Table 2.2.1. The maximum deflection of the cantilevered structure is provided in Table 2.2.1 and Figure 2.2.3 shows the convergence of this deflection with respect to the number of layers modeled.

Table 2.2.1. Number of Layers Evaluation Results

Number of layers	Layer Thicknesses (in.)	Maximum Deflection (in.)
1	2.0	17.50
2	1.0	7.16
3	0.6667	6.44
4	0.5	6.43
5	0.4	6.44
6	0.3333	6.30

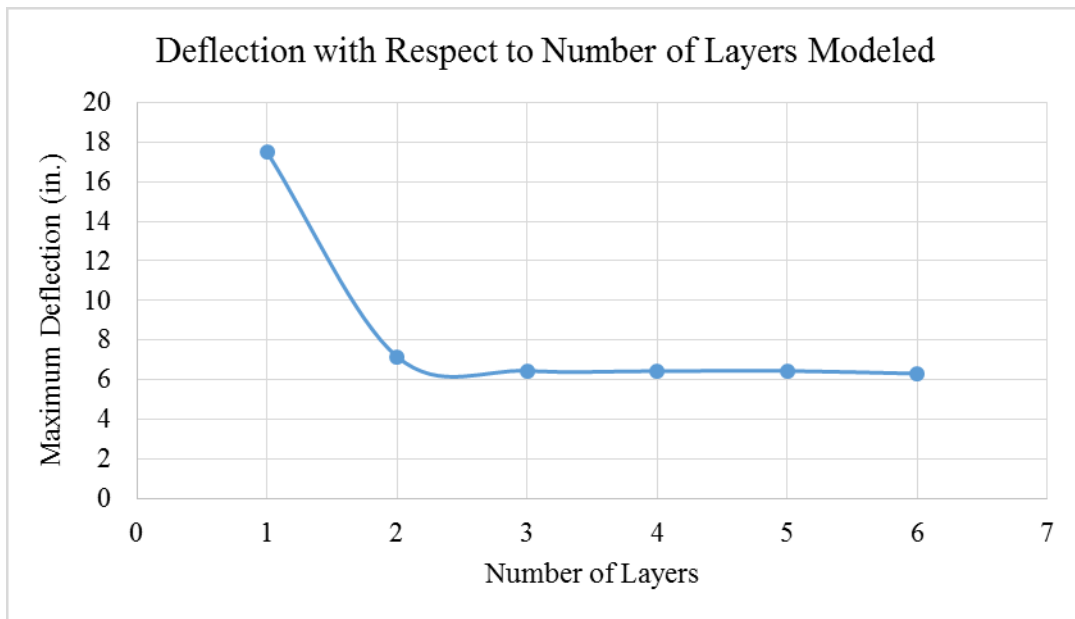


Figure 2.2.3. Number of Layers Evaluations Results

From Figure 2.2.3, there are limitations to computing accurate deflection results with only one 2.0 inch laminate layer. However, the maximum displacement results demonstrate convergence when three or more layers are defined. Therefore, throughout the optimization process, any solution containing only one or two composite layers will be split equivalently into at least three layers prior to LS-DYNA analysis.

An additional eight test models demonstrates the effects of layer thicknesses on analysis results. Each test consisted of the same cantilever composite structure and steel ball shown in Figures 2.2.1 and 2.2.2; however, for these tests, the composite structure has an increased plate thickness of 8.0 inches. The thickness to bending span ratio is 2.7% such that the elements can be acceptably modeled as thin shells. Throughout the eight tests, the number of layers composing the structure vary from a maximum of ten to a minimum of three. As a result, the individual layer thicknesses vary from a maximum of 2.667 inches to 0.8 inch as presented in Table 2.2.2. Figure 2.2.4 shows the resulting maximum nodal deflection of the cantilevered structure.

Table 2.2.2. Layer Thickness Evaluation Results

<b>Number of layers</b>	<b>Layer Thickness (in.)</b>	<b>Maximum Deflection (in.)</b>
10	0.8	0.455
9	0.8889	0.449
8	1.0	0.439
7	1.1429	0.426
6	1.3333	0.436
5	1.60	0.452
4	2.0	0.459
3	2.6667	0.459

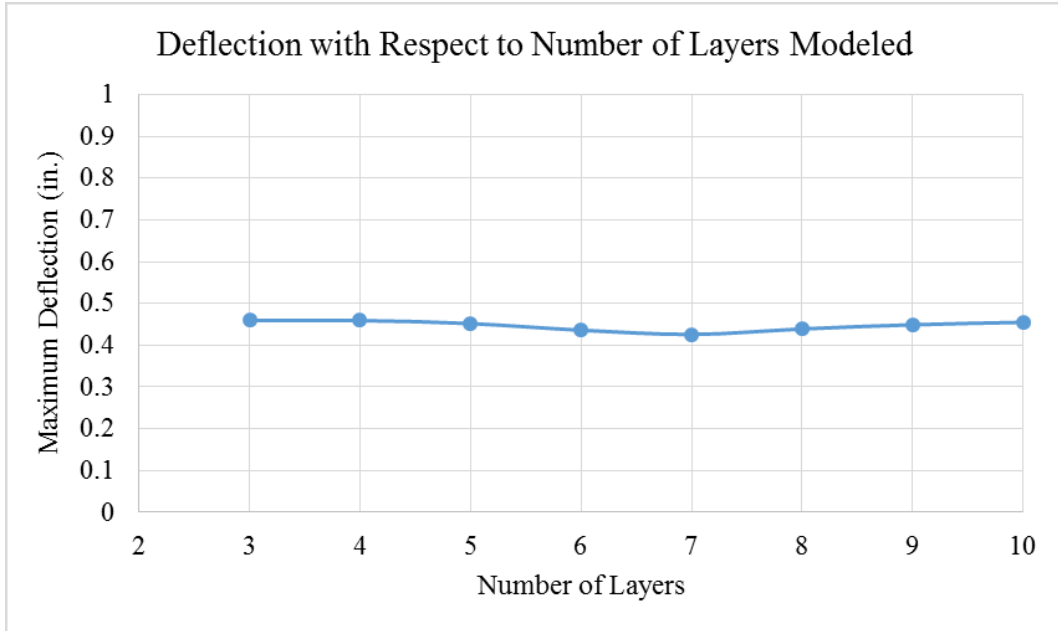


Figure 2.2.4. Layer Thickness Evaluation Results

The maximum displacement results from the eight tests provided in Figure 2.2.4 are within a 3.5% range of each other. As such, there appears to be no maximum layer thickness constraints inherent within the \*PART\_COMPOSITE modeling methodology. However, different mesh densities and problem parameters may result in a larger effect from individual layer thicknesses. Optimized solutions utilizing the \*PART\_COMPOSITE card can be evaluated with a similar layer refinement process in order to identify if any layer thickness dependencies are prevalent for the optimized problem set up.

### 3. COMPOSITE MATERIAL OPTIMIZATION

#### 3.1. Optimization Theory

The COMP-OPT program is equipped with both population and gradient based optimization methods. Specifically, the COMP-OPT program has the ability to use the GA, DE, and MFD optimization methods (Dhandapani, Jain, & Rajan, 2013).

Algorithmic details and references for these three optimization techniques can be found in various sources (Rao S. S., 2009), (Storn & Price, 1997), (Goldberg, 1989).

##### 3.1.1. Genetic Algorithm

The GA optimization method is used in the COMP-OPT program for sizing, topology, and shape optimization. This population based search method can optimize continuous, discrete, and Boolean design variables. The default replacement strategy for GA is elitist replacement, where the top performing design transfers to the next iteration. However, when specifying that the GA optimizer should be used by the COMP-OPT program, the replacement strategy can be changed to “none” or “topfew” (Dhandapani, Jain, & Rajan, 2013). A replacement strategy of “none” would result in no replacement preference for the next generation based upon fitness value and a replacement strategy of “topfew” would entail that the top designs are transferred to the next generation. The default probability of crossover and mutation for the GA optimization are 0.8 and 0.03, respectively (Dhandapani, Jain, & Rajan, 2013). These defaults can be overridden with appropriate changes within the COMP-OPT algorithm. The verification examples that utilize GA in chapter 4 use the “topfew” replacement strategy and default crossover and mutation probabilities.

### 3.1.2. Differential Evolution

The DE optimization method is also used in the COMP-OPT program for sizing, topology, and shape optimization. The DE optimization method is a population based search method that optimizes continuous, discrete, and Boolean design variables. Similarly to the GA optimization characteristics, the default selection strategy for the DE optimizer, the default differentiation constant of 1.0, the crossover constant of 0.9, and the seed value of 3 can be overridden with the appropriate functions within the COMP-OPT algorithm (Dhandapani, Jain, & Rajan, 2013). The verification tests in chapter 4 that use the DE optimizer use the default DE characteristics.

### 3.1.3. Method of Feasible Directions

Within the COMP-OPT program, MFD is used for sizing and topology optimization. The design variables for optimization problems using this gradient based method must be continuous. The objective function and constraints are not represented as explicit equations, so the gradients are completed numerically. The numerical gradient computation of relatively noisy or discontinuous objective functions can prevent the optimization method from functioning as expected (Lund, 2009). As a result, the MFD optimization technique cannot be applied to all dynamically loaded composite optimization models. The default number of search directions used in the MFD algorithm in the COMP-OPT program is 3 and can be adjusted using appropriate functions (Dhandapani, Jain, & Rajan, 2013). The verification and validation tests that used the MFD optimizer used the default number of search directions.

### 3.2. Optimization Problem Formulation

The COMP-OPT program optimization procedure minimizes the mass, volume, cost, or maximum displacement of a laminated composite structure by changing the material layup and structural shape. The general optimization problem can be stated as follows:

$$\text{Find } \mathbf{x}[\mathbf{x}^{Sizing}, \mathbf{x}^{Topology}, \mathbf{x}^{Shape}] \quad (1.a)$$

$$\text{Minimize } F(\mathbf{x}) \quad (1.b)$$

$$\text{Subject to } \frac{d_{j,o}}{d_{j,o}^{allowable}} - 1 \leq 0 \quad (1.c)$$

$$\frac{\sigma_i^k}{\sigma_i^{allowable}} - 1 \leq 0 \quad (1.d)$$

$$\frac{n_{j_1,o_1} - n_{j_2,o_2}}{b} + 1 \leq 0 \quad (1.e)$$

$$\frac{\tau_{max}}{\tau^{allowable}} - 1 \leq 0 \quad (1.f)$$

$$\text{when } \tau_{max} = \frac{|\sigma_{max} - \sigma_{min}|}{2} \quad (1.g)$$

$$\frac{\sigma_1^2}{F_1^2} + \frac{\sigma_2^2 + \sigma_3^2}{F_2^2} + \frac{\tau_4^2}{F_4^2} + \frac{\tau_5^2 + \tau_6^2}{F_6^2} - \frac{\sigma_1\sigma_2}{F_1^2} - \frac{\sigma_2\sigma_3}{F_2^2} - \frac{\sigma_1\sigma_3}{F_1^2} - 1 \leq 0 \quad (1.h)$$

$$\text{when } F_r = \sigma_i^{allowable} \quad (1.i)$$

$F(\mathbf{x})$  represents the objective function equation and  $\mathbf{x}$  represents the vector of design variable values. The design variable vector can contain sizing, shape, and/or topology design variables depending on the optimization problem posed. Eq. (1.c), (1.d), (1.e), and (1.h) are normalized displacement, material principal stress, geometric, and

Tsai-Hill failure criterion respectively. The maximum shear stress, computed by Eq. (1.g), is used to evaluate shear failure through Eq. (1.f) as per the maximum shear stress failure theory (Kaw, 2005).

The sizing design variables optimize a) the individual layer thickness within an element group and b) the constant layer thickness for all layers within an element group. The topology design variables optimize the individual layer orientation within an element group, the individual layer material within an element group, and the individual layer status within an element group. The shape optimization design variable represents the amplitude of the shape change expressed by a provided velocity field. Specific details of the sizing, topology, and shape design variables will be addressed in section 3.2.1, 3.2.2, and 3.2.3, respectively.

The constraints used in the COMP-OPT program are similar to what Almeida and Awruch (Almeida & Awruch, 2008) use for composite material optimization. The maximum nodal displacement in the global coordinate directions, maximum principal material normal stress, maximum shear stress, and maximum nodal location difference between nodes are the design constraints for COMP-OPT problems. As shown in Eq. (1.c), (1.d), (1.e), and (1.f), the constraint values are normalized to eliminate the differences in the characteristic magnitudes. The displacement constraint verifies that the absolute value of the displacement in the identified axis direction for a specific node does not exceed the allotted maximum throughout analysis. Similarly, the geometric constraint penalizes excessive mesh distortion by limiting the minimum distance between identified nodes.

The maximum normal stress and shear stress or Tsai-Hill criteria (Daniel & Ishai, 2006) can be adopted as the failure criteria within the COMP-OPT program. For the maximum normal stress criteria, “failure occurs when at least one stress component along one of the principal material axes exceeds the corresponding strength in that direction” (Daniel & Ishai, 2006). The maximum stress failure criteria is regularly used for composite material design optimization as noted by Narayana Naik et al. (Narayana Naik, Gopalakrishnan, & Ganguli, 2008) and Gurdal and Hajela (Gurdal, Haftka, & Hajela, 1999). Similarly, the maximum shear stress failure theory (Kaw, 2005) is used to evaluate the experienced shear stress. This theory assumes that composite failure occurs when the shear stress in any of the material planes exceeds the shear strength of the material (Kaw, 2005). The Tsai-Hill criteria (Daniel & Ishai, 2006) offers a more conservative failure criteria approach when large stresses are observed in multiple principal material directions. One or both criteria can be used as optimization problem constraints.

### 3.2.1. Composite Material Sizing Optimization

The laminated composite material sizing optimization problem designs the structural and layer thicknesses. The composite material sizing optimization problem is stated as follows:

$$\text{Find} \quad x^{sizing} [t_{p,l}, t_p] \quad (2.a)$$

$$\text{Minimize} \quad F(x) \quad (2.b)$$

$$\text{Subject to} \quad \frac{d_{j,o}}{d_{j,o}^{allowable}} - 1 \leq 0 \quad (2.c)$$

$$\frac{\sigma_i^k}{\sigma_i^{allowable}} - 1 \leq 0 \quad (2.d)$$

$$\frac{n_{j_1, \theta_1} - n_{j_2, \theta_2}}{b} + 1 \leq 0 \quad (2.e)$$

$$\frac{\tau_{\max}}{\tau_{\text{allowable}}} - 1 \leq 0 \quad (2.f)$$

$$\frac{\sigma_1^2}{F_1^2} + \frac{\sigma_2^2 + \sigma_3^2}{F_2^2} + \frac{\tau_4^2}{F_4^2} + \frac{\tau_5^2 + \tau_6^2}{F_6^2} - \frac{\sigma_1\sigma_2}{F_1^2} - \frac{\sigma_2\sigma_3}{F_2^2} - \frac{\sigma_1\sigma_3}{F_1^2} - 1 \leq 0 \quad (2.g)$$

$$x^L \leq t_{p,l} \leq x^U \quad (2.h)$$

$$x^L \leq t_p \leq x^U \quad (2.i)$$

Section 3.2.1.1 provides additional details regarding the sizing optimization design variables.

#### 3.2.1.1. Layer Thickness

Two types of layer thickness design variables are available within the COMPT-OPT program. The first is assigned to a specific layer within an element property group as shown in Eq. (2.h). Using this design variable, the optimal thickness of a specific layer in the laminated composite is determined. The second sizing design variable type is assigned to a specific element property group and assigns all layers within that property group a consistent thickness as shown in Eq. (2.i). This design variable does not allow for layer thickness variability within a given element property group; however, this design variable is used when the orientation and stacking sequence is pre-defined and constant throughout the thickness of the composite. By assigning all layers the same thickness, the total thickness of the composite for a constant orientation can be determined with a reduced number of design variables. As shown in Eq. (2.h) and (2.i), the sizing design variables are continuous between lower and upper bounds. Both layer thickness design variable types are demonstrated in verification tests in chapter 4.

### 3.2.2. Composite Material Topology Optimization

As laminated layers are orthotropic, the orientation and the material of the layers directly impacts the composite's performance. Composite material topology optimization involves optimization of the material stacking sequence through the use of the layer orientation, layer material, and layer status design variables. The composite material topology optimization problem would be stated as follows:

$$\text{Find } x^{topology} [\beta_{p,l}, m_{p,l}, s_{p,l}] \quad (3.a)$$

$$\text{Minimize } F(x) \quad (3.b)$$

$$\text{Subject to } \frac{d_{j,o}}{d_{j,o}^{allowable}} - 1 \leq 0 \quad (3.c)$$

$$\frac{\sigma_i^k}{\sigma_i^{allowable}} - 1 \leq 0 \quad (3.d)$$

$$\frac{n_{j_1,o_1} - n_{j_2,o_2}}{b} + 1 \leq 0 \quad (3.e)$$

$$\frac{\tau_{max}}{\tau^{allowable}} - 1 \leq 0 \quad (3.f)$$

$$\frac{\sigma_1^2}{F_1^2} + \frac{\sigma_2^2 + \sigma_3^2}{F_2^2} + \frac{\tau_4^2}{F_4^2} + \frac{\tau_5^2 + \tau_6^2}{F_6^2} - \frac{\sigma_1\sigma_2}{F_1^2} - \frac{\sigma_2\sigma_3}{F_2^2} - \frac{\sigma_1\sigma_3}{F_1^2} - 1 \leq 0 \quad (3.g)$$

$$\beta_{p,l} \in B_{p,l} \quad B_{p,l}(\beta_1, \beta_2, \dots, \beta_{m_o}) \quad (3.h)$$

$$m_{p,l} \in M_{p,l} \quad M_{p,l}(m_1, m_2, \dots, m_{m_m}) \quad (3.i)$$

$$x^L \leq \beta_{p,l} \leq x^U \quad (3.j)$$

$$s_{p,l} = 0, 1 \quad (3.k)$$

Sections 3.2.2.1, 3.2.2.2, and 3.2.2.3 provide additional details regarding the topology optimization design variables.

### 3.2.2.1. Layer Orientation

The orientation angle is defined as the angle  $\beta$  shown in Figure 3.2.2.1. Vectors  $a$ ,  $v$ , and  $n$  (1, 2, and 3) define the material coordinate systems for the LS-DYNA composite material model. Therefore, the material coordinate system for each layer can be rotated as defined by the layer angle  $\beta_{p,l}$ .

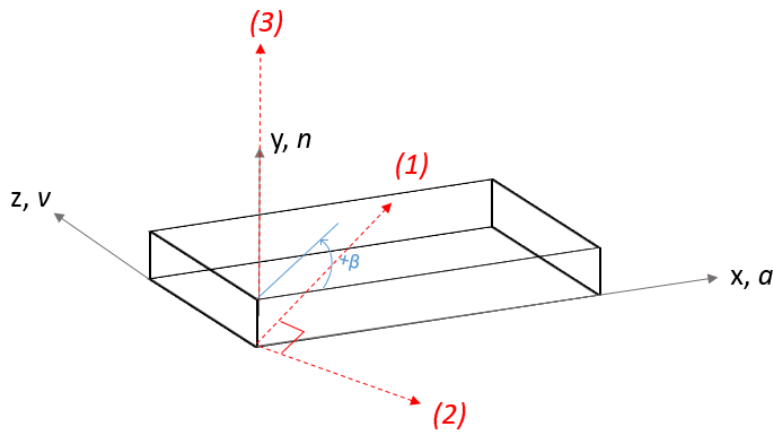


Figure 3.2.2.1. Layer Orientation Coordinate System Definition

The layer orientation design variables are designed on an element group individual layer basis in order to account for stacking sequence effects. The orientation of each layer in the composite is determined as necessary based on the stresses experienced at the through thickness integration points.

The layer orientation design variables found in Eq. (3.h) and Eq. (3.i) are discrete and continuous design variables, respectively. The continuous design variable requires a lower bound and upper bound; whereas, the discrete design variable requires a list of the

possible orientation angles to be defined,  $B_{p,l}$ . The preference for use of discrete or continuous orientation variables is problem dependent. The continuous orientation design variable is advantageous when gradient based optimization methods are used. However, from a manufacturing perspective, discrete angle orientation optimization may be preferred as the fabrication process may restrict the number of possible orientation angles that can be achieved within a necessary tolerance (Suresh, Sujit, & Rao, 2007), (Rao & Arvind, 2007).

#### 3.2.2.2. Layer Material

Topology design of laminate composites typically involves layer material design in addition to orientation design (Stegmann & Lund, 2005). The layer material design variable in Eq. (3.i) is available for optimization problems of multi-material laminate structures. The layer material design variable enables individual layers within an element group to have different orthotropic material properties based upon a discrete list of possible materials defined by  $M_{p,l}$ . When the layer material design variable is used within the COMP-OPT program, a material card (\*MAT\_22) for each possible material must be provided. The layer material optimization process within the COMP-OPT program is applicable to multi-material stacking sequence optimization like the design that Lund (Lund, 2009) completed for a wind turbine blade involving E-glass/epoxy and Wood-carbon/epoxy laminate layers.

#### 3.2.2.3. Layer Status

The layer status design variable in Eq. (3.k) is representative of the layer's presence. This design variable is a Boolean design variable that is equal to 1 if the layer is present or equal to 0 if the layer is not. As a result, the layer status design variable has the

ability to remove layers when their presence is not necessary for the laminated composite performance. The layer status design variable is applied on an individual layer per element group basis. As there must be a minimum of at least one layer present in the composite structure for LS-DYNA to execute analysis, at least one layer per element group should not be assigned a layer status design variable.

The examination of the minimum number of layers required to be modeled in the composite structure completed in section 2.2 demonstrate that a minimum number of layers are necessary. Therefore, when the layer status design variable is used and one or two layers are present in the composite for any given element group, the layers of this element group are subdivided for the purpose of modeling within the LS-DYNA \*PART\_COMPOSITE card. When two layers are present, each layer is divided in half to result in four layers of total equivalent thickness, material, and orientation sequence in the LS-DYNA model. Similarly, when only one layer is present, the layer is divided into four layers for LS-DYNA analysis. This division process ensures that an appropriate number of through thickness integration points are used within the analysis model.

### 3.2.3. Composite Material Shape Optimization

Composite material shape optimization designs the composite structure boundary shape. This functionality is executed through the use of pre-defined velocity fields and shape change magnifiers. The composite material shape optimization problem statement is presented as follows:

$$\text{Find } \mathbf{x}^{shape} [x_{k \times 1}] \quad (4.a)$$

$$\text{Minimize } F(\mathbf{x}) \quad (4.b)$$

$$\text{Subject to } \frac{d_{j,o}}{d_{j,o}^{allowable}} - 1 \leq 0 \quad (4.c)$$

$$\frac{\sigma_i^k}{\sigma_i^{allowable}} - 1 \leq 0 \quad (4.d)$$

$$\frac{n_{j_1,o_1} - n_{j_2,o_2}}{b} + 1 \leq 0 \quad (4.e)$$

$$\frac{\tau_{max}}{\tau^{allowable}} - 1 \leq 0 \quad (4.f)$$

$$\frac{\sigma_1^2}{F_1^2} + \frac{\sigma_2^2 + \sigma_3^2}{F_2^2} + \frac{\tau_4^2}{F_4^2} + \frac{\tau_5^2 + \tau_6^2}{F_6^2} - \frac{\sigma_1\sigma_2}{F_1^2} - \frac{\sigma_2\sigma_3}{F_2^2} - \frac{\sigma_1\sigma_3}{F_1^2} - 1 \leq 0 \quad (4.g)$$

$$\mathbf{x}_{k \times 1} [a_1, a_2, \dots, a_k] \quad (4.h)$$

$$a_k = \alpha_k \mathfrak{R}_o \Delta \quad -1 \leq \alpha_k \leq 1, \quad o = x, y, z - axis \quad (4.i)$$

The shape optimization problem requires user-defined velocity fields that contain nodal translation information with respect to the x, y, and z-coordinates. The primary methodology used to formulate the velocity fields is to compute the nodal location differences between an initial and perturbed finite element model. Any symmetry requirements for the shape change are enforced within the perturbed model to ensure symmetry is maintained throughout the optimization process. For example, a velocity field vector representing a Biezer curve or a vector containing nodal relationships such that a straight boundary line is always achieved within the finite element mesh can be used. The geometric constraints present in the shape optimization problem, Eq. (4.e), are designed to prevent excessive mesh distortion by limiting the minimum distance between control nodes.

The optimization process will utilize the velocity fields in the form of the velocity field matrix,  $\mathbf{Q}_{3n_p \times k}$  - where  $k$  is the number of velocity fields and  $n$  is the number of nodes that make up the laminated composite model. The shape change scale vector,  $\mathbf{X}_{k \times 1}$ , in Eq. (4.g) contains multipliers,  $a_k$ , that define the magnification for corresponding velocity fields. The shape optimization methodology utilized within the COMP-OPT program is to use a maximum allowable nodal coordinate change percentage,  $\Delta$ , of the nodal coordinate range,  $\mathfrak{R}_o$ , in order to limit the amount of shape alteration (Rajan, Chin, & Gani, 1996). The percent change allowable is chosen to avoid large mesh distortions as a large allowable change percentage may result in highly distorted finite element meshes (Rajan, Chin, & Gani, 1996). The optimization process determines the amplitude of shape change,  $a_k$ , for each velocity field. The amplitude can vary between -1.0 and 1.0, as seen in Eq. (4.h), to determine the magnitude of the shape change.

The resulting shape change scale vector that determines the level of translation from each velocity field is composed of the optimized shape change magnification factors as computed from Eq. (4.i). The shape optimization procedure updates the nodal locations of the laminate composite finite element mesh during each iteration according to Eq. (5).

$$[\mathbf{G}_{new}]_{3n_p \times 1} = [\mathbf{G}_{initial}]_{3n_p \times 1} + \mathbf{Q}_{3n_p \times k} \mathbf{X}_{k \times 1} \quad (5)$$

$$a_{\max} = \pm \Delta \mathfrak{R}_o \quad o = x, y, z - axis \quad (6)$$

As the amplitude of shape change cannot be greater than positive or negative one, the maximum shape change magnifier possible in any given axis direction is as defined in Eq. (6).

### 3.3. General Solution and Algorithm

The general COMP-OPT program algorithm is as follows:

1. Read the design input file. (See Appendix A for details.)
2. Store finite element model data and initialize appropriate optimizer.
3. Begin the design process.
  - a. Update all design variables.
  - b. Update the LS-DYNA input files to prepare for analysis. The \*MAT\_22 material and composite part cards as well as the composite structural mesh are updated.
  - c. Complete function evaluation in LS-DYNA.
  - d. Compute the objective function value.
  - e. Post-process LS-DYNA analysis results to evaluate constraints.
  - f. Export results for this iteration to the output file based upon desired output detail level.
  - g. If the objective function is the best thus far and all constraints are satisfied, save the structural mesh and laminate composite material layup in the LS-DYNA input files specified to hold the best design.
  - h. Check for termination condition. If yes, continue to Step 4, otherwise, return to Step 3, Part (a). For population based methods, check for termination based on if the maximum number of iterations is reached. For

gradient based methods, check if solution has converged within a specified tolerance.

4. Create output file summarizing optimization results from each iteration, the final design variable values, and final composite model layup details. (See Appendix B for details.)

## 4. NUMERICAL RESULTS

In the following sections, verification and validation tests are discussed.

Verification test cases demonstrate the functionality of the various problem formulations.

The validation test consists of design optimization of an automobile leaf spring.

### 4.1. Verification Tests

A number of verification tests were completed with the T800-F3900 fiber/resin composite material (Hoffarth, et al., 2014). The material properties (Raju & Acosta, 2010) are listed in Table 4.1.1. The a-b-c directions correspond to the 1-2-3 principal material directions shown in Figure 3.2.2.1.

Table 4.1.1. T800-F3900 Fiber/Resin Composite Material Properties (US)

<b>Material Property</b>	<b>Value</b>
Density (slug/in <sup>3</sup> )	$1.457 \times 10^{-4}$
Young's Modulus, a-direction (psi)	$2.183 \times 10^7$
Young's Modulus, b-direction (psi)	$1.145 \times 10^6$
Young's Modulus, c-direction (psi)	$1.145 \times 10^6$
Shear Modulus, ab-direction (psi)	$5.796 \times 10^5$
Shear Modulus, bc-direction (psi)	$3.243 \times 10^5$
Shear Modulus, ca-direction (psi)	$5.796 \times 10^5$
Poisson's Ratio, ba	0.013847
Poisson's Ratio, ca	0.013847
Poisson's Ratio, cb	0.3792
Longitudinal Tensile Strength, a-axis (psi)	$4.20 \times 10^5$
Transverse Tensile Strength, b-axis (psi)	$2.5 \times 10^4$
Longitudinal Compressive Strength, a-axis (psi)	$4.20 \times 10^5$
Transverse Compressive Strength, b-axis (psi)	$2.5 \times 10^4$
Shear strength (psi)	$7.5 \times 10^3$

All optimization techniques, GA, DE, and MFD, are demonstrated with at least one verification test. DE is selected as the optimization method for the majority of the

tests because the population based method is more equipped to handle the unpredictable composite material design space. As previously discussed, many composite optimization resources suggest that population based optimization methods are preferable (Almeida & Awruch, 2008), (Muc & Gurba, 2001), (Narayana Naik, Gopalakrishnan, & Ganguli, 2008), (Soremekun, 1997), (Rao & Arvind, 2007). (Ghiasi, Pasini, & Lessard, 2009). Additionally, the finite element models of the verification tests are completed with minimal damping characteristics as the optimization is completed for the initial response of the dynamic system. The total energy is maintained throughout each simulation.

#### 4.1.1. Cantilever Beam for Sizing Optimization

In order to verify the sizing optimization capabilities, a cantilever beam is optimized for thickness. The initial design is a 300 inch by 90 inch composite plate composed of 4 layers. All of the layers are assumed to be at the same orientation parallel to the positive x-axis. A steel ball with a radius of 20 inches is dropped vertically upon the free end of the cantilever beam at a velocity of 100 inch per second as shown in Figure 4.1.1.

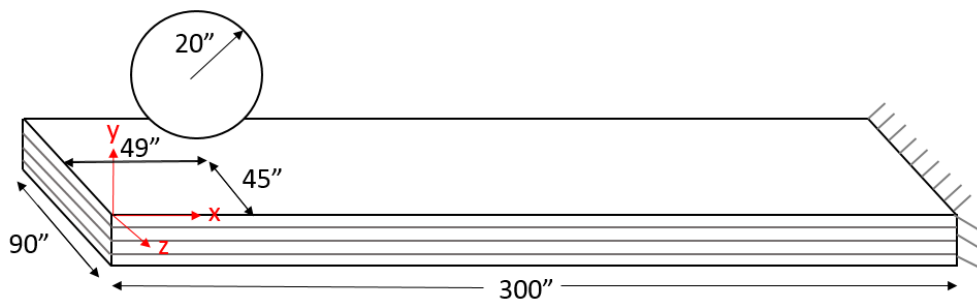


Figure 4.1.1. Initial Model for Thickness Verification

The plate is represented by a coarse finite element mesh composed of 4-noded, reduced integration shell elements. Figs. 4.1.2 shows the composite structure finite element mesh and Table 4.1.2 provides a summary of the finite element model.

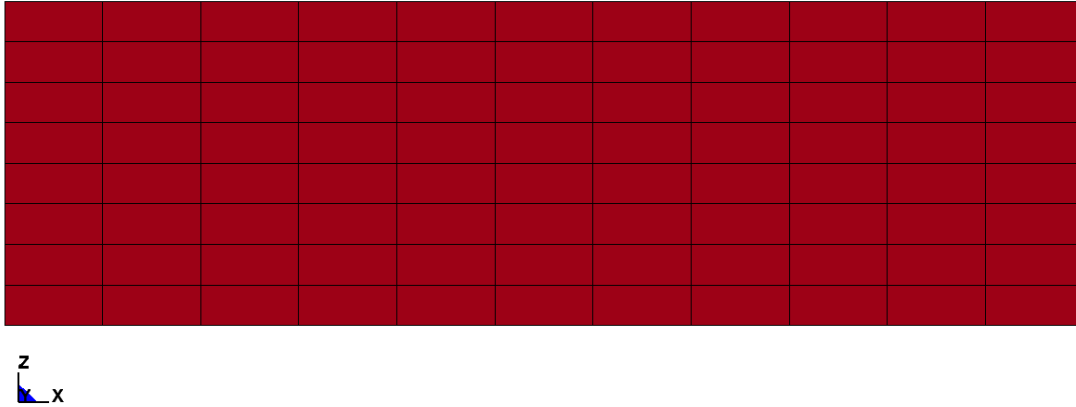


Figure 4.1.2. Element Formulation of Initial Model for Thickness Verification

Table 4.1.2. Summary of Finite Element Model

Part	Material	Num. of Nodes	Num. of Elements
Plate (PART_COMPOSITE)	Composite (MAT_22)	108	88
Ball (SECTION_SHELL)	Steel (MAT_PLASTIC_KINEMATIC)	149	151

Three thickness optimization test cases demonstrate the use of sizing optimization for laminate composites. Each has a continuous thickness design variable assigned on a per element group basis. The optimization problem is as follows:

$$\text{Find } x^{sizing} [t_1, t_2, \dots, t_p] \quad (7.a)$$

$$\text{Minimize } F(x) \quad (7.b)$$

$$\text{Subject to } \frac{d_{5,y}}{d_{5,y}^{allowable}} - 1 \leq 0 \quad (7.c)$$

$$\frac{\sigma_i^k}{\sigma_i^{allowable}} - 1 \leq 0 \quad (7.d)$$

$$\frac{\tau_{max}}{\tau^{allowable}} - 1 \leq 0 \quad (7.e)$$

$$0.1 \leq t_p \leq 1.0 \quad \text{inch} \quad (7.f)$$

The objective function is to minimize the mass of the composite structure. The allowable stress is assumed to be  $4.20 \times 10^5$  psi for longitudinal tensile and compressive stress,  $2.50 \times 10^4$  for transverse tensile and compressive stress, and  $7.5 \times 10^3$  psi for shear stress as per Table 4.1.1. The maximum allowable displacement, Eq. (7.c), imposed in the y-direction at node 5 (Figure 4.1.3) is 4.3 inch.

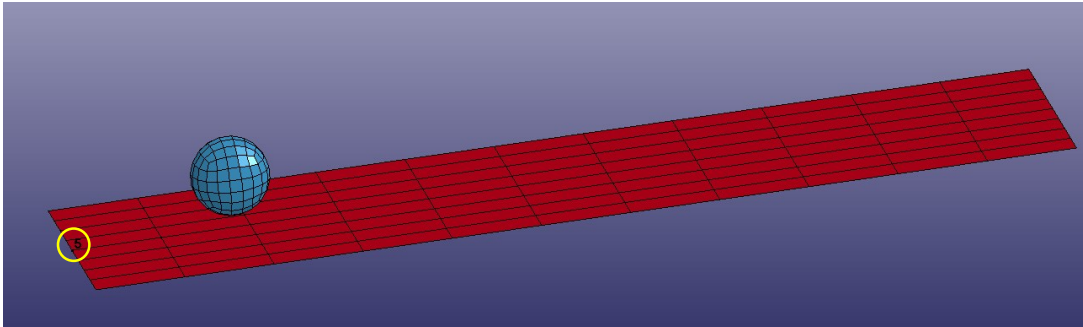


Figure 4.1.3. Node 5 Location in Cantilever Beam Model

The Test Case 1 assumes that the entire plate must be of the same thickness as shown in Figure 4.1.4. The second test case, Test Case 2, separates the composite structure into two element groups (Figure 4.1.5) that have independent thicknesses. The separation is parallel to the z-axis as the optimal thickness distribution for cantilever structures is assumed to be variables along the x-axis with increasing thickness toward the fixed support. Test Case 3 assumes the plate is composed of 4 element groups with

independent thicknesses (Figure 4.1.6). All of the test cases start with the initial solution of four 1.0 inch thick layers, uniform throughout the plate. As a result, the initial objective function,  $F(\mathbf{x})$ , value is 15.7356 slugs.



Figure 4.1.4. Element Group Definition for Test Case 1

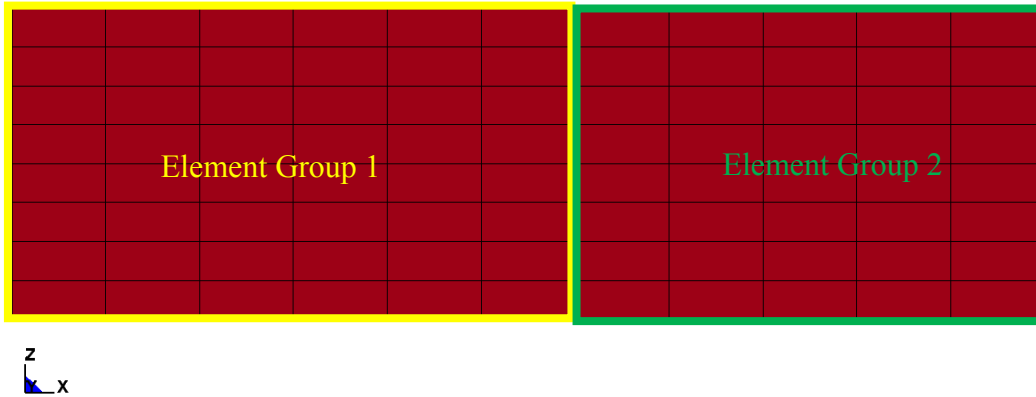


Figure 4.1.5. Element Group Definition for Test Case 2

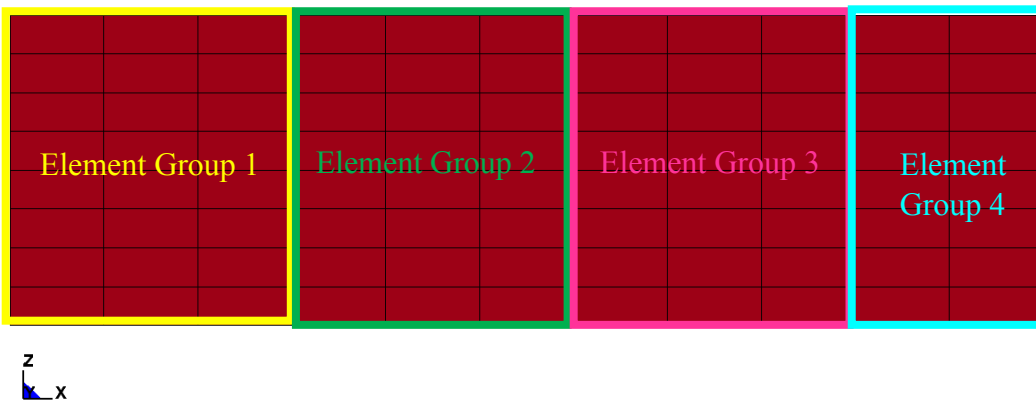


Figure 4.1.6. Element Group Definition for Test Case 3

The results of the optimization process for Test Case 1, 2, and 3 are summarized in Table 4.1.3. The active constraint for all three test cases is the nodal displacement at node 5.

Table 4.1.3. Results of Layer Thickness Demonstrations

	Test Case 1	Test Case 2	Test Case 3
<b>Num. of Element Groups</b>	1	2	4
<b>Num. of Design Variables</b>	1	2	4
<b>Optimizer</b>	DE	DE	DE
<b>Max Iterations</b>	10	20	20
<b>Population Size</b>	10	20	20
<b>Final Objective Function (slug)</b>	9.76	9.29	8.68
<b>Num. of Function Evaluations</b>	92	382	382
<b>Time to Complete (s)</b>	5327	22507	23156
<b>Max. Constraint Value</b>	-0.000372171	-0.00106978	-0.00360465
<b>Max. Nodal Deflection (inch)</b>	4.298	4.295	4.285
<b>Max. Principal Stress</b>	$\sigma_{xx} = -5012.5$	$\sigma_{xx} = 4677.8$	$\sigma_{xx} = 5543.3$
<b>Max. Shear Stress</b>	2506.3	2338.9	2771.6

The final design variable for Test Case 1 is 0.62 inch; therefore, the plate model has a total thickness of 2.48 inches uniformly across the plate as shown in Figure 4.1.7.

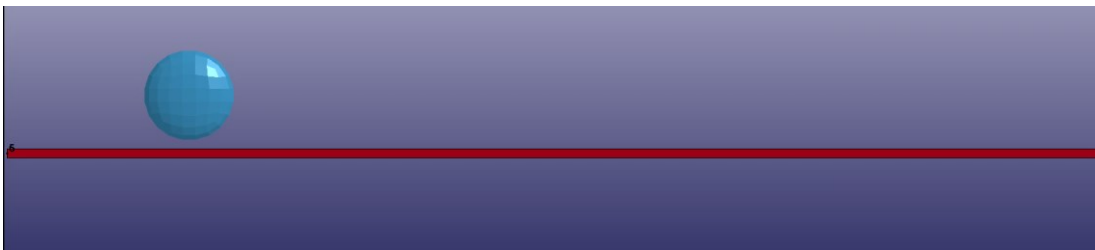


Figure 4.1.7. Results of Test Case 1

The final model for Test Case 2 has different thicknesses for Element Group 1 and Element Group 2 as expected as shown in Figure 4.1.8. The design variable values

are 0.518 inch and 0.676 inch, respectively. Therefore, Element Group 1 containing elements further away from the fixed support have a total thickness of 2.07 inch and Element Group 2 has a total thickness of 2.71 inch.

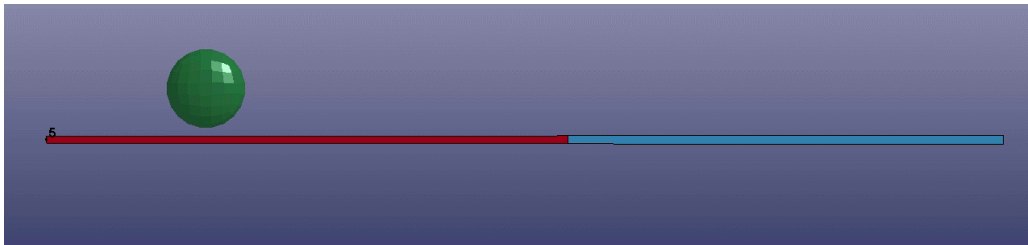


Figure 4.1.8. Results of Test Case 2

The final model for Test Case 3 (Figure 4.1.9) has different total thicknesses for each of the four element groups. The thickness distribution demonstrates that the optimal design has an increasing part thickness towards the fixed support. Element Group 1 is 1.37 inch thick, Element Group 2 is 1.93 inch thick, Element Group 3 is 2.78 inch thick, and Element Group 4 is 3.01 inch thick. Respectively, the design variable values are 0.34 inch, 0.48 inch, 0.70 inch, and 0.75 inch.

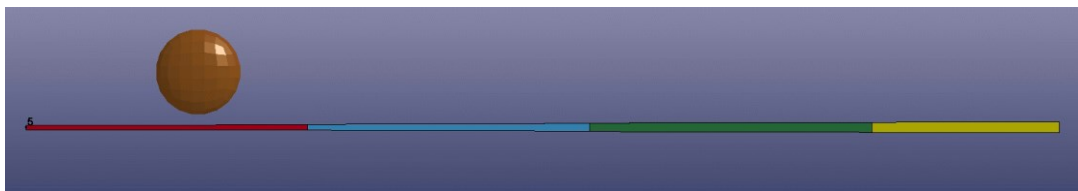


Figure 4.1.9. Results of Test Case 3

The three test cases presented for composite layer thickness optimization demonstrates the prediction of the thickness distribution of the optimal cantilever structure for minimizing weight. The part thickness decreases as the distance from the

fixed support is increased. Additionally, Test Case 3 demonstrates that as the number of element groups is increased, the objective function value can be reduced to a more optimum solution.

The optimization for Test Case 2 and Test Case 3 was initially completed with 10 iterations of populations with size 10. However, after completion of the optimization process, the maximum constraint value was larger than -10% of zero demonstrating that no constraint was active. As a result, the number of iterations was increased to 20 and the population size increased to 20 in order to achieve solutions that are governed displacement as the active constraint as shown in Table 4.1.3.

#### 4.1.2. Pinned Structure for Sizing and Topology Optimization

In order to demonstrate sizing and topology optimization, test cases using layer thickness, layer orientation, and layer status are provided. Test Case 4 and Test Case 5 utilize the continuous layer thickness and layer orientation design variables. The layer status design variables are used in Test Case 6 and Test Case 7. This finite element model for Test Case 4 through Test Case 7 (Figure 4.1.11) is similar to the cantilever model discussed in section 4.1.1, however, the boundary conditions of the model are changed (Figure 4.1.10). Test Case 4 through Test Case 7 is pinned along the 90 inch sides of the structure. In this way, when the 20 inch ball is vertically dropped upon the plate at 100 inches per second, the composite structure is expected to behave similar to a three-point bending test.

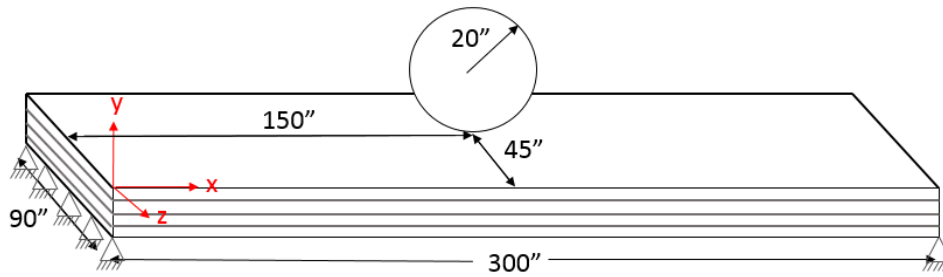


Figure 4.1.10. Simply Supported Structure Model

The finite element mesh in Figure 4.1.11 has refined elements located along the x-axis center of the plate. This refinement places a node directly at the location of impact from the ball for maximum displacement measurement. A summary of the finite element model is provided in Table 4.1.4.

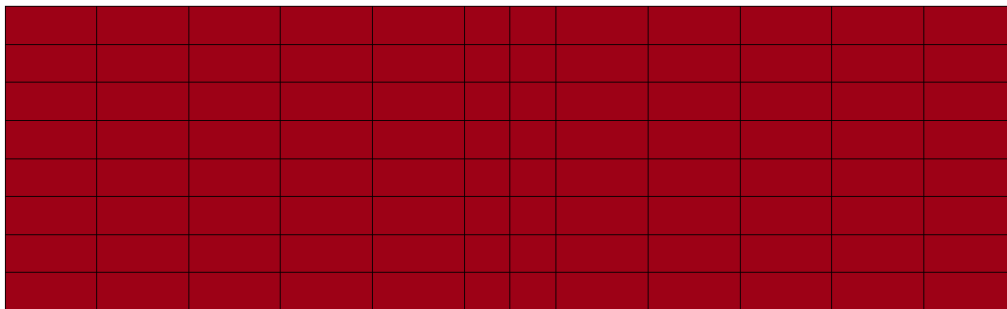


Figure 4.1.11. Element Formulation for Pinned Structure Model

Table 4.1.4. Summary of Finite Element Model for Pinned Structure

Part	Material	Num. of Nodes	Num. of Elements
Plate (PART_COMPOSITE)	Composite (MAT_22)	117	96
Ball (SECTION_SHELL)	Steel (MAT_PLASTIC_KINEMATIC)	149	151

Test Case 4 and Test Case 5 utilize the continuous layer thickness and layer orientation design variables. The layer thickness design variable is assigned on a per element group basis and the layer orientation is designed per layer. The optimization problem is posed as follows:

$$\text{Find } x\{x^{sizing}[t_1, t_2, \dots, t_p], x^{topology}[\beta_{1,1}, \beta_{1,2}, \dots, \beta_{p,l}]\} \quad (8.a)$$

$$\text{Minimize } F(x) \quad (8.b)$$

$$\text{Subject to } \frac{d_{115,y}}{d_{115,y}^{allowable}} - 1 \leq 0 \quad (8.c)$$

$$\frac{\sigma_i^k}{\sigma_i^{allowable}} - 1 \leq 0 \quad (8.d)$$

$$\frac{\tau_{max}}{\tau^{allowable}} - 1 \leq 0 \quad (8.e)$$

$$0.1 \leq t_p \leq 1.0 \quad \text{inch} \quad (8.f)$$

$$0.0 \leq \beta_{p,l} \leq 135.0 \quad (8.g)$$

The objective function is to minimize the mass of the composite structure. The allowable stress is assumed to be  $4.20 \times 10^5$  psi for longitudinal tensile and compressive stress,  $2.50 \times 10^4$  for transverse tensile and compressive stress, and  $7.5 \times 10^3$  psi for shear stress as per Table 4.1.1. The maximum allowable displacement, Eq. (8.c), imposed in the

y-direction at node 115 is 1.0 inch. Figure 4.1.12 identifies the location of node 115 as the node located directly at the point of impact from the steel ball.

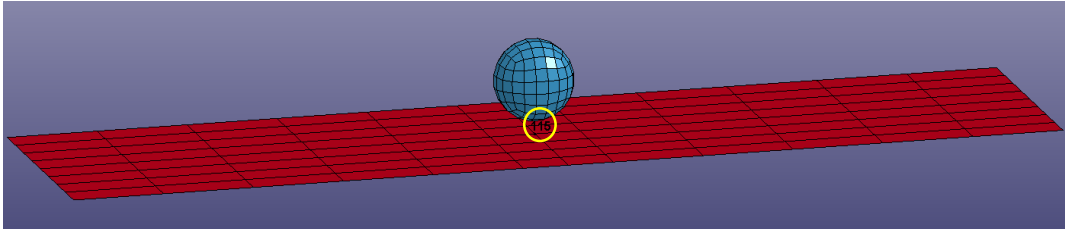


Figure 4.1.12. Node 115 Location In Pinned Model

Test Case 4 contains one element property group of which all of the plate elements belong to (Figure 4.1.13). Alternatively, Test Case 5 uses two element property groups. Figure 4.1.14 shows that the element group separation for Test Case 5 is symmetric about the center of the structural x-axis span. This separation is based upon the optimal solution assumed to be when the material near the pinned edges are thin and complemented by thicker layers toward the center of the plate. This assumption is based upon demonstration of large stresses and displacements located at the center of specimens subjected to three point bending tests. Additionally, it is expected that some of the material layers will be orientated parallel to the global x-axis to accommodate bending in the long spanning x-axis dimension and the remaining layers will be oriented off axis to account for curvature effects. Both test cases start with the initial solution of four 1.0 inch thick layers, uniform throughout the plate, oriented parallel to the global x-axis. As a result, the initial objective function,  $F(\mathbf{x})$ , value is 15.7356 slugs.

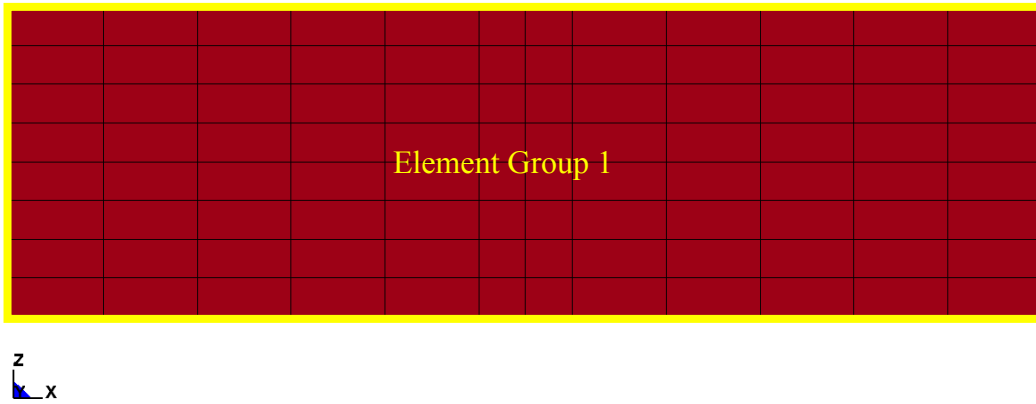


Figure 4.1.13. Element Groups for Test Case 4

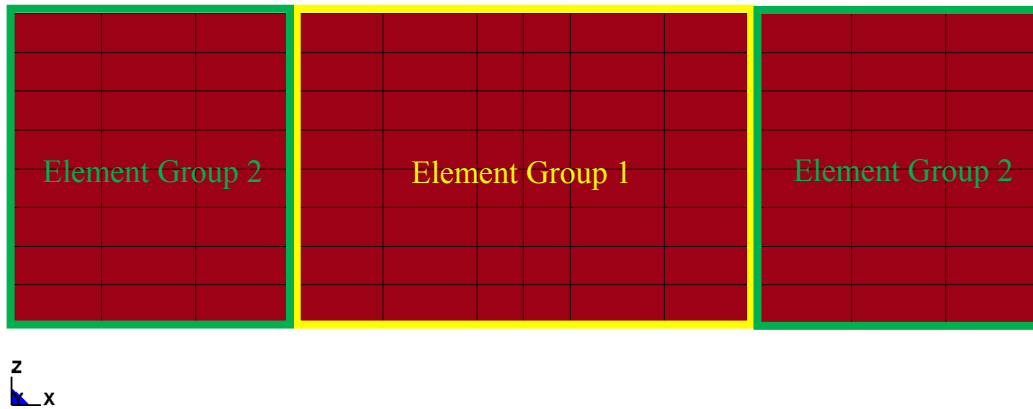


Figure 4.1.14. Element Groups for Test Case 5

The results for Test Case 4 and Test Case 5 are summarized in Table 4.1.5. The active constraint for both optimized solutions is the maximum displacement at node 115.

Table 4.1.5. Results from Sizing and Topology Optimization

	Test Case 4	Test Case 5
<b>Num. of Element Groups</b>	1	2
<b>Num. of Design Variables</b>	5	10
<b>Optimizer</b>	DE	DE
<b>Max Iterations</b>	30	50
<b>Population Size</b>	30	30
<b>Final Objective Function (slugs)</b>	9.4	8.5
<b>Num. of Function Evaluations</b>	884	1432
<b>Time to Complete (s)</b>	20844	43404
<b>Max. Constraint Value</b>	-0.01567	-0.00019002
<b>Max. Nodal Deflection (inch)</b>	-0.98	-0.99
<b>Max. Principal Stress (psi)</b>	$\sigma_{xx} = 5159.8$	$\sigma_{xx} = 10822.0$
<b>Max. Shear Stress (psi)</b>	2579.9	5411.0

The final model for Test Case 4 has a plate thickness of 2.4 inches uniformly across the plate as shown in Figure 4.1.15. Table 4.1.6 details the layer thicknesses and orientations throughout the thickness of the laminate composite.

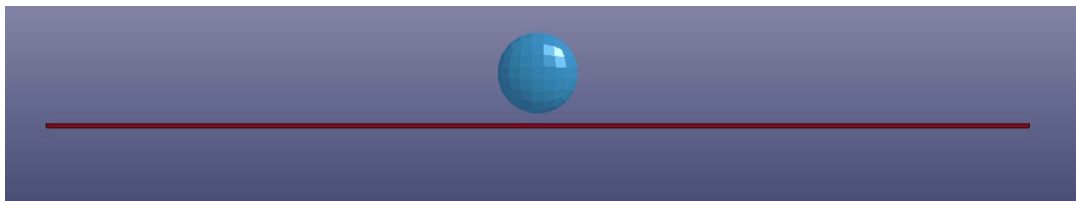


Figure 4.1.15. Final Model for Test Case 4

Table 4.1.6. Details of Final Model for Test Case 4

<b>Element Group 1</b>		
<b>Layer</b>	<b>Thickness (in.)</b>	<b>Orientation (deg.)</b>
4	0.6	10.1
3	0.6	0.0
2	0.6	0.0
1	0.6	14.9

The final stacking sequence for Test Case 4 is representative of a balanced laminate composite. The bottom and top layers are oriented at 14.94 degrees and 10.12 degrees, respectively, to account for large curvature effects from the ball impact. The remaining interior layers are oriented parallel to the global x-axis as expected to provide strength in the long spanning direction.

As with traditional three point bending tests, the maximum principal material stresses were experienced in the bottom layer of the in elements located near the center of the composite part. Tensile stress in the longitudinal direction of the top layer is the largest principal material stress throughout the simulation. The maximum principal material stresses for Test Case 4 are provided in Table 4.1.7

Table 4.1.7. Maximum Stresses in Final Model for Test Case 4

	<b>Time (s)</b>	<b>Element Number</b>	<b>Layer Number</b>	<b>Stress (psi)</b>
$\sigma_{xx}$	0.0074	95	4	5159.8
$\sigma_{yy}$	0.13	96	4	-842.8
$\sigma_{zz}$	-	-	-	0.0
$\tau_{max}$	0.0074	95	4	2579.9

The final model for Test Case 5 has different thicknesses for Element Group 1 and Element Group 2 as shown in Figure 4.1.16. Element Group 1 containing elements in the center portion of the composite plate has a thickness of 3.55 inch and Element Group 2 has a thickness of 0.99 inch. Layer orientation and thickness values for Element Group 1 and Element Group 2 are detailed in Table 4.1.8.

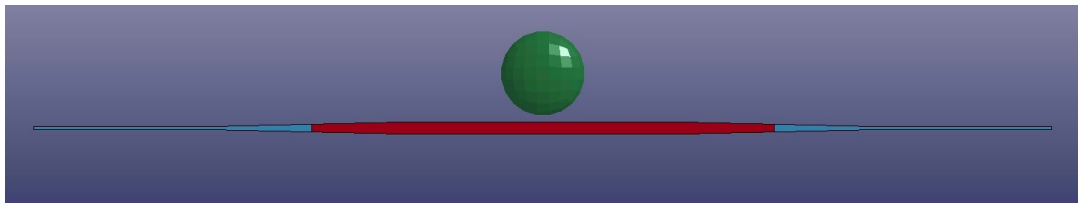


Figure 4.1.16. Final Model for Test Case 5

Table 4.1.8. Details of Final Model for Test Case 5

Layer	Element Group 1		Element Group 2	
	Thickness (in.)	Orientation (deg.)	Thickness (in.)	Orientation (deg.)
4	0.89	0.0	0.247	0.8
3	0.89	64.9	0.247	135.0
2	0.89	3.6	0.247	134.3
1	0.89	26.0	0.247	9.0

The stacking sequence in Element Group 2 resembles a symmetric sequence. This symmetry minimizes asymmetric bending coupling and curvature effects (Daniel & Ishai, 2006). Element Group 1 stacking sequence does not demonstrate this same symmetry, however, the sequence aligns with the principal material stresses experienced in the elements within this element group.

The maximum principal material stresses were experienced in the top and bottom layers of the elements located near the center of the composite structure. Details of the

maximum principal material stresses are provided in Table 4.1.9. The top layer in Element Group 1 experiences maximum longitudinal stresses. As a result, this layer is oriented parallel to the x-axis to ensure that the longitudinal material axis is engaged.

Table 4.1.9. Maximum Stresses in Final Model for Demonstration 5

	<b>Time (s)</b>	<b>Element Number</b>	<b>Layer Number</b>	<b>Stress (psi)</b>
$\sigma_{xx}$	0.0085	65	4	10822.0
$\sigma_{yy}$	0.025	46	1	-943.0
$\sigma_{zz}$	-	-	-	0.0
$\tau_{max}$	0.0085	65	4	5411.0

Overall, the orientation results from Test Case 4 and Test Case 5 demonstrate that to meet the displacement constraint, approximately one half of the laminate layers are oriented parallel to the 300 inch span and the other oriented off-axis to help mitigate curvature effects. By utilizing the layer orientation design variable in tandem with the layer thickness design variable, the optimization process orients layers to allow for reduction in the objective function value. This increase in the number of design variables also results in an increase in required computation time in order to find a solution with an active constraint as can be noted from Table 4.1.5.

A demonstration of the discrete layer orientation design variable is not presented here as the results and methodology are similar to that of the continuous orientation design variable. The primary reason to favor the discrete orientation design variable is when fabrication constraints limit the number of possible layup orientations.

In order to demonstrate the layer status design variable and use of the Genetic Algorithm optimization procedure, an additional two test cases are completed as an expansion to Test Case 4 and Test Case 5. Test Case 6 uses the same finite element model as Test Case 4 (Figure 4.1.13) with one element group; however, the design variables are the layer status of each layer with in the element group. Similarly, Test Case 7 uses the same finite element model as Test Case 5 (Figure 4.1.14) with layer status design variables. The layer status design variables are assigned on a per layer basis. The optimization problem for Test Case 6 and Test Case 7 is posed as follows:

$$\text{Find } x \{x^{topology} [s_{1,1}, s_{1,2}, \dots, s_{p,l}]\} \quad (9.a)$$

$$\text{Minimize } F(x) \quad (9.b)$$

$$\text{Subject to } \frac{d_{115,y}}{d_{115,y}^{allowable}} - 1 \leq 0 \quad (9.c)$$

$$\frac{\sigma_i^k}{\sigma_i^{allowable}} - 1 \leq 0 \quad (9.d)$$

$$\frac{\tau_{max}}{\tau^{allowable}} - 1 \leq 0 \quad (9.e)$$

$$s_{p,l} = 0, 1 \quad (9.f)$$

The layer status design variable is assigned to all layers except the top layer for of each element group. The objective function is still to minimize the mass of the composite structure. The allowable stress is assumed to be  $4.20 \times 10^5$  psi for longitudinal tensile and compressive stress,  $2.50 \times 10^4$  for transverse tensile and compressive stress, and  $7.5 \times 10^3$  psi for shear stress as per Table 4.1.1. The maximum allowable displacement, Eq. (7.c), imposed in the y-direction at node 115 is 1.0 inch (Figure 4.1.12). Each test case has an

initial design of 10 layers of 0.4 inch thick oriented parallel to the x-axis, giving an initial objective function value of 17.31 slugs.

The results of Test Case 6 and Test Case 7 are provided in Table 4.1.10. The active constraint in both test cases is the maximum displacement of node 115. The GA optimizer was used for these test cases to demonstrate the COMP-OPT GA optimization capabilities. However, DE could have also have been used for the optimization problem presented in Eq. (9.a) – (9.f).

Table 4.1.10. Results from Layer Status Topology Optimization

	Test Case 6	Test Case 7
<b>Num. of Element Groups</b>	1	2
<b>Num. of Design Variables</b>	9	18
<b>Optimizer</b>	GA-TOPFEW	GA-TOPFEW
<b>Max Iterations</b>	15	30
<b>Population Size</b>	15	30
<b>Final Objective Function (slugs)</b>	11.0	8.3
<b>Num. of Function Evaluations</b>	134	379
<b>Time to Complete (s)</b>	5449	13949
<b>Max. Constraint Value</b>	-0.22981	-0.09232
<b>Max. Nodal Deflection (inch)</b>	-0.77	-0.91
<b>Max. Principal Stress</b>	$\sigma_{xx} = 5381.4$	$\sigma_{xx} = 6691.4$
<b>Max. Shear Stress</b>	2690.7	3345.7

The final model for Test Case 6 has seven layers of 0.4 inches and, therefore, a total structural thickness of 2.8 inches as shown in Figure 4.1.17.

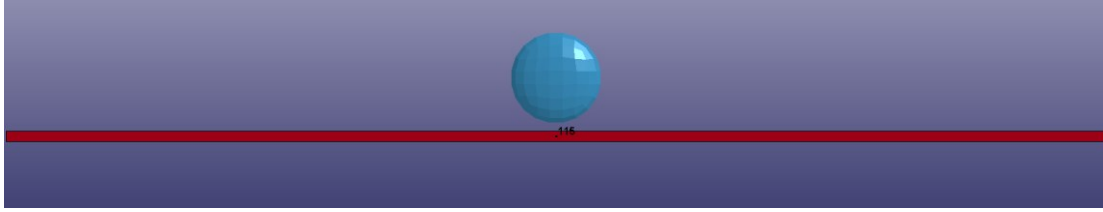


Figure 4.1.17. Final Model for Test Case 6

The final model for Test Case 7 has a different number of layers for Element Group 1 and Element Group 2 as shown in Figure 4.1.18. Element Group 1 containing elements in the center span of the composite structure has a total of 8 layers and a uniform thickness of 3.2 inch. Element Group 2 has a total of 3 layers summing to a total thickness of 1.2 inch.

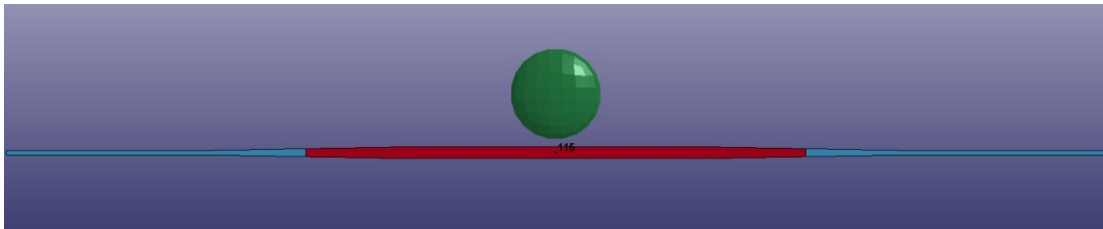


Figure 4.1.18. Final Model for Test Case 7

As expected, the final results from Test Case 6 and Test Case 7 utilizing the layer status design variables provide solutions similar to the results from Test Case 4 and Test Case 5. For two element groups, enabling the optimization process to remove unnecessary layers provided a more optimum solution than found through optimization of layer thickness and orientation design variables. Alternatively, when only one element group was used, Test Case 4 provided a more desirable solution than Test Case 6. It is expected that by utilizing the layer status, thickness, and orientation design variables together, the final material design could be further optimized.

#### 4.1.3. Cantilever Beam for Expected Shape Optimization

Shape optimization is completed on the cantilever composite structure presented in section 4.1.1 to demonstrate the shape optimization capabilities of the COMP-OPT program. Test Case 8 uses the details of the single element group finite element mesh found in Figure 4.1.4 and Table 4.1.4; however, the new shape optimization problem will be stated as follows:

$$\text{Find } x\{x^{shape}[x_{k \times 1}], x^{sizing}[t_1, t_2, \dots, t_p]\} \quad (10.a)$$

$$\text{Minimize } F(x) \quad (10.b)$$

$$\text{Subject to } \frac{d_{5,y}}{d_{5,y}^{allowable}} - 1 \leq 0 \quad (10.c)$$

$$\frac{\sigma_i^k}{\sigma_i^{allowable}} - 1 \leq 0 \quad (10.d)$$

$$\frac{n_{1,z} - n_{0,z}}{20} + 1 \leq 0 \quad (10.e)$$

$$\frac{\tau_{max}}{\tau^{allowable}} - 1 \leq 0 \quad (10.f)$$

$$x_{k \times 1}[a_1] \quad (10.g)$$

$$a_k = \alpha_k \mathfrak{R}_0 \Delta \quad -1 \leq \alpha_k \leq 1, \quad o = x, y, z - axis \quad (10.h)$$

$$\Delta_1 = 45.0\% \quad (10.i)$$

$$0.1 \leq t_p \leq 1.0 \quad \text{inch} \quad (10.j)$$

The objective function is to minimize the mass of the composite structure. The allowable stress is assumed to be  $4.20 \times 10^5$  psi for longitudinal tensile and compressive stress,  $2.50 \times 10^4$  for transverse tensile and compressive stress, and  $7.5 \times 10^3$  psi for shear

stress as per Table 4.1.1. The maximum allowable displacement, Eq. (10.c), imposed in the y-direction at node 5 (Figure 4.1.3) is 4.3 inch. Eq. (10.e) represents the geometric constraint that requires the z-coordinate of node 1 and node 9 is at least 20.0 inches apart (Figure 4.1.19).

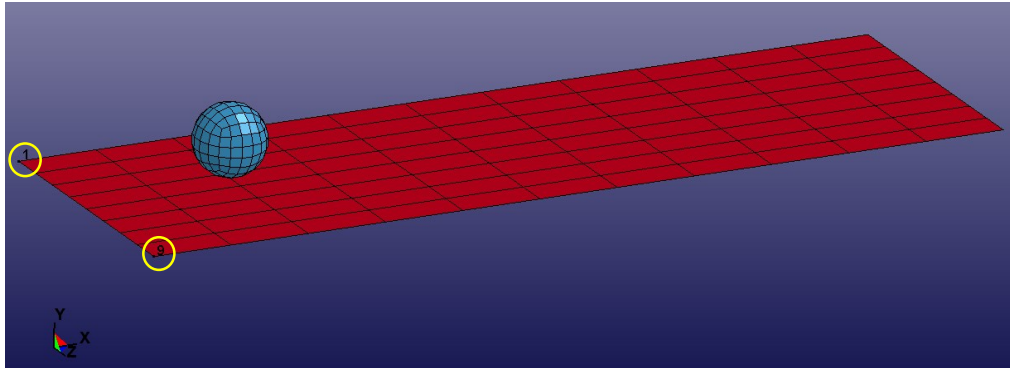


Figure 4.1.19. Shape Optimization Geometric Constraint Nodes

The shape optimization process in the COMP-OPT program is completed through use Eq. (5). Therefore, velocity fields must be provided based on the type of desired results from the shape optimization process. Only one velocity field is used for the shape optimization problem for Test Case 8. The velocity field vector is such that the 300 inch edges of the cantilever plate mesh maintain a straight line form with no adjustment of the fixed nodal supports. Additionally, the velocity field is created such that symmetry is maintained about the center line of the structure parallel to the x-axis. The Figure 4.1.20 demonstrates the range of possible optimized shapes. This vector was computed utilizing the methodology proposed by Rajan et al. through comparison of an initial finite element mesh and a perturbed mesh (Rajan, Chin, & Gani, 1996).

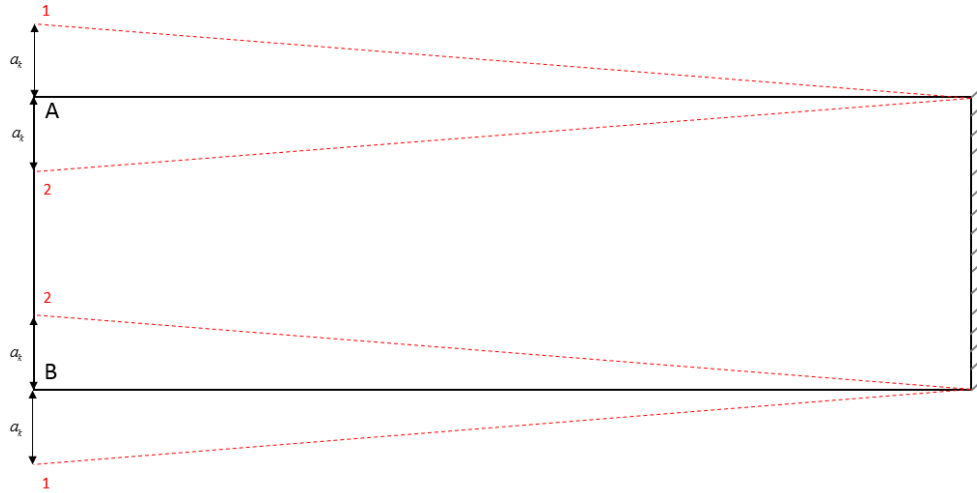


Figure 4.1.20. Possible Shape Changes for Test Case 8

In Figure 4.1.20, node A will be moved a distance specified by the design variable  $\mathbf{x}$ . Node B will be moved the same distance in the opposite direction to ensure symmetry is maintained. In a similar fashion, all of the consecutive nodes along the edges of the plate will be moved such that they form a line as identified by the red, dotted lines above. The nodes that form the fixed edge of the plate are not permitted to move in the shape optimization process, but all successive nodes will be adjusted by an appropriate fraction of the relocation magnitude of nodes A and B.

The design variable for the vector field used in this demonstration has an allowable per iteration change of 45.0% as shown in Eq. (10.i). Additionally, the thickness of the composite layers is optimized as completed in section 4.1.1 between the bounds defined in Eq. (10.j). The optimized result from Test Case 8 is expected to provide a solution shape along some magnitude of movement #2 as identified in Figure 4.1.20 as this is the optimal shape of a cantilevered structure. Test Case 8 starts with the initial solution of four 1.0 inch thick layers, uniform throughout the plate. As a result, the initial objective function,  $F(\mathbf{x})$ , value is 15.7356 slugs.

The results of the optimization process are summarized below. The active constraint for the final solution is the displacement at node 5.

Table 4.1.11. Results from Shape Optimization Test Case 8

	Test Case 8
<b>Num. of Element Groups</b>	1
<b>Num. of Design Variables</b>	2
<b>Optimizer</b>	DE
<b>Max Iterations</b>	15
<b>Population Size</b>	15
<b>Final Objective Function (slugs)</b>	7.3
<b>Num. of Function Evaluations</b>	212
<b>Time to Complete (s)</b>	15427
<b>Max. Constraint Value</b>	-0.0351629
<b>Max. Nodal Deflection (inch)</b>	4.15
<b>Max. Principal Stress (psi)</b>	$\sigma_{xx} = 8620.2$
<b>Max. Shear Stress (psi)</b>	4310.1

The final model shape and thickness is shown in Figures 4.1.21 and 4.1.22. The optimized shape is as expected.

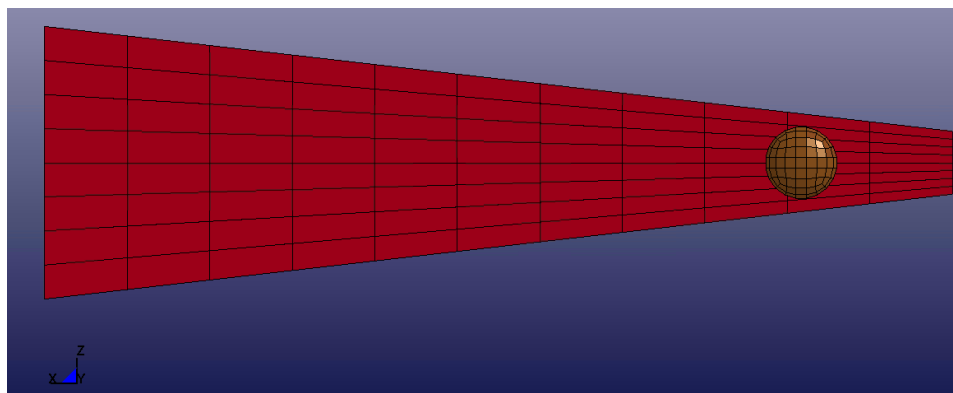


Figure 4.1.21. Final Model Shape of Test Case 8



Figure 4.1.22. Final Model Thickness of Test Case 8

In comparison to the Test Case 1 completed in section 4.1.1, the optimization process was executed for an additional number of iterations to find a solution with an active constraint. This additional number of iterations increase the computation time for the optimization process, however, the final result was reduced by 25%, from 9.76 slugs (Table 4.1.3) to 7.32 slugs (Table 4.1.11). Therefore, shape optimization may be a desired addition to a realistic laminate composite optimization problem when additional computation time from additional design variables is acceptable.

#### 4.1.3.1. Mesh Convergence Study

The optimization results from laminate composite material design problems are loading and finite element mesh dependent (Muc & Gurba, 2001). The shape and sizing optimization problem solved in section 4.1.3 will be used to demonstrate mesh dependency. The final model of the laminate composite plate shown in Figure 4.1.21 was refined to contain 207 nodes and 176 elements as shown in Figure 4.1.23.

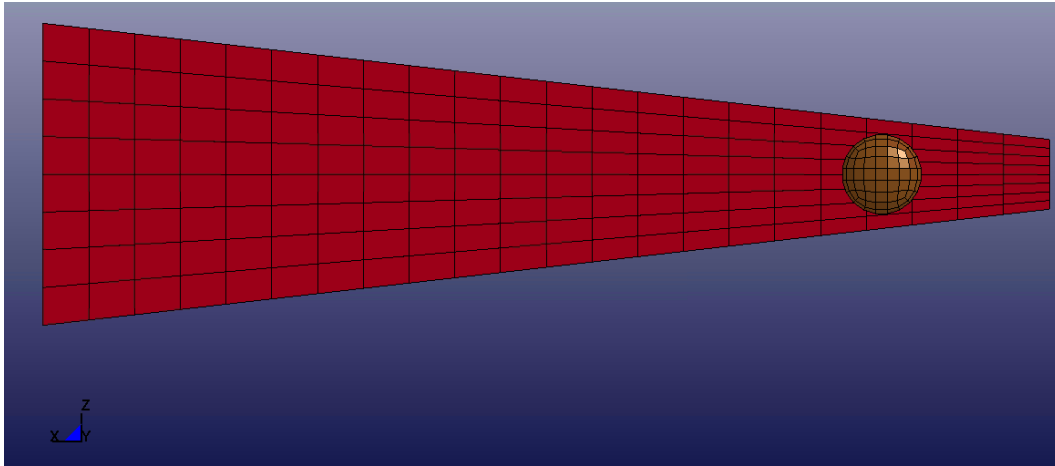


Figure 4.1.23. Refined Mesh from Test Case 8

The finite element results of the refined mesh shown in Figure 4.1.23 differ slightly from those the final Test Case 8 model. As the active constraint in Test Case 8 was the displacement at node 5, a comparison of the y-axis displacement curves for the Test Case 8 solution (Figure 4.1.24) and the refined mesh shown in Figure 4.1.23 (Figure 4.1.25) demonstrates that the maximum displacement of node 5 for the refined mesh is no longer an active constraint. The Test Case 8 solution has a maximum y-displacement of 4.15 inches at node 5, whereas the refined mesh experiences a maximum y-displacement of 3.99 inches.

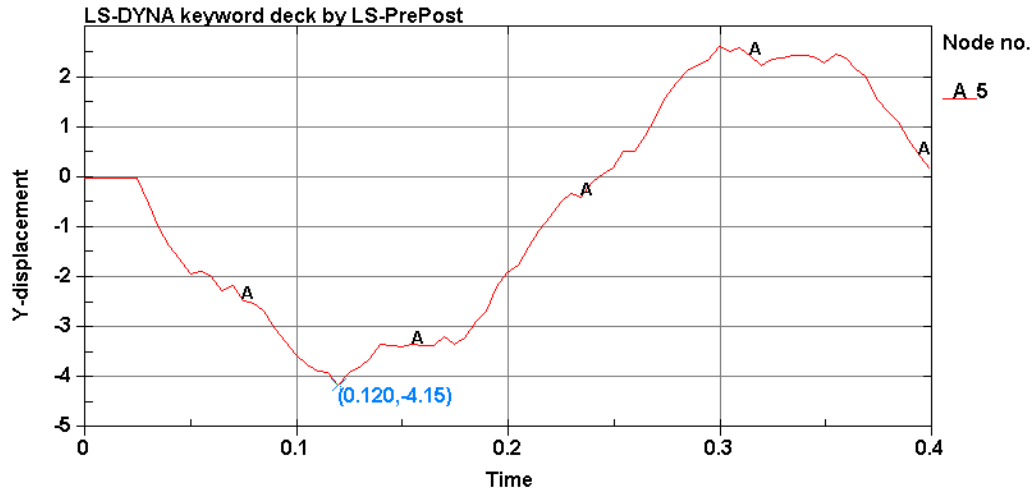


Figure 4.1.24. Node 5 Deflection on Test Case 8

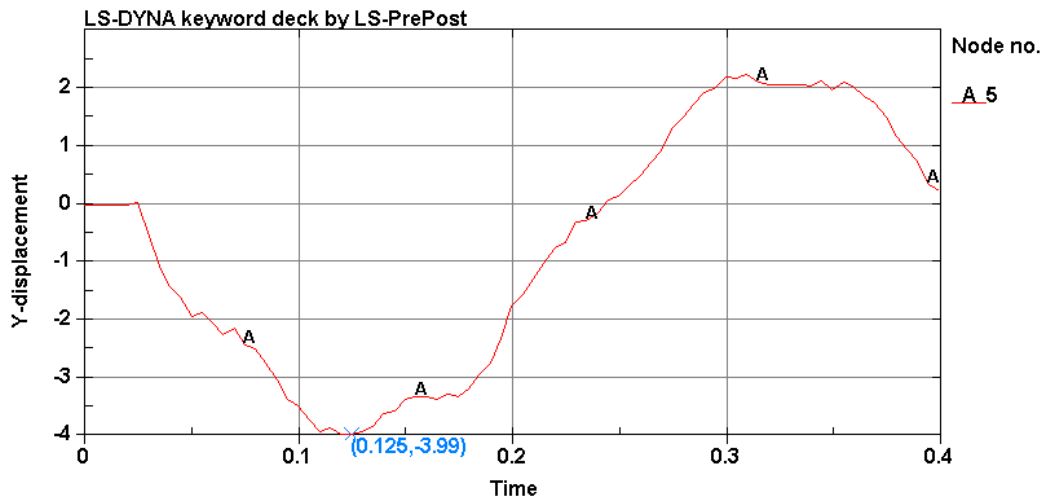


Figure 4.1.25. Node 5 Deflection on Refined Mesh of Test Case 8 Model

The displacement results for the Test Case 8 and the Test Case 8 refined mesh are compared with a further refined mesh that doubled the number of elements in a similar manner. The maximum displacement of node 5 in the three models are used to compute the grid convergence index of the solution. Neither refined model was re-optimized and each successive model refinement doubled the number of elements present, such that the grid density increases by a factor of 2. The grid convergence index is a measure of the

computed result values with respect to the expected, mathematical asymptotic values in order to demonstrate mesh convergence (Slater, 2008). The grid convergence index was computed utilizing the data provided in Table 4.1.12 for the three cantilevered structure models discussed.

Table 4.1.12. Data for Grid Convergence Index Computations

Normalized Grid Spacing	Node 5 Absolute Maximum Deflection (inch)
4	4.14
2	3.99
1	3.93

Application of the Richardson extrapolation predicts that the exact maximum deflection is expected to be 3.905 inch (Slater, 2008). The following graph demonstrates the expected grid convergence path for the Test Case 8 model. The asymptotic range of convergence is computed as 0.962 (Slater, 2008). This range is close to 1.0, therefore, the results from the mesh refinement process of the optimized model from Test Case 8 are within an appropriate range of convergence.

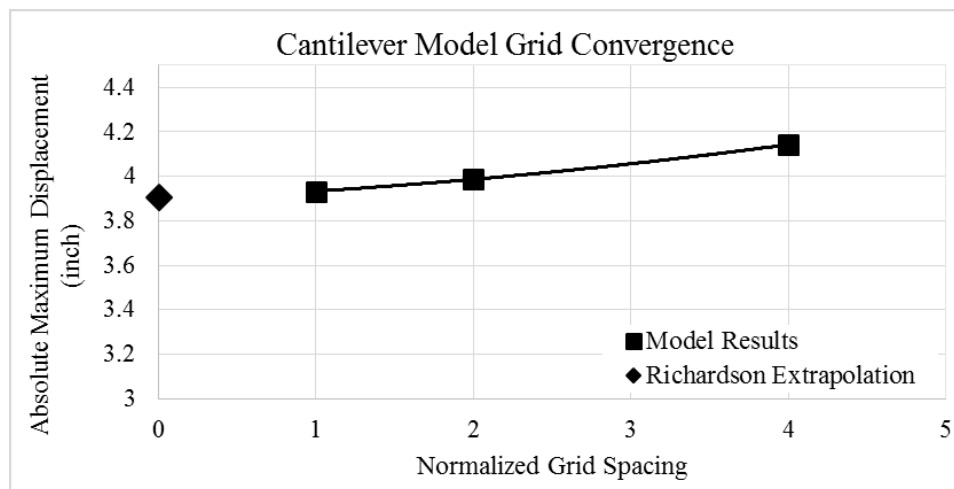


Figure 4.1.26. Grid Convergence Analysis

As the refined Test Case 8 optimized mesh, Figure 4.1.23, demonstrates that the maximum displacement constraint is no longer considered active, the refined mesh is optimized using the same optimization problem presented in section 4.1.3 and Eq. (10.a) – (10.j). The initial shape for Test Case 8.1 is similar to the initial shape used for Test Case 8 with the exception of additional, refined elements. The initial composite layup is four layers of 1.0 inch thickness throughout the plate oriented parallel to the global x-axis. For the same optimization problem statement (Eq. (10.a) – (10.j)), the following optimization results were obtained.

Table 4.1.13. Results from Shape Optimization of Test Case 8.1

	<b>Test Case 8.1</b>
<b>Num. of Element Groups</b>	1
<b>Num. of Design Variables</b>	2
<b>Optimizer</b>	DE
<b>Max Iterations</b>	15
<b>Population Size</b>	15
<b>Final Objective Function (slugs)</b>	7.2
<b>Num. of Function Evaluations</b>	212
<b>Time to Complete (s)</b>	24476
<b>Max. Constraint Value</b>	-0.0189535
<b>Max. Nodal Deflection (inch)</b>	4.22
<b>Max. Principal Stress (psi)</b>	$\sigma_{xx} = 9997.0$
<b>Max. Shear Stress (psi)</b>	4998.5

The final optimized shape and composite thickness for Test Case 8.1 is shown below in Figure 4.1.27 and Figure 4.1.28.

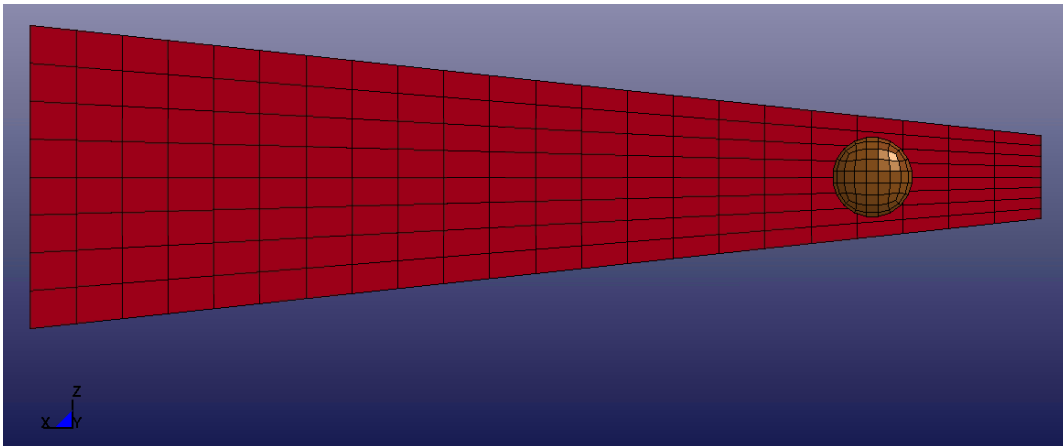


Figure 4.1.27. Final Model Shape for Test Case 8.1



Figure 4.1.28. Final Model Thickness for Test Case 8.1

The final optimized shapes for Test Case 8 and Test Case 8.1 are similar. The final model for Test Case 8.1 results in a slightly lower objective function. A comparison of the final design variables values for Test Case 8 and Test Case 8.1 in Table 4.1.14 demonstrate that the optimization solution changes based upon the level of mesh density. Test Case 8.1 optimized to a thinner laminate composite structure and did not change the shape to the same amplitude as in Test Case 8.

Table 4.1.14. Result Comparison of Test Case 8 and Test Case 8.1

	Test Case 8	Test Case 8.1
<b>Thickness of Layers (inch)</b>	0.76	0.71
<b>Shape Change Amplitude</b>	-0.855	-0.807
<b>Objective Function Value</b>	7.3	7.2
<b>Max. Constraint Value</b>	-0.0351629	-0.0189535
<b>Max. Displacement of Node 5 (inch)</b>	4.15	4.22

The optimization results obtained from Test Case 8.1 are further refined to verify the displacement constraint is still active (Figure 4.1.29). Analysis results from the additional refinement show a maximum displacement of node 5 as -4.22, as was found in Test Case 8.1. As a result, the displacement constraint remains active.

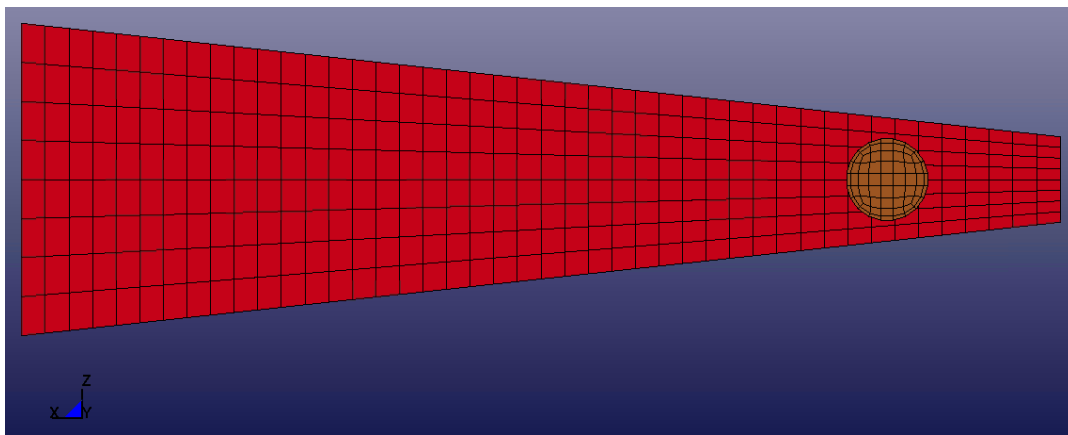


Figure 4.1.29. Refined Test Case 8.1 Model

In addition to the grid refinement process demonstrated with Test Case 8 and Test Case 8.1, time refinement can also be completed to ensure results are capturing full structural response behavior. All previous test cases have exported displacement and stress results every 0.005 seconds, so the model in Figure 4.1.29 was refined with respect

to time to record performance results every 0.0005 seconds. The y-displacement over time output curves are provided in Figure 4.1.30 and 4.1.31, respectively.

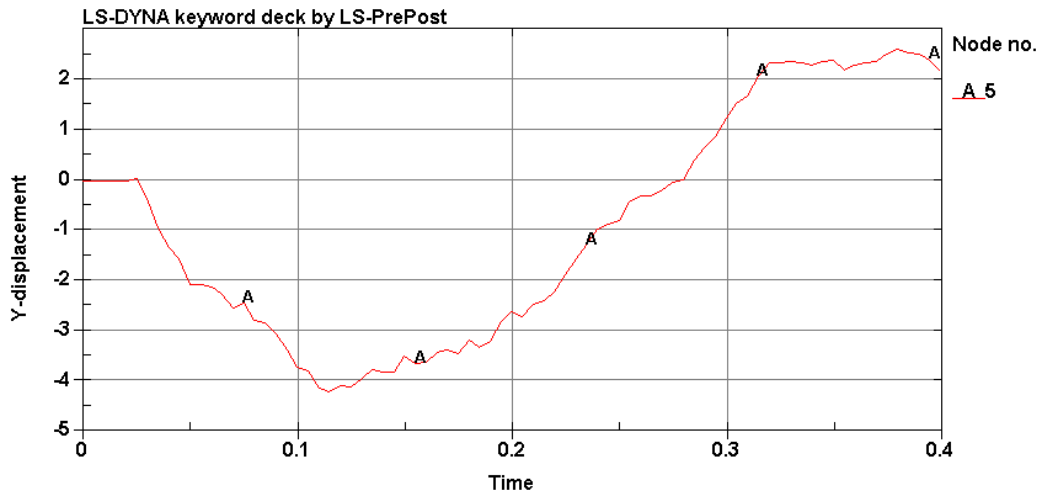


Figure 4.1.30. Node 5 Displacement of Mesh Refined Test Case 8.1 Model

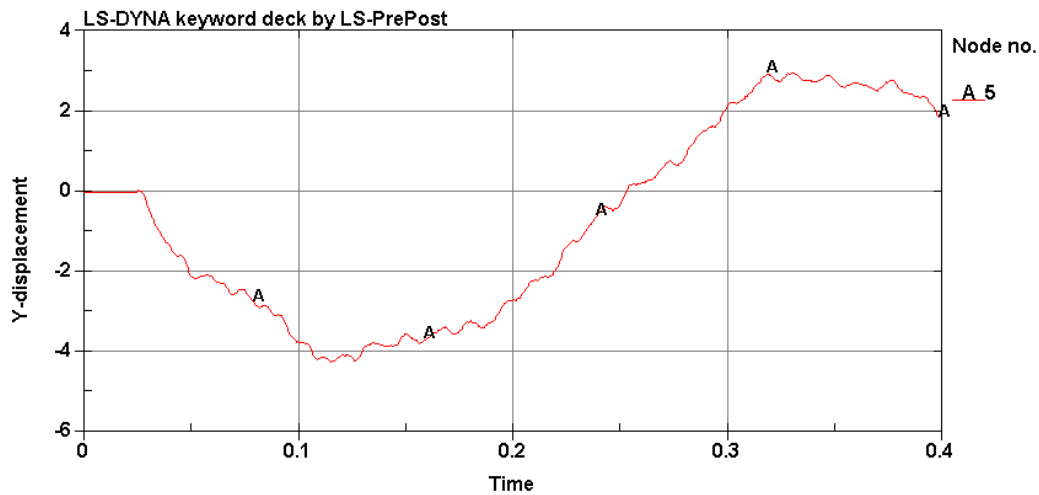


Figure 4.1.31. Node 5 Displacement of Time Refined Test Case 8.1 Model

A comparison of the y-displacement of node 5 over time plots demonstrates that reducing the time between each response record provides a smoother curve with less sharp peaks. However, from comparison of the plots in Figure 4.1.30 and Figure 4.1.31, the maximum displacement does not differ dramatically. As such, the original time step

for the result output of 0.005 seconds appears to sufficiently capture the laminate composite structure displacement behavior.

#### 4.1.4. Oblique Ball Drop Demonstration

All demonstrations thus far have utilized a pure vertical ball drop impact loading scenario. Final verification tests, Test Case 9 and Test Case 10, utilize a steel ball impacting laminate composite structure at a prescribed angle. In a similar manner, the presented optimization algorithm is equipped to handle a range of composite structural dynamic loading scenarios. The model and finite element mesh is the same as used for demonstration purposes in section 4.1.2 and shown figuratively in Figure 4.1.10 and Figure 4.2.11 and explicitly in Table 4.1.4.

Test Case 9 is completed with the DE optimizer and utilizes individual layer thickness variability, layer orientation design and layer status design variables. The optimization problem for Test Case 9 is stated as follows:

$$\text{Find } x \{ x^{\text{sizing}} [t_{1,1}, t_{1,2}, \dots, t_{p,l}], x^{\text{topology}} [\beta_{1,1}, \beta_{1,2}, \dots, \beta_{p,l}, s_{1,1}, s_{1,2}, \dots, s_{p,l}] \} \quad (11.a)$$

$$\text{Minimize } F(x) \quad (11.b)$$

$$\text{Subject to } \frac{d_{112,y}}{d_{112,y}^{\text{allowable}}} - 1 \leq 0 \quad (11.c)$$

$$\frac{d_{116,y}}{d_{116,y}^{\text{allowable}}} - 1 \leq 0 \quad (11.d)$$

$$\frac{\sigma_i^k}{\sigma_i^{\text{allowable}}} - 1 \leq 0 \quad (11.e)$$

$$\frac{\tau_{\max}}{\tau^{\text{allowable}}} - 1 \leq 0 \quad (11.f)$$

$$0.1 \leq t_p \leq 1.0 \quad \text{inch} \quad (11.g)$$

$$0.0 \leq \beta_{p,l} \leq 135.0 \quad (11.h)$$

Test Case 10 is optimized with the MFD optimizer with only the individual layer thickness and orientation design variables. The layer status design variable cannot be used with the MFD optimizer because the design variables are not continuous.

$$\text{Find } x\{x^{sizing}[t_{1,1}, t_{1,2}, \dots, t_{p,l}], x^{topology}[\beta_{1,1}, \beta_{1,2}, \dots, \beta_{p,l}]\} \quad (12.a)$$

$$\text{Minimize } F(\mathbf{x}) \quad (12.b)$$

$$\text{Subject to } \frac{d_{112,y}}{d_{112,y}^{allowable}} - 1 \leq 0 \quad (12.c)$$

$$\frac{d_{116,y}}{d_{116,y}^{allowable}} - 1 \leq 0 \quad (12.d)$$

$$\frac{\sigma_i^k}{\sigma_i^{allowable}} - 1 \leq 0 \quad (12.3)$$

$$\frac{\tau_{max}}{\tau^{allowable}} - 1 \leq 0 \quad (12.4)$$

$$0.1 \leq t_{p,l} \leq 1.0 \quad \text{inch} \quad (12.g)$$

$$0.0 \leq \beta_{p,l} \leq 135.0 \quad (12.h)$$

The objective function is to minimize the mass of the composite structure. The allowable stress is assumed to be  $4.20 \times 10^5$  psi for longitudinal tensile and compressive stress,  $2.50 \times 10^4$  for transverse tensile and compressive stress, and  $7.5 \times 10^3$  psi for shear stress as per Table 4.1.1. The maximum allowable displacement, Eq. (11.c), Eq. (12.c), Eq. (11.d), and Eq. (12.d), imposed in the y-direction at node 112 and node 116 is 1.5 inch. Figure 4.1.12 identifies the location of node 115 as the node located directly at the point of impact from the steel ball. Figure 4.1.32 identifies the location of nodes 112 and 116 as the nodes located at the center upon the composite structure's 300 inch edges.

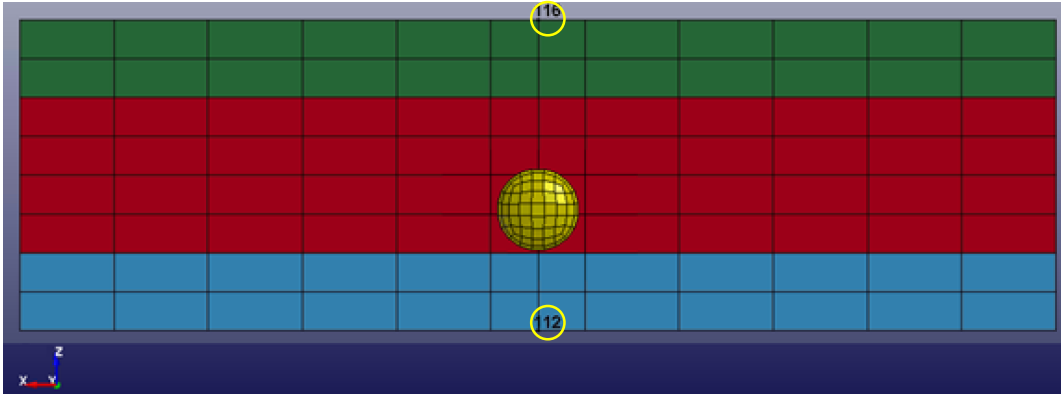


Figure 4.1.32. Node 112 and 116 Location on Oblique Ball Drop Composite Model

The 20 inch diameter steel ball is given an initial velocity of 100.0 inches per second in the negative y-axis direction and 100.0 inches per second in the positive z-axis direction. Therefore, the ball will follow an impact path as described in Figure 4.1.33.

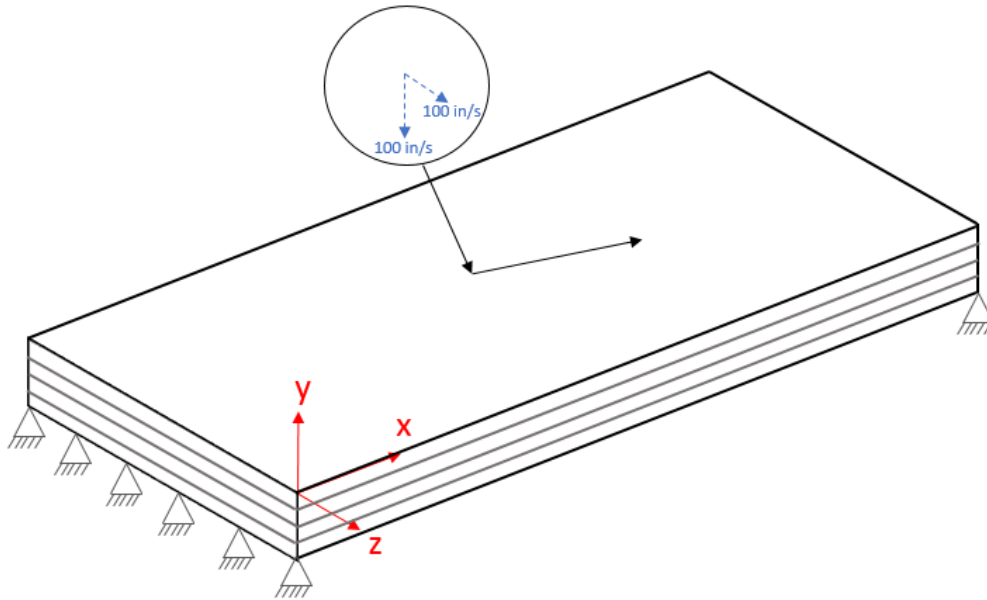


Figure 4.1.33. Impact Path of Oblique Ball Drop Demonstration

For both test cases, the laminated composite structure is composed of three element property groups. Figure 4.1.34 demonstrates the property group distribution within the composite structure. The structure was divided into groups parallel to the x-axis as the optimal solution is assumed to have thickness variability along the z-axis. The optimal solution is assumed to be when the material at the center of the composite plate is thinner than the elements located along the long-span edges as elements closer to the 300 inch edge are predicted to experience larger stresses. Both test cases start with the initial solution of four 1.0 inch thick layers oriented parallel to the positive x-axis. As a result, the initial objective function,  $F(x)$ , value is 15.74 slugs.



Figure 4.1.34. Element Groups for Test Case 9 and Test Case 10

The purpose of optimizing the oblique ball drop problem with both the DE and MFD optimizers is to demonstrate the performance of population based and gradient based methods for laminate composite material optimization. The comparison between the results for both methods is not an absolute evaluation of the efficacy of these methods, as the efficiency of both methods is problem and model dependent. The results

from the optimization processes are summarized below. The active constraint for both Test Case 9 and Test Case 10 is the maximum nodal displacement of node 112.

Table 4.1.15. Results for Oblique Ball Drop Sizing and Topology Optimization

	Test Case 9	Test Case 10
<b>Num. of Element Groups</b>	3	3
<b>Num. of Design Variables</b>	33	24
<b>Optimizer</b>	DE	MFD
<b>Max Iterations</b>	10	20
<b>Population Size</b>	10	-
<b>Final Objective Function (slugs)</b>	9.9	7.8
<b>Num. of Function Evaluations</b>	92	444
<b>Time to Complete (s)</b>	2954	14560
<b>Max. Constraint Value</b>	-0.0914667	-0.000200033
<b>Max. Nodal Deflection (inch)</b>	1.36	1.49
<b>Max. Principal Stress (psi)</b>	$\sigma_{xx} = 6796.3$	$\sigma_{xx} = 5362.8$
<b>Max. Shear Stress (psi)</b>	3398.1	2681.4

The results from the DE problem statement and optimization process, Test Case 9, resulted in three layers present in Element Group 1 and four layers present in Element Group 2 and 3. The total thicknesses of the Element Groups are 2.18 inch for group 1, 2.74 inch for group 2, and 2.99 inch for group 3. The Figure 4.1.35 demonstrates the varying plate thickness from a side view where the ball is located at its initial position. The layer details are provided in Table 4.1.16. The table is organized to reflect the element group ordering of Figure 4.1.35.

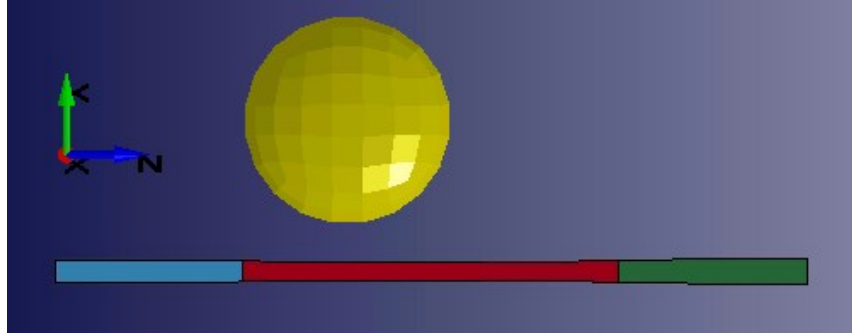


Figure 4.1.35. Final Model of Test Case 9

Table 4.1.16. Details of Final Model of Test Case 9

Layer	Element Group 2		Element Group 1		Element Group 3	
	Thickness (in.)	Orientation (deg.)	Thickness (in.)	Orientation (deg.)	Thickness (in.)	Orientation (deg.)
4	0.96	71.3	0.83	0.0	0.68	39.8
3	0.43	62.9	0.61	45.8	0.61	26.1
2	0.38	80.9	0.74	0.0	0.83	45.1
1	0.97	25.1	-	-	0.87	38.2

Even though the problem presented to the MFD optimization process, Test Case 10, was not able to remove layers through the layer status Boolean design variable, the final solution results in a lower objective function value. The final MFD solution contains three element property groups each containing four layers. The total thicknesses of the property groups are 1.72 inches for group 1, 2.54 inches for group 2, and 1.92 inches for group 3. Figure 4.1.36 and Table 4.1.17 demonstrate the varying plate thickness side view and layer details where the steel ball is located at its initial position. The optimized solution orients all layers parallel to the global x-axis in order to utilize the strong material axis again bending along the long span of the composite part. Table 4.1.17 is organized to reflect the element group order in Figure 4.1.36.

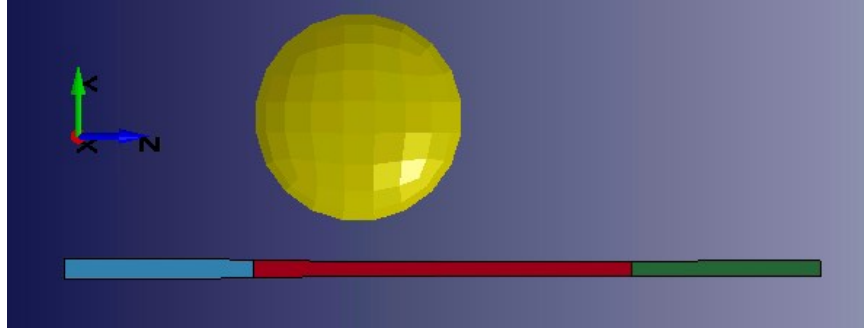


Figure 4.1.36. Final Model of Test Case 10

Table 4.1.17. Details of Final Model of Test Case 10

Layer	Element Group 2		Element Group 1		Element Group 3	
	Thickness (in.)	Orientation (deg.)	Thickness (in.)	Orientation (deg.)	Thickness (in.)	Orientation (deg.)
4	0.53	0.0	0.50	0.0	0.59	0.0
3	0.76	0.0	0.41	0.0	0.58	0.0
2	0.77	0.0	0.29	0.0	0.37	0.0
1	0.47	0.0	0.52	0.0	0.37	0.0

The center of the plate (Element Group 1) contains the thinnest elements complimented by thicker elements located along the 300 inch long edges of the structure for both Test Case 9 and Test Case 10. However, the MFD optimizer was able to further refine the element thickness while maintaining feasibility of the constraints to result in a lower objective function value. The material layup results presented in Table 4.1.17 are dependent upon the initial solution used for the MFD optimization process. A different initial layup may cause the gradient based optimization technique to converge to a different local optimal solution as the design space as multiple local optimums.

#### 4.2. Validation Test of the COMP-OPT program

The laminate composite optimization problems presented thus far serve the purpose of demonstrating the functionality of the COMP-OPT program and optimization

procedures. The design of a mono-leaf laminate composite leaf spring is presented in section 4.2.1 as a validation test of the COMP-OPT program. Traditionally, leaf springs are a steel component in automobile suspension systems. However, there is an interest in the automotive industry to reduce the weight of the leaf spring by replacing the part with an equivalently or better performing composite substitute. (Rajendran & Vijayarangan, 2001), (Kumar, Charyulu, & Ramesh, 2012), (Patunkar & Dolas, 2011), (Zheng Yinhuan & Zhigao, 2011).

#### 4.2.1. Optimization of a Laminate Composite Leaf Spring

The traditional multi-layered steel leaf spring is a heavy component in automobile suspension systems. The steel leaf springs contribute about 10%-20% of the unsprung weight, which is weight that is not supported by the suspension system of a vehicle, that effects vehicle ride performance and handling (Rajendran & Vijayarangan, 2001). As a result, attention has been given to designing a mono-layer composite leaf spring to take advantage of composite's high strength-to-weight ratio and reduce the unsprung weight contribution of the leaf spring (Kumar, Charyulu, & Ramesh, 2012).

The optimization problem to be solved with the COMP-OPT program is based upon the leaf spring design problem that Rajendran and Vijayarangan (Rajendran & Vijayarangan, 2001) present to establish an optimum spring design with respect to sizing and shape optimization. Rajendran and Vijayarangan posed a GA optimization problem to design a mono-leaf composite spring to minimize weight for a static load application of 4500 N. The optimization process designed the thickness at the center of the spring,  $t$ , and the width at the center of the spring,  $b$  with maximum stress and vertical deflection

constraints. Figure 4.2.1 shows the final optimized shape of the composite leaf spring designed Rajendran and Vijayarangan (Rajendran & Vijayarangan, 2001).

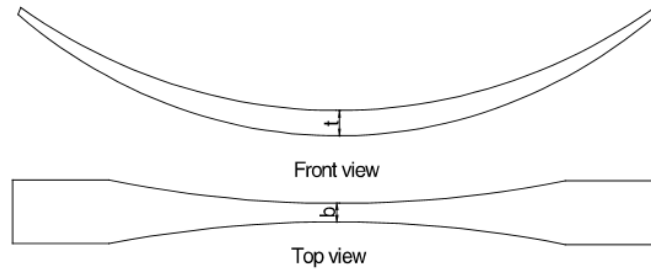


Figure 4.2.1. Composite Leaf Spring Optimized Model (Graphic Provided by Rajendran & Vijayarangan, 2001)

The final spring width in the center,  $b$ , is 28.475 mm with a center thickness,  $t$ , of 25.015 mm (Rajendran & Vijayarangan, 2001). This results in an estimated objective function weight of 2.26 kg. The maximum bending stress and maximum deflection experienced in this final design is 462.17 MPa and 141.03 mm, respectively.

The COMP-OPT program solves an optimization problem similar to the problem that Rajendran and Vijayarangan (Rajendran & Vijayarangan, 2001) pose to validate the proposed optimum shape and thickness design of composite leaf springs. The composite leaf spring model used by the COMP-OPT program utilizes the same dimensions as the problem presented by Rajendran and Vijayarangan. The initial model shown in Figure 4.2.2 assumes that all layers are oriented parallel to the global x-axis.

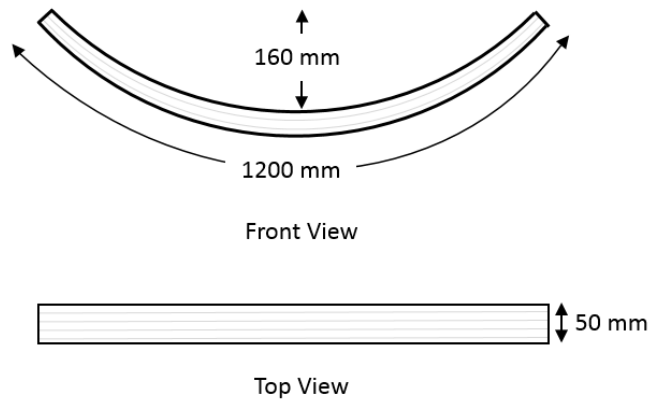


Figure 4.2.2. Initial Laminate Composite Leaf Spring Model

The composite leaf spring is assumed to be simply supported with pins as shown in Figure 4.2.3 as the boundary conditions of Rajendran and Vijayarangan's (Rajendran & Vijayarangan, 2001) finite element model are not detailed. Realistically, one end of the leaf spring is allowed a degree of translation along the x-axis by means of a lever arm (Patnaik, Yadav, & Dewangan, 2012). However, for simplicity, the lever arm component is not included in the optimization model and the spring is constrained from translating. This pin-pin boundary condition is a conservative assumption as higher stress concentrations are observed when compared to pin and roller supported models.



Figure 4.2.3. Boundary Conditions for Laminate Composite Leaf Spring Model

The COMP-OPT optimization problem uses layer thickness and shape design variables subjected to maximum stresses and displacements. The optimization problem is stated as follows:

$$\text{Find } \mathbf{x} \{ \mathbf{x}^{shape} [x_{k \times 1}], \mathbf{x}^{sizing} [t_1, t_2, \dots, t_p] \} \quad (13.a)$$

$$\text{Minimize } F(\mathbf{x}) \quad (13.b)$$

$$\text{Subject to } \frac{d_{199,y}}{d_{199,y}^{allowable}} - 1 \leq 0 \quad (13.c)$$

$$\frac{\sigma_i^k}{\sigma_i^{allowable}} - 1 \leq 0 \quad (13.d)$$

$$\frac{n_{25,z} - n_{66,z}}{20} + 1 \leq 0 \quad (13.e)$$

$$\frac{\tau_{max}}{\tau^{allowable}} - 1 \leq 0 \quad (13.f)$$

$$\mathbf{x}_{k \times 1} [a_1] \quad (13.g)$$

$$a_k = \alpha_k \mathcal{R}_o \Delta \quad -1 \leq \alpha_k \leq 1, \quad o = x, y, z - axis \quad (13.h)$$

$$\Delta_1 = 15.0\% \quad (13.i)$$

$$\Delta_2 = 15.0\% \quad (13.j)$$

$$1.0 \leq t_p \leq 5.0 \quad \text{mm} \quad (13.k)$$

The objective function is to minimize the mass of the composite spring. The allowable normal and shear stresses are provided in Table 4.2.1. The T800-F3900 fiber/resin composite material (Hoffarth, et al., 2014) utilized by Hoffarth, et al. is used as the leaf spring composite material. The material properties (Raju & Acosta, 2010) are

listed in metric units in Table 4.2.1. The a-b-c directions correspond to the 1-2-3 principal material directions shown in Figure 3.2.2.1.

Table 4.2.1. T800-F3900 Fiber/Resin Composite Material Properties (Metric)

Material Property	Value
Density (kg/mm <sup>3</sup> )	1.297 x 10 <sup>-7</sup>
Young's Modulus, a-direction (MPa)	1.505 x 10 <sup>5</sup>
Young's Modulus, b-direction (MPa)	7.894 x 10 <sup>3</sup>
Young's Modulus, c-direction (MPa)	7.894 x 10 <sup>3</sup>
Shear Modulus, ab-direction (MPa)	3.996 x 10 <sup>4</sup>
Shear Modulus, bc-direction (MPa)	2.223 x 10 <sup>4</sup>
Shear Modulus, ca-direction (MPa)	3.996 x 10 <sup>4</sup>
Poisson's Ratio, ba	0.013847
Poisson's Ratio, ca	0.013847
Poisson's Ratio, cb	0.3792
Longitudinal Tensile Strength, a-axis (MPa)	2.895 x 10 <sup>3</sup>
Transverse Tensile Strength, b-axis (MPa)	1.724 x 10 <sup>2</sup>
Longitudinal Compressive Strength, a-axis (MPa)	2.895 x 10 <sup>3</sup>
Transverse Compressive Strength, b-axis (MPa)	1.724 x 10 <sup>2</sup>
Shear strength (MPa)	5.17 x 10 <sup>1</sup>

The maximum allowable displacement, Eq. (13.c), imposed in the y-direction at node 199 (Figure 4.2.4) is 160 mm as proposed by Rajendran and Vijayarangan (Rajendran & Vijayarangan, 2001). Additionally, Eq. (13.e) represents the geometric constraint that requires that the z-coordinate of node 25 and node 66 are at least 10.0 mm apart (Figure 4.2.5).

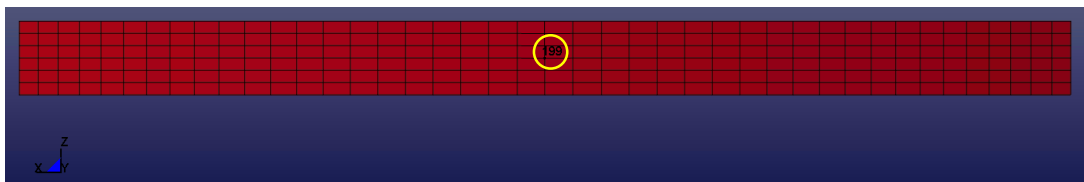


Figure 4.2.4. Location of Leaf Spring Displacement Constraint

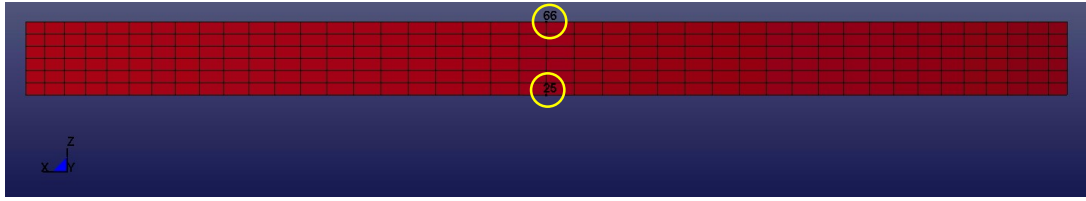


Figure 4.2.5. Location of Leaf Spring Geometric Constraint

There are two velocity field vectors used to define the shape change optimization of the leaf spring model (Eq. (13.i) and Eq. (13.j)). Bezier curves define the outer edge shapes resulting in allowed curvature and translational movement. Figure 4.2.6 details the possible shape change types. The magnitude of the shape change contribution from each velocity field is computed as described in section 3.2.3 with Eq. (5).

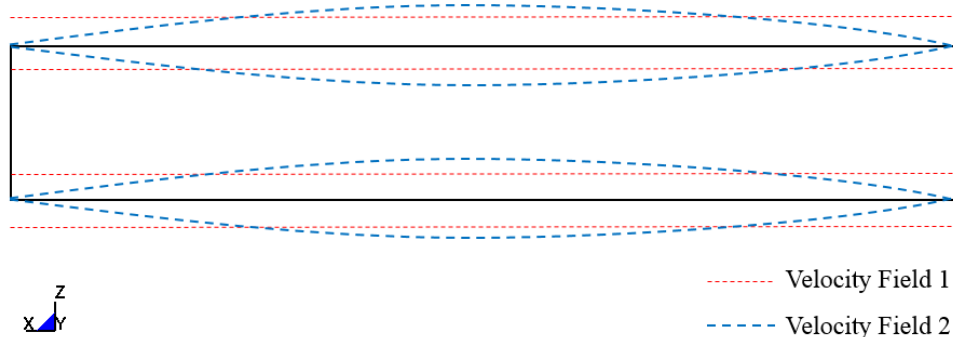


Figure 4.2.6. Leaf Spring Shape Optimization Velocity Fields

The finite element model that is optimized in the COMP-OPT program utilizes a time dependent applied force in place of the 4500 N static force that Rajendran and Vijayarangan (Rajendran & Vijayarangan, 2001) applied. One period of a sinusoidal curve is defined in order to simulate the dynamic force imposed upon suspension systems from speed bump impact (Blundell & Harty, 2004). Figure 4.2.7 represents the load applied over time to the composite leaf spring model. A negative, downward force is

included to simulate the spring behavior when vehicles impact potholes. Once the force is applied, the system response is observed for residual frequency effects of the load curve.

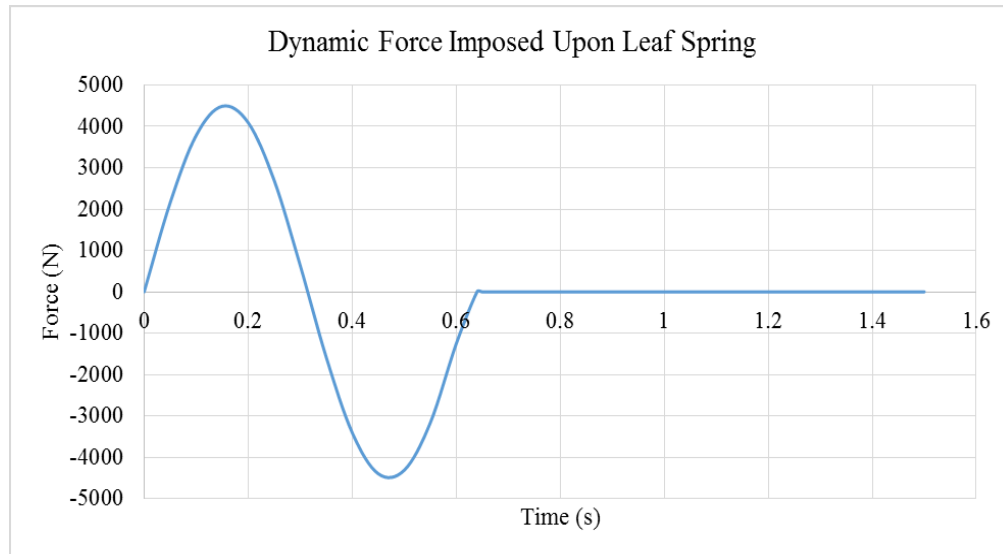


Figure 4.2.7. Dynamic Force Imposed Upon Leaf Spring

The variations in the time that the loading curve is applied to the leaf spring model did not demonstrate a large effect on the resulting stresses and displacements in comparison to variations in the maximum load magnitude. In this case, the load is applied over an arbitrary 0.55 seconds and the amplitude of the sinusoidal curve used to define the dynamic force is 4500 N. Thus, the maximum applied force is of the same magnitude as the optimization problem completed by Rajendran and Vijayarangan (Rajendran & Vijayarangan, 2001). As the loading is represented by a sinusoidal curve, the load magnitude caused by a speed bump and caused by a pothole or downward force is assumed to be the same. The dynamic force curve in Figure 4.2.7 is applied along the center nodes of the finite element model. Figure 4.2.8 shows the location of the load and direction of the positive load values.

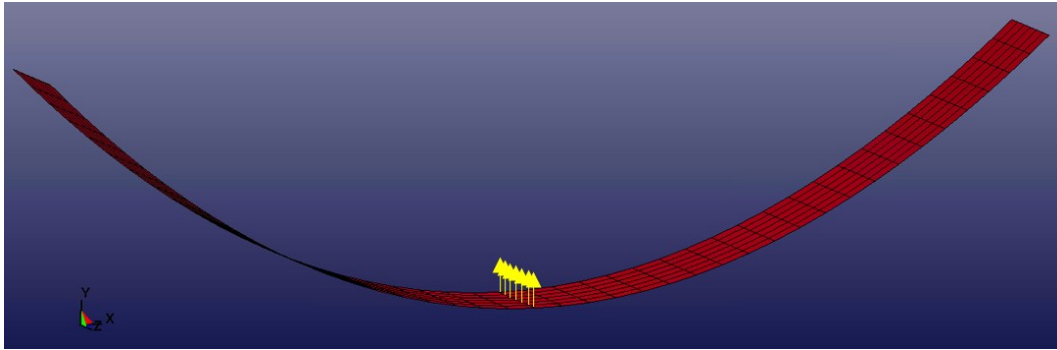


Figure 4.2.8. Composite Leaf Spring Loading Application

The leaf spring finite element mesh is separated into eleven different element groups. The element groups are defined such that the thickness of the leaf spring can vary throughout the span, but maintain symmetry. Figure 4.2.9 details the element group definition sequence.

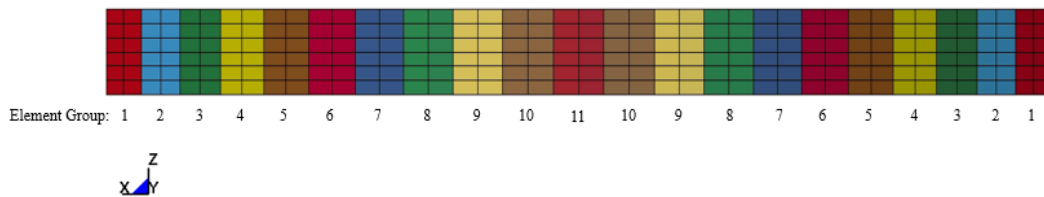


Figure 4.2.9. Leaf Spring Element Group Definition

The initial leaf spring model has a constant thickness of 50 mm, resulting in an objective function value of 0.39 kg. Ten layers are modeled within the laminate spring. As a result the maximum composite thickness is 50 mm and the minimum is 10 mm as described with Eq. (13.k). MFD is used to optimize the leaf spring model because the design variables are continuous. Gradient methods do not terminate until a specified

convergence tolerance is reached and tend to demonstrate good convergence as shown in section 4.1.4. Population based methods can also be used to solve the optimization problem presented in Eq. (13.a) – (13.k); however, MFD is preferred as quick and thorough convergence is desired. The optimized solution details are provided in Table 4.2.2. The active constraint for the optimum design is the maximum shear stress criteria.

Table 4.2.2. Optimization of Leaf Spring

	<b>Leaf Spring</b>
<b>Num. of Element Groups</b>	11
<b>Num. of Design Variables</b>	13
<b>Optimizer</b>	MFD
<b>Max Iterations</b>	20
<b>Final Objective Function (kg)</b>	0.14
<b>Num. of Function Evaluations</b>	334
<b>Time to Complete (s)</b>	161028
<b>Max. Constraint Value</b>	0.000
<b>Max. Nodal Deflection (mm)</b>	0.324
<b>Max. Principal Stress (MPa)</b>	$\sigma_{xx} = 103.4$
<b>Max. Shear Stress (MPa)</b>	51.7

The final thickness distribution and plan view shape are shown in Figure 4.2.10 and Figure 4.2.11, respectively. Both the thickness distribution and width shape are similar to the optimized design reported by Rajendran and Vijayarangan (Rajendran & Vijayarangan, 2001) in Figure 4.2.1.

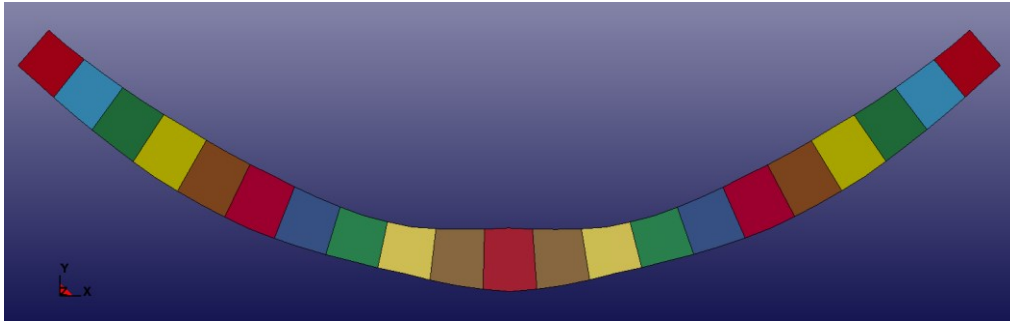


Figure 4.2.10. Optimum Leaf Spring Thickness Distribution

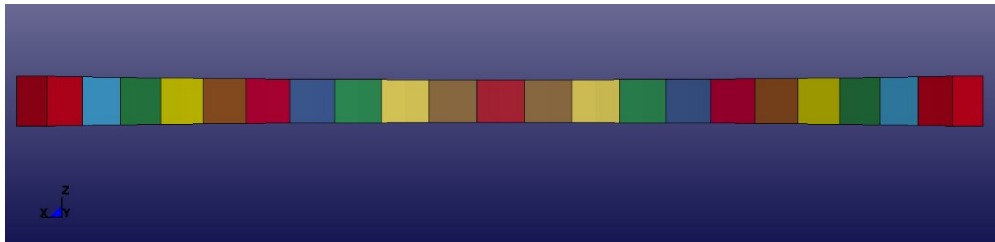


Figure 4.2.11. Optimum Leaf Spring Plan View Shape

The optimized leaf spring shape dimensions are shown in Figure 4.2.12. The element group total thicknesses are provided in Table 4.2.3 to demonstrate the thickness variability throughout the spring.

Table 4.2.3. Element Group Thicknesses for Optimized Leaf Spring

Element Group Number	Thickness (mm)
1	35.3
2	38.0
3	40.5
4	43.9
5	43.9
6	43.7
7	39.4
8	35.3
9	35.3
10	42.3
11	47.7

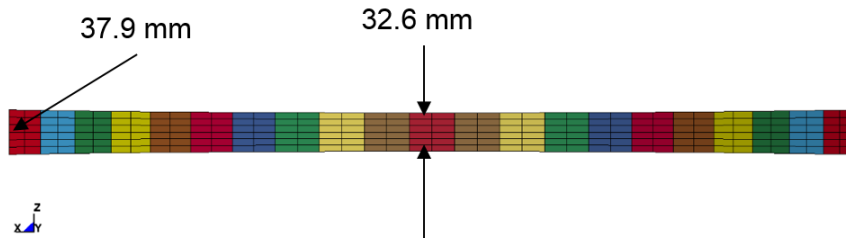


Figure 4.2.12. Optimized Leaf Spring Shape Dimensions

The plots of the 1<sup>st</sup> principal stresses in the global x-y coordinate system at the peak forces, 4500 N and -4500 N are shown in Figure 4.2.13 and Figure 4.2.14. When the force is applied in the positive y-axis direction, the largest global x-y coordinate system 1<sup>st</sup> principal stresses are experienced in the central area of the spring. Alternatively, when the force is applied in the negative y-axis direction, the largest global x-y coordinate system 1<sup>st</sup> principal stresses are experienced near the outer edges of the spring where Element Groups 3, 4, 5, and 6 are noticeably thicker than surrounding element groups.

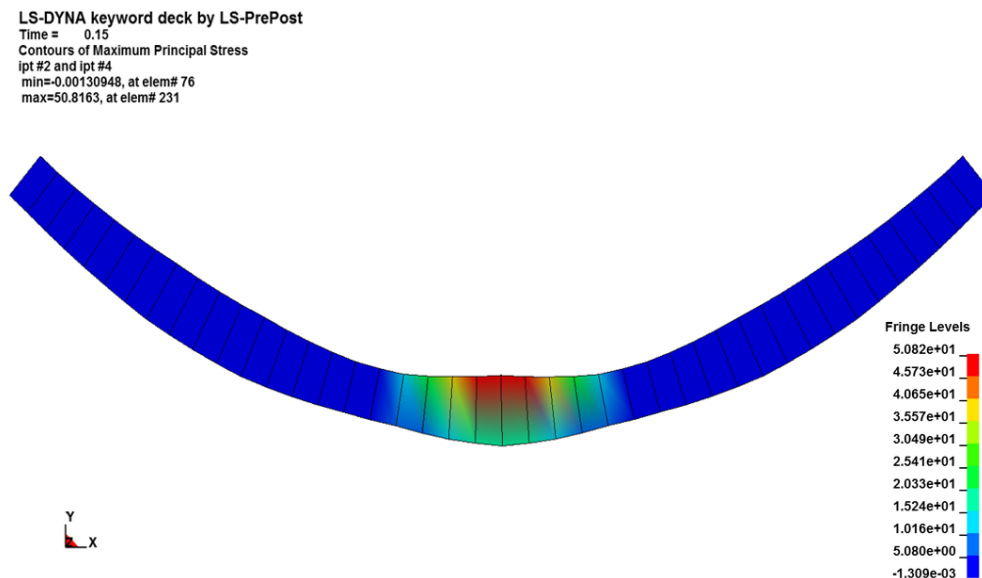


Figure 4.2.13. 1<sup>st</sup> Global Principal Stress Plot for Positive Peak Load

LS-DYNA keyword deck by LS-PrePost  
 Time = 0.46  
 Contours of Maximum Principal Stress  
 ipt #2 and ipt #4  
 min=1.58361, at elem# 105  
 max=53.4121, at elem# 90

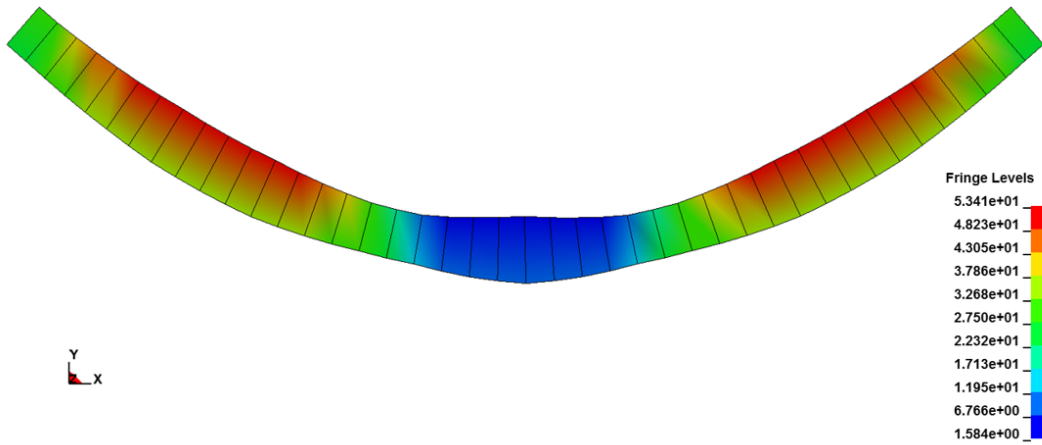


Figure 4.2.14. 1<sup>st</sup> Global Principal Stress Plot for Negative Peak Load

The overall maximum normal and shear principal material stresses experienced in the optimized leaf spring model are provided in Table 4.2.4. The center of the leaf spring has a greatest thicknesses to accommodate for these stresses.

Table 4.2.4. Maximum Stress in Optimized Leaf Spring

	Time (s)	Element Number	Layer Number	Stress (MPa)
$\sigma_{xx}$	0.15	21	10	-103.4
$\sigma_{yy}$	0.15	147	10	1.0
$\sigma_{zz}$	-	-	-	0.0
$\tau_{max}$	0.15	21	10	51.7

The displacement plot of center nodes of the leaf spring where the force is applied is shown in Figure 4.2.15. There is no displacement response lag time demonstrated.

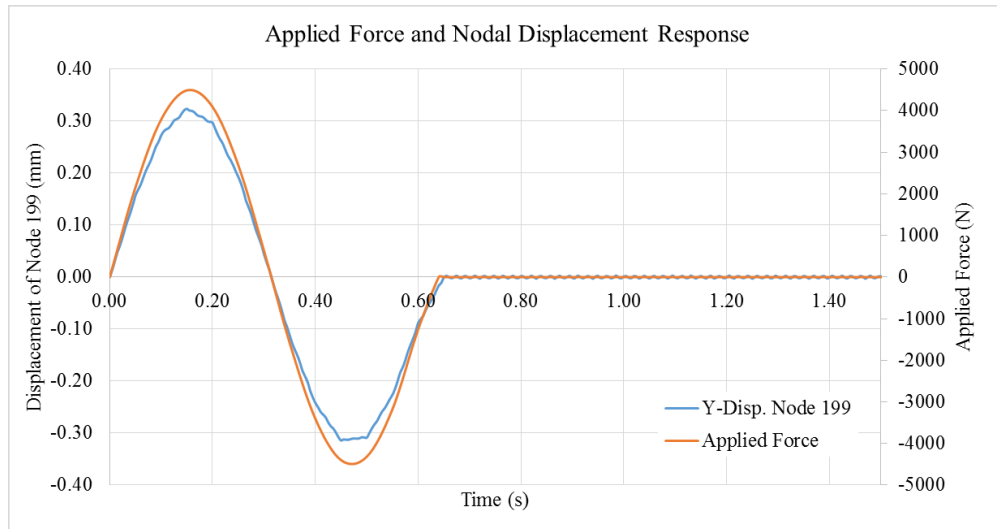


Figure 4.2.15. Plot of Leaf Spring Displacement Response

The maximum displacement of the optimized leaf spring model is 0.315 mm. As the spring is modeled with pin-pin boundaries (Figure 4.2.3), no translation or flattening of the spring is permitted. As a result, the maximum displacement experienced is relatively small. If the pin support on one end is released to allow for x-axis translation, more leaf spring displacement is observed. The energy in the system is represented by Figure 4.2.16 and 4.2.17. The damping imposed in the problem was minimal as the initial response of the spring to the load curve shown in Figure 4.2.15 is of interest.

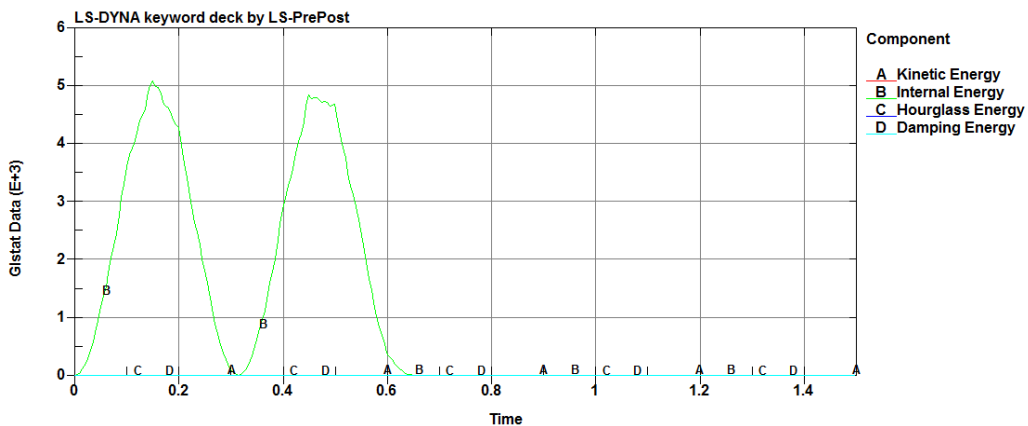


Figure 4.2.16. Internal Energy of Leaf Spring Model

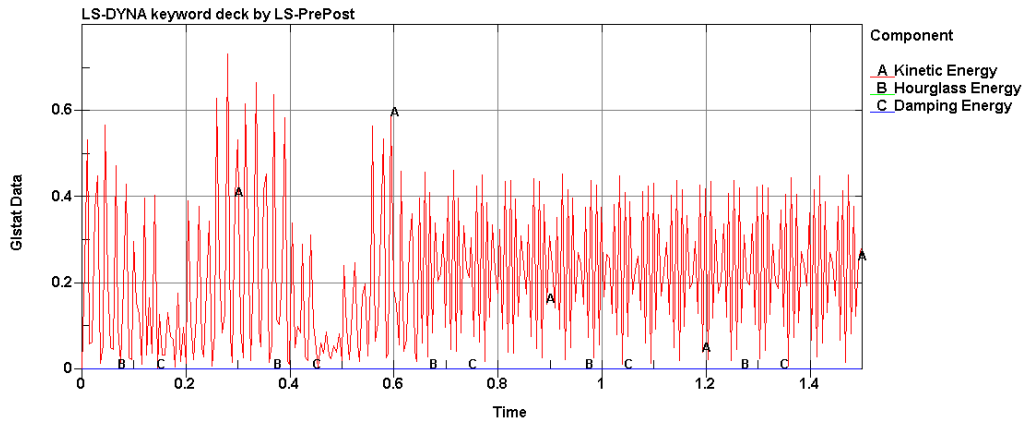


Figure 4.2.17. Kinetic Energy of Leaf Spring Model

The peaks in the internal energy shown in Figure 4.2.16 correspond to the peaks in the applied force as presented in Figure 4.2.7. As such, Figure 4.2.17 demonstrates that although the kinetic energy of the system is magnitudes smaller than the internal energy, decreasing kinetic energy trends are observed during the times when internal energy is at maximums. The kinetic energy of the system is small relative to the internal energy of the system, because the displacements observed in Figure 4.2.15 are small with respect to the problem dimensions.

#### 4.2.2. Leaf Spring Mesh Refinement

The leaf spring finite element mesh presented in section 4.2.1 is further refined and the optimization problem presented in Eq. (13.a) – (13.k) resolved. The refined mesh model has an additional 756 shell elements, resulting in a total of 1008 elements. The design variable bounds and initial solution utilized in section 4.2.1 is no longer a feasible range for the refined mesh as the maximum stress constraints presented in Eq. (13.d) are violated at the maximum thickness. As a result, the upper bound on the layer thickness



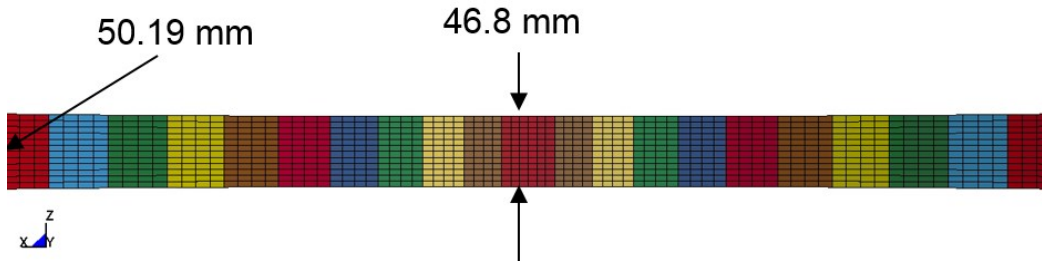


Figure 4.2.19. Refined Optimum Leaf Spring Shape Distribution

The final mass of the optimized model is 0.24 kg. The stress responses of the optimized solution for the refined and original model presented in section 4.2.1 are alike resulting in similar thickness and shape distributions. The final maximum stress values for the original and refined optimal solutions are presented in Table 4.2.5. As the active constraint at the optimum for both problems is the maximum shear stress in the top layer in the middle of element group 1, the stress similarities between the optimized solutions are expected.

Table 4.2.5. Stress Results for Original and Refined Leaf Spring Optimum

Stress	Time (s)	Location	Layer	Max Value (MPa)	
				Original Mesh	Refined Mesh
$\sigma_{xx}$	0.15	Center	Top	-103.4	-103.2
$\sigma_{yy}$	0.15	Center	Top	1.0	1.53
$\sigma_{zz}$	-	-	-	0.0	0.0
$\tau_{max}$	0.15	Center	Top	51.7	51.6

This comparison of the thickness and shape distributions from original and refined leaf spring optimization problems further demonstrates the mesh density dependency of the optimization process.

## 5. CONCLUSIONS

The COMP-OPT program executes a variety of laminated composite material optimization problems. Sizing, topology and shape optimization are applied to the laminate composite material layup and structural shape design. The ability to optimize laminate composites for a required performance is a beneficial design tool for realistic structural applications as demonstrated with the composite leaf spring design validation test. The optimization process utilizes explicit finite element analysis through LS-DYNA for performance and constraint evaluation. The LS-DYNA composite part card, \*PART\_COMPOSITE, is a straightforward method to model thin shell composite elements. The shell elements defined with the \*PART\_COMPOSITE card use through thickness integration points to identify the individual composite layers. As a result, layer thicknesses, layer orientations, and layer materials can be defined and altered with ease.

The verification design optimization problems utilize sizing, topology, shape or a combination of these optimization methodologies. As a result, the layer and part thicknesses, the number of layers present in the part, the layer orientation and material, and the part shape are available design variables. This optimization methodology and available design variables can be optimized with a number of optimization techniques. The GA, DE, and MFD methods are utilized in the verification and validation demonstrations of the COMP-OPT program. The population based techniques, GA and DE, are able to optimize all available design variables (continuous, discrete, and Boolean). Alternatively, gradient based techniques, such as MFD, can only be applied to optimization problems utilizing continuous design variables. The appropriate optimization technique must be selected for each particular problem. The benefits and

disadvantages of both population and gradient based methods contribute to choice of optimization technique for a given optimization problem.

### 5.1 Future Work

The COMP-OPT program functionally is currently limited to the design variables types and constraints discussed. The laminate composite material model utilized for finite element analysis is a linear stress-strain model; however, composite materials may be better represented with non-linear material relationships. The non-linear stress-strain behavior of a laminate composite results from successive ply failures and complex composite failure mechanisms. Laminate composite materials experience internal failures from ply failures and delamination that causes complex behavior (Shi, Swait, & Soutis, 2012). The maximum stress failure criteria utilized by the COMP-OPT program does not account for this non-linear response. Such response mechanisms can be integrated into the optimization process for further precise estimations of composite part response due to dynamic loading. This integration can be completed by allowing the constitutive properties of the composite material to change based on a function of experienced stresses or strains.

Additionally, this study only utilized shell elements. The COMP-OPT program algorithm and processes can be extended into the utilization of solid element modeling within LS-DYNA. The expansion to solid elements will increase the range of problems that can be designed with the optimization procedure presented as the maximum part thickness to span ratio required for shell element modeling is no longer necessary.

The primary loading situations examined involved impact systems. Other loading cases that can be analyzed with explicit finite element analysis can be modeled and

optimized with the COMP-OPT program. Demonstrations involving alternative dynamic loading situations, like blast loading or machinery vibrations, can be completed in order to demonstrate the versatile nature of the COMP-OPT program.

## REFERENCES

- Almeida, F., & Awruch, A. (2008). Design Optimization of Composite Laminated Structures Using Genetic Algorithms and Finite Element Analysis. *Composite Structures*, 88, 443-454.
- Altair Engineering, Inc. (2011). *Optimization of Composite: Recent Advances and Application*. Irvine: Altair Product Design.
- Bank, L. C., Gentry, T. R., Thompson, B. P., & Russell, J. S. (2003). A Model Specification for FRP Composites for Civil Engineering Structures. *Construction and Building Materials (Elsevier)*, 405-437.
- Belegundu, A., & Rajan, S. (1988). A Shape Optimization Approach Based on Natural Design Variables and Shape Functions. *Computer Methods in Applied Mechanics and Engineering*, 87-106.
- Bendsoe, M. (1989). Optimal Shape Design as a Material Distribution Problem. *Structural Optimization*, 193-202.
- Biswal, B., Deepak, B., & Bahubalendruni, M. (2014). *Study of Optimization of Composite Structures with Respect to Industrial Applications*. Coimbatore: IEEE.
- Blundell, M., & Harty, D. (2004). *The Multibody Systems Approach to Vehicle Dynamics*. Burlington: Elsevier Butterworth-Heinemann.
- Calard, V. (2011). *Formulas and Equations for the Classical Laminate Theory*.
- Chatiri, M., Gull, T., & Matzenmiller, P. (2009). An Assessment of the New LS-DYNA layered solid element: Basics, Patch Simulation and its Potential for Thick Composite Structure Analysis. *7th European LS-DYNA Conference*.
- Daniel, I. M., & Ishai, O. (2006). *Engineering Mechanics of Composite Materials, Second Edition*. Oxford: Oxford University Press, Inc.
- Daudeville, L., & Malecot, Y. (2011). Concrete Structures Under Impact. *European Journal of Environmental and Civil Engineering Volume 15(SI)*, 101-140.

- Dhandapani, K., Jain, R., & Rajan, S. (2013). *Engineering Design Optimization (EDO) Workbench User's Manual Version 1.1*. Tempe: School of Sustainable Engineering & the Built Environment, Arizona State University.
- Frecker, M. I. (2003). Recent Advances in Optimization of Smart Structures and Actuators. *Journal of Intelligent Material Systems and Structures*, 14(207).
- Ghiasi, H., Pasini, D., & Lessard, L. (2009). Optimum Stacking Sequence Design of Composite Materials Part I: Constant Stiffness Design. *Composite Structures (Elsevier)*, 1-11.
- Goldberg, D. E. (1989). *Genetic Algorithms in Search, Optimization & Machine Learning*. Reading: Addison-Wesley Professional.
- Greenlee, R. (2010, January 12). *Index of ME360, Impact Loads*. Retrieved from The University of New Mexico: <http://www.unm.edu/~bgreen/ME360/>
- Gurdal, Z., Haftka, R. T., & Hajela, P. (1999). *Design and Optimization of Laminated Composite Materials*. New York: John Wiley & Sons.
- Hoffarth, C., Harrington, J., Rajan, S., Goldberg, R., Carney, K., Du Bois, P., & Blakenhorn, G. (2014). Verification and Validation of a Three-Dimensional Generalized Composite Material Model. *13th International LS-DYNA Users Conference*. Dearborn: LSTC.
- Kathiravan, R., & Ganguli, R. (2007). Strength Design of Composite Beam Using Gradient and Particle Swarm Optimization. *Composite Structures (Elsevier)*, 471-479.
- Kaw, A. K. (2005). *Mechanics of Composite Materials, Second Edition*. Boca Raton: CRC Press.
- Kumar, M. A., Charyulu, T. N., & Ramesh, C. (2012). Design Optimization of Leaf Spring. *International Journal of Engineering Research and Applications (IJERA)*, 759-765.

- Livermore Software Technology Corporation (LSTC). (2012). LS-DYNA Keyword User's Manual Volume II Material Models Version 971 (Revision: 1275). Livermore: Livermore Software Technology Corporation.
- Livermore Software Technology Corporation. (2003, September 10). *LS-DYNA Support: Define Composites*. (Livermore Software Technology Corporation) Retrieved October 19, 2014, from <http://www.dynasupport.com/howtos/material/define-composites/?searchterm=composite>
- LSTC. (2014). *LS-DYNA Computer Program*. Retrieved from <http://www.lstc.com>
- Lund, E. (2009). Buckling Topology Optimization of Laminated Multi-material Composite Shell Structures. *Composite Structures*(91), 158-167.
- Lund, E., & Stegmann, J. (2004). Structural Optimization of Composite Shell Structures Using a Discrete Constitutive Parameterization. *Mechanics of 21st Century*, 15-21.
- Muc, A. (2007). Optimal Design of Composite Multilayered Plated and Shell Structures. *Thin-Walled Structures (Elsevier)*, 816-820.
- Muc, A., & Gurba, W. (2001). Genetic Algorithms and Finite Element Analysis in Optimization of Composite Structures. *Composite Structures (Elsevier)*, 275-281.
- Narayana Naik, G., Gopalakrishnan, S., & Ganguli, R. (2008). Design Optimization of Composites using Genetic Algorithm and Failure Mechanism Based Failure Criterion. *Composite Structures (Elsevier)*, 354-367.
- Patnaik, M., Yadav, N., & Dewangan, R. (2012). Study of a Parabolic Leaf Spring by Finite Element Method & Design of Experiments. *International Journal of Modern Engineering Research*, 1920-1922.
- Patunkar, M., & Dolas, D. (2011). Modelling and Analysis of Composite Leaf Spring under the Static Load Condition by using FEA. *International Journal of Mechanical & Industrial Engineering*, 1-4.
- Rajan, S., Chin, S.-W., & Gani, L. (1996). Towards a Practical Design Optimization Tool. *Computer-Aided Civil and Infrastructure Engineering*, 259-274.

- Rajendran, I., & Vijayarangan, S. (2001). Optimal Design of a Composite Leaf Spring Using Genetic Algorithms. *Computers and Structures*, 1121-1129.
- Raju, K., & Acosta, J. (2010). *CRASHWORTHINESS OF COMPOSITE FUSELAGE STRUCTURES - MATERIAL DYNAMIC PROPERTIES, PHASE I*. Washington: U.S. Department of Transportation Federal Aviation Administration.
- Rao, A., & Arvind, N. (2007). Optimal Stacking Sequence Design of Laminate Composite Structures Using Tabu Embedded Simulated Annealing. *Structural Engineering and Mechanics*, 239-268.
- Rao, S. S. (2009). *Engineering Optimization: Theory and Practice, Fourth Edition*. Hoboken: John Wiley & Sons, Inc.
- Shi, Y., Swait, T., & Soutis, C. (2012). Modelling Damage Evolution in Composite Laminates Subjected to Low Velocity Impact. *Composite Structures (Elsevier)*, 2902-2913.
- Shokrieh, M. M., & Rezaei, D. (2003). Analysis and Optimization of a Composite Leaf Spring. *Composite Structures (Elsevier)*, 317-325.
- Sigmund, O., & Torquato, S. (1999). Design of Smart Composite Materials Using Topology Optimization. *Smart Materials and Structures*, 365-379.
- Slater, J. W. (2008, July 17). *NPARC Alliance CFD Verification and Validation: Examining Spatial (Grid) Convergence*. Retrieved from National Aeronautics and Space Administration:  
<http://www.grc.nasa.gov/WWW/wind/valid/tutorial/spatconv.html>
- Soremekun, G. A. (1997). *Genetic Algorithms for Composite Laminate Design and Optimization*. Blacksburg: Virginia Polytechnic Institute and State University.
- Stegmann, J., & Lund, E. (2005). Discrete Material Optimization of General Composite Shell Structures. *International Journal for Numerical Methods in Engineering*, 2009-2027.

- Stelzmann, D.-I., & Hormann, D.-I. (2011). *Ply-based Composite Modeling with the new \*ELEMENT\_SHELL\_COMPOSITE Keyword*. Strasbourg: 8th European LS-DYNA Users Conference.
- Storn, R., & Price, K. (n.d.). *"Differential Evolution (DE) for Continuous Function Optimization"*. Retrieved September 28, 2014, from <http://www.icsi.berkeley.edu/~storn/code.html>
- Storn, R., & Price, K. (1997). Differential Evolution - A Simple and Efficient Heuristic for Global Optimization over Continuous Spaces. *Journal of Global Optimization*, 11, 341-359.
- Suresh, S., Sujit, P., & Rao, A. (2007). Particle Swarm Optimization Approach for Multi-objective Composite Box-beam Design. *Composite Structures (Elsevier)*, 598-605.
- Vaidya, A., Yang, S., St. Ville, J., Nguyen, D., & Rajan, S. (2005). *Multiphysics CAD-Based Design Optimization*.
- Wade, B., Feraboli, P., & Osborne, M. (2012). *Simulating Laminated Composites Using LS-DYNA Material Model MAT54 Part I: [0] and [90] Ply Single-element Investigation*. Seattle: University of Washington & The Boeing Company.
- Zhang, Y., & Yang, C. (2009). Recent Developments in Finite Element Analysis for Laminated Composite Plates. *Composite Structures (Elsevier)*, 147-157.
- Zheng Yinhan, X., & Zhigao, H. (2011). Finite Element Analysis of Composite Leaf Spring. *The 6th International Conference on Computer Science & Education*.

## APPENDIX A

### DESIGN INPUT FILE FORMAT

The design input file is read by the COMP-OPT program. The file must be in the following format with all required information. The control cards within the file all begin with a “\*”. The following description will demonstrate the formation and information required for each card. All successive entries shown here separated with commas should be separated with a space in the design input file.

\$comment – Any comment lines describing the problem must be located at the beginning of the file with a “\$” as the first character to identify the line as a comment

\*Heading  
description of problem statement

\*FE\_Model  
No data is required. This card identifies the start of the finite element model information.

\*Node  
the node number, x-coordinate, y-coordinate, and z-coordinate

\*Nodal\_BC  
the node number, the condition in the global x-axis, global y-axis, and global z-axis – the condition can be SPECIFIED or FREE. Only nodes that have at least one specified constraint should be included here

\*Material\_Property  
the material number, the material density, elastic modulus for a-axis, elastic modulus for b-axis, elastic modulus for c-axis, Poisson’s ratio of BA, Poisson’s ratio of CA, Poisson’s ratio of CB, shear modulus of AB, shear modulus of BC, shear modulus of CA, shear strength in AB plane, longitudinal tensile strength, transverse tensile strength, transverse compressive strength,  $a_1$  component of vector  $\mathbf{a}$ ,  $a_2$  component of vector  $\mathbf{a}$ ,  $a_3$  component of vector  $\mathbf{a}$ ,  $v_1$  component of vector  $\mathbf{v}$ ,  $v_2$  component of vector  $\mathbf{v}$ ,  $v_3$  component of vector  $\mathbf{v}$ , beta for global material axis, cost per unit of mass. See LS-DYNA material manual for details regarding coordinate system definition for the material card \*MAT\_022, \*MAT\_COMPOSITE\_DAMAGE (Livermore Software Technology Corporation (LSTC), 2012)

\*Cross-section\_Property  
the property group number, the number of layers in the initial model, the layer thickness of layer  $i$ , the layer orientation of layer  $i$ , the material property of layer  $i$ , the layer thickness of layer  $i+1$ , ... - all of the layer data for the property group should be listed separated by a space

**\*Element**

the element number, “q4” to identify the elements as 4-noded quadratic shell elements, node number for first node, node number for second node, and the node number for fourth node. All elements should be defined in a counter clockwise manner

**\*Num\_Element\_Outputs**

the number of time steps that displacement and stress results will be outputted for

**\*Design\_Model**

No data is required. This card identifies the beginning of the design problem information.

**\*Objective\_function**

mass, volume, cost, or maxdisp

**\*Design\_Variable**

- layer\_thickness, the element group number, the layer number, the lower bound, the upper bound, desired precision
- layer\_thickness\_all, the element group number, the lower bound, the upper bound, desired precision
- layer\_status, the element group number, the layer number
- material, the element group number, the layer number, the number of possible materials, a list of all possible material group numbers
- layer\_orientation, the element group number, the layer number, the number of possible orientations, a list of all possible orientations
- layer\_orientation\_cont, the element group number, the layer number, the lower bound, the upper bound, desired precision
- shape\_optimization, the velocity field value, the percent change allowable (integer), desired precision

**\*Constraint**

- displacement, node number, number to identify the displacement direction degree of freedom (1, 2, or 3 to represent x, y, and z-axes, respectively), absolute value of maximum allowable displacement
- stress\_mpd (maximum material principal direction criteria), material group number, maximum allowable longitudinal tensile stress, maximum allowable transverse tensile stress, maximum allowable longitudinal compressive stress, maximum allowable transverse compressive stress, maximum allowable shear stress.
- stress\_th (Tsai-Hill criteria), material group number, maximum allowable longitudinal tensile stress, maximum allowable transverse tensile stress, maximum allowable longitudinal compressive stress, maximum allowable transverse compressive stress, maximum allowable shear stress.

- geometry, node 1, number to identify the constrained direction, node 2, number to identify the constrained direction, minimum allowable distance

\*Velocity\_fields (3 lines of data)

the velocity field number, velocity vector data for x-axis direction

velocity vector data for y-axis direction

velocity vector data for z-axis direction

\*optimizer

“GA”, “DE”, or “MFD”

\*Replacement\_strategy (for GA only, optional)

elitist, none, topfew

\*max\_iterations (for GA, DE, and MFD)

maximum number of iterations

\*Population\_size (for GA and DE only)

population size

\*output (optional)

silent, minimal, detailed

\*End\_Design\_Model

No data. Card identifies that all design model information has been inputted.

\*End

No data. Card identifies that all input data has been read.

## APPENDIX B

### DESIGN OUTPUT FILE FORMAT

A truncated sample output file is provided for a sample leaf spring optimization problem as presented in section 4.2.1. The output file begins by summarizing the details of the finite element model. The number of layers and layer details (thickness, orientation, and material group) for the initial model are detailed.

Next, the optimization problem details are presented. The optimizer in use, optimizer parameters, design variable, and constraint data is presented. As the optimization process begins, the level of detail included in the output file is dependent upon the output detail level selected. If minimal output is desired, then the objective function and maximum constraint violation will be presented for each iteration. If detailed output is desired, then all design variable values and all constraint evaluation computations will be presented.

When the convergence criteria is met and a final solution is found, the generation/iteration history is summarized and the final design variable values are presented along with the best objective function and maximum constraint value. The final design model information is recorded including details with respect to the final mesh and element group layer sequence and characteristics. The maximum stresses experienced in the principal material directions is presented as well as the nodal deflection for each result output time step.

The following output file is a sample file for a leaf spring model as presented in section 4.2.1 and is truncated to only show the nodal displacements experienced at the first result output time step.

---

COMP-OPT  
A Composite Optimization Program  
2014, K.Mika

---

Start at : Sun Nov 09 12:19:51 2014

Number of nodes: 301  
 Number of elements: 252  
 Number of x/s property groups: 11  
 Number of material groups: 1

X/S Property Data

EPG	Num. of Layers
1	10
2	10
3	10
4	10
5	10
6	10
7	10
8	10
9	10
10	10
11	10

Layer Data

EPG	Layer	Thickness	Theta	MPG
1	1	3.54926	0	1
1	2	3.54926	0	1
1	3	3.54926	0	1
1	4	3.54926	0	1
1	5	3.54926	0	1
1	6	3.54926	0	1
1	7	3.54926	0	1
1	8	3.54926	0	1
1	9	3.54926	0	1
1	10	3.54926	0	1
2	1	3.8206	0	1
2	2	3.8206	0	1
2	3	3.8206	0	1
2	4	3.8206	0	1
2	5	3.8206	0	1
2	6	3.8206	0	1
2	7	3.8206	0	1
2	8	3.8206	0	1
2	9	3.8206	0	1
2	10	3.8206	0	1
3	1	4.03524	0	1
3	2	4.03524	0	1
3	3	4.03524	0	1
3	4	4.03524	0	1
3	5	4.03524	0	1
3	6	4.03524	0	1
3	7	4.03524	0	1
3	8	4.03524	0	1
3	9	4.03524	0	1
3	10	4.03524	0	1
4	1	4.37872	0	1
4	2	4.37872	0	1
4	3	4.37872	0	1
4	4	4.37872	0	1
4	5	4.37872	0	1
4	6	4.37872	0	1
4	7	4.37872	0	1
4	8	4.37872	0	1
4	9	4.37872	0	1
4	10	4.37872	0	1
5	1	4.37872	0	1

5	2	4.37872	0	1
5	3	4.37872	0	1
5	4	4.37872	0	1
5	5	4.37872	0	1
5	6	4.37872	0	1
5	7	4.37872	0	1
5	8	4.37872	0	1
5	9	4.37872	0	1
5	10	4.37872	0	1
6	1	4.37872	0	1
6	2	4.37872	0	1
6	3	4.37872	0	1
6	4	4.37872	0	1
6	5	4.37872	0	1
6	6	4.37872	0	1
6	7	4.37872	0	1
6	8	4.37872	0	1
6	9	4.37872	0	1
6	10	4.37872	0	1
7	1	3.96353	0	1
7	2	3.96353	0	1
7	3	3.96353	0	1
7	4	3.96353	0	1
7	5	3.96353	0	1
7	6	3.96353	0	1
7	7	3.96353	0	1
7	8	3.96353	0	1
7	9	3.96353	0	1
7	10	3.96353	0	1
8	1	3.54926	0	1
8	2	3.54926	0	1
8	3	3.54926	0	1
8	4	3.54926	0	1
8	5	3.54926	0	1
8	6	3.54926	0	1
8	7	3.54926	0	1
8	8	3.54926	0	1
8	9	3.54926	0	1
8	10	3.54926	0	1
9	1	3.54926	0	1
9	2	3.54926	0	1
9	3	3.54926	0	1
9	4	3.54926	0	1
9	5	3.54926	0	1
9	6	3.54926	0	1
9	7	3.54926	0	1
9	8	3.54926	0	1
9	9	3.54926	0	1
9	10	3.54926	0	1
10	1	4.21549	0	1
10	2	4.21549	0	1
10	3	4.21549	0	1
10	4	4.21549	0	1
10	5	4.21549	0	1
10	6	4.21549	0	1
10	7	4.21549	0	1
10	8	4.21549	0	1
10	9	4.21549	0	1
10	10	4.21549	0	1
11	1	4.79425	0	1
11	2	4.79425	0	1
11	3	4.79425	0	1
11	4	4.79425	0	1
11	5	4.79425	0	1
11	6	4.79425	0	1
11	7	4.79425	0	1
11	8	4.79425	0	1
11	9	4.79425	0	1
11	10	4.79425	0	1

Number of Material Properties

-----  
 MPG  
 -----  
 1

Optimizer in Use: MFD  
 Objective Function: Mass

Number of Continuous Design Variables: 13  
 Number of Discrete Design Variables: 0  
 Number of Boolean Design Variables: 0  
 Number of constraints: 308

Design Variable Data

DV	Type	Detail	Detail	Lower	Upper	Precision
		1	2	Bound	Bound	
1	Thickness All-C	1	1	1	5	0.1
2	Thickness All-C	2	1	1	5	0.1
3	Thickness All-C	3	1	1	5	0.1
4	Thickness All-C	4	1	1	5	0.1
5	Thickness All-C	5	1	1	5	0.1
6	Thickness All-C	6	1	1	5	0.1
7	Thickness All-C	7	1	1	5	0.1
8	Thickness All-C	8	1	1	5	0.1
9	Thickness All-C	9	1	1	5	0.1
10	Thickness All-C	10	1	1	5	0.1
11	Thickness All-C	11	1	1	5	0.1
12	shape_optimization	1	15	-1	1	0.1
13	shape_optimization	2	15	-1	1	0.1

Constraint Data

CN	Type	Target	Target	Allowable	Allowable	Allowable	Allowable	Allowable
		1	2	1	2	3	4	5
1	Displacement	199	2	160				
2	Stress	1		2895.8	172.4	2895.8	172.4	51.7
3	Geometry	25	3	66	3			

MFD (Method of Feasible Directions) V1.02

Number of Continuous Design Variables: 13  
 Max Iterations: 20  
 Number of function evaluations: 122  
 Number of gradient evaluations: 6  
 No. of Function Evaluations in Line Search: 29  
 Final Objective Function Value: 0.143746

MFD History

Iter	Objective	Active	Max Constr	Cum. FE	Cum. GE
	Function	Constraints	Value		
1	0.145316	1	-0.00512571	15	1
2	0.14495	1	-0.00483559	33	2
3	0.143923	1	-0.00174082	61	3
4	0.143749	1	-9.67325e-005	79	4
5	0.143746	1	0	98	5
6	0.143746	1	0	116	6
7	0.143746	1	0	122	6

Continuous Design Variables

DV	Lower	Upper	Final
	Bound	Bound	Value
1	1	5	3.53075
2	1	5	3.80209
3	1	5	4.05346
4	1	5	4.39723
5	1	5	4.39723
6	1	5	4.37544
7	1	5	3.94502
8	1	5	3.53075
9	1	5	3.53075
10	1	5	4.22979
11	1	5	4.77574

12	-1	1	-0.0184509
13	-1	1	-0.018218

---

Post-Design Information

---

Start at : Sun Nov 09 12:19:51 2014

End at : Mon Nov 10 09:03:39 2014

Total Computation Time : 74628 seconds

Total mass : 0.143746

Total volume : 1.1083e+006

Total cost : 0.143746

Nodal Data

NN	X-Coordinate	Y-Coordinate	Z-Coordinate	X-Fixity	Y-Fixity	Z-Fixity
1	0	0	6.00277	Specified	Specified	Specified
2	716.697	0.000970995	6.00277	Specified	Specified	Specified
3	0	0	43.9972	Specified	Specified	Specified
4	716.697	0.000970995	43.9972	Specified	Specified	Specified
5	13.098	-11.4188	6.25186	Free	Free	Free
6	26.7765	-22.8899	6.4888	Free	Free	Free
7	41.0063	-34.3313	6.71358	Free	Free	Free
8	55.7585	-45.6629	6.92622	Free	Free	Free
9	71.0041	-56.8069	7.12671	Free	Free	Free
10	86.714	-67.6877	7.31504	Free	Free	Free
11	102.859	-78.2326	7.49123	Free	Free	Free
12	119.411	-88.3727	7.65526	Free	Free	Free
13	136.339	-98.041	7.80714	Free	Free	Free
14	153.616	-107.176	7.94688	Free	Free	Free
15	171.213	-115.72	8.07447	Free	Free	Free
16	189.099	-123.619	8.18989	Free	Free	Free
17	207.247	-130.822	8.29317	Free	Free	Free
18	225.627	-137.286	8.3843	Free	Free	Free
19	244.21	-142.97	8.46329	Free	Free	Free
20	262.967	-147.839	8.53011	Free	Free	Free
21	281.869	-151.864	8.5848	Free	Free	Free
22	300.887	-155.021	8.62732	Free	Free	Free
23	319.992	-157.289	8.6577	Free	Free	Free
24	339.156	-158.655	8.67592	Free	Free	Free
25	358.348	-159.112	8.682	Free	Free	Free
26	377.541	-158.655	8.67592	Free	Free	Free
27	396.704	-157.289	8.6577	Free	Free	Free
28	415.809	-155.021	8.62732	Free	Free	Free
29	434.828	-151.864	8.5848	Free	Free	Free
30	453.73	-147.839	8.53011	Free	Free	Free
31	472.487	-142.97	8.46328	Free	Free	Free
32	491.07	-137.286	8.3843	Free	Free	Free
33	509.45	-130.822	8.29317	Free	Free	Free
34	527.597	-123.619	8.18989	Free	Free	Free
35	545.484	-115.72	8.07447	Free	Free	Free
36	563.08	-107.176	7.94688	Free	Free	Free
37	580.357	-98.0409	7.80714	Free	Free	Free
38	597.286	-88.3721	7.65526	Free	Free	Free
39	613.838	-78.2319	7.49123	Free	Free	Free
40	629.983	-67.6869	7.31504	Free	Free	Free
41	645.693	-56.806	7.12671	Free	Free	Free
42	660.939	-45.6617	6.92622	Free	Free	Free
43	675.691	-34.3302	6.71358	Free	Free	Free
44	689.921	-22.8886	6.48879	Free	Free	Free
45	703.599	-11.4179	6.25186	Free	Free	Free
46	13.098	-11.4188	43.7482	Free	Free	Free
47	26.7765	-22.8899	43.5112	Free	Free	Free
48	41.0063	-34.3313	43.2864	Free	Free	Free
49	55.7585	-45.6629	43.0738	Free	Free	Free
50	71.0041	-56.8069	42.8732	Free	Free	Free
51	86.714	-67.6877	42.6849	Free	Free	Free
52	102.859	-78.2326	42.5088	Free	Free	Free
53	119.411	-88.3727	42.3447	Free	Free	Free
54	136.339	-98.041	42.1929	Free	Free	Free
55	153.616	-107.176	42.0531	Free	Free	Free
56	171.213	-115.72	41.9255	Free	Free	Free
57	189.099	-123.619	41.8101	Free	Free	Free
58	207.247	-130.822	41.7068	Free	Free	Free

59	225.627	-137.286	41.6156	Free	Free	Free
60	244.21	-142.97	41.5367	Free	Free	Free
61	262.967	-147.839	41.4698	Free	Free	Free
62	281.869	-151.864	41.4152	Free	Free	Free
63	300.887	-155.021	41.3727	Free	Free	Free
64	319.992	-157.289	41.3423	Free	Free	Free
65	339.156	-158.655	41.3241	Free	Free	Free
66	358.348	-159.112	41.318	Free	Free	Free
67	377.541	-158.655	41.3241	Free	Free	Free
68	396.704	-157.289	41.3423	Free	Free	Free
69	415.809	-155.021	41.3727	Free	Free	Free
70	434.828	-151.864	41.4152	Free	Free	Free
71	453.73	-147.839	41.4698	Free	Free	Free
72	472.487	-142.97	41.5367	Free	Free	Free
73	491.07	-137.286	41.6156	Free	Free	Free
74	509.45	-130.822	41.7068	Free	Free	Free
75	527.597	-123.619	41.8101	Free	Free	Free
76	545.484	-115.72	41.9255	Free	Free	Free
77	563.08	-107.176	42.0531	Free	Free	Free
78	580.357	-98.0409	42.1929	Free	Free	Free
79	597.286	-88.3721	42.3448	Free	Free	Free
80	613.838	-78.2319	42.5088	Free	Free	Free
81	629.983	-67.6869	42.6849	Free	Free	Free
82	645.693	-56.806	42.8733	Free	Free	Free
83	660.939	-45.6617	43.0738	Free	Free	Free
84	675.691	-34.3302	43.2864	Free	Free	Free
85	689.921	-22.8886	43.5112	Free	Free	Free
86	703.599	-11.4179	43.7482	Free	Free	Free
87	716.697	0.000970995	12.3352	Specified	Specified	Specified
88	716.697	0.000970995	18.6676	Specified	Specified	Specified
89	716.697	0.000970995	25	Specified	Specified	Specified
90	716.697	0.000970995	31.3324	Specified	Specified	Specified
91	716.697	0.000970995	37.6649	Specified	Specified	Specified
92	0	0	37.6649	Specified	Specified	Specified
93	0	0	31.3324	Specified	Specified	Specified
94	0	0	25	Specified	Specified	Specified
95	0	0	18.6676	Specified	Specified	Specified
96	0	0	12.3352	Specified	Specified	Specified
97	13.098	-11.4188	12.5012	Free	Free	Free
98	26.7765	-22.8899	12.6592	Free	Free	Free
99	41.0063	-34.3313	12.8091	Free	Free	Free
100	55.7585	-45.6629	12.9508	Free	Free	Free
101	71.0041	-56.8069	13.0844	Free	Free	Free
102	86.714	-67.6877	13.2101	Free	Free	Free
103	102.859	-78.2326	13.3275	Free	Free	Free
104	119.411	-88.3727	13.4368	Free	Free	Free
105	136.339	-98.041	13.5381	Free	Free	Free
106	153.616	-107.176	13.6313	Free	Free	Free
107	171.213	-115.72	13.7163	Free	Free	Free
108	189.099	-123.619	13.7933	Free	Free	Free
109	207.247	-130.822	13.8621	Free	Free	Free
110	225.627	-137.286	13.9229	Free	Free	Free
111	244.21	-142.97	13.9755	Free	Free	Free
112	262.967	-147.839	14.0201	Free	Free	Free
113	281.869	-151.864	14.0565	Free	Free	Free
114	300.887	-155.021	14.0849	Free	Free	Free
115	319.992	-157.289	14.1052	Free	Free	Free
116	339.156	-158.655	14.1173	Free	Free	Free
117	358.348	-159.112	14.1213	Free	Free	Free
118	377.541	-158.655	14.1173	Free	Free	Free
119	396.704	-157.289	14.1052	Free	Free	Free
120	415.809	-155.021	14.0849	Free	Free	Free
121	434.828	-151.864	14.0565	Free	Free	Free
122	453.73	-147.839	14.0201	Free	Free	Free
123	472.487	-142.97	13.9755	Free	Free	Free
124	491.07	-137.286	13.9229	Free	Free	Free
125	509.45	-130.822	13.8621	Free	Free	Free
126	527.597	-123.619	13.7933	Free	Free	Free
127	545.484	-115.72	13.7163	Free	Free	Free
128	563.08	-107.176	13.6312	Free	Free	Free
129	580.357	-98.0409	13.5381	Free	Free	Free
130	597.286	-88.3721	13.4368	Free	Free	Free
131	613.838	-78.2319	13.3275	Free	Free	Free
132	629.983	-67.6869	13.2101	Free	Free	Free
133	645.693	-56.806	13.0844	Free	Free	Free
134	660.939	-45.6617	12.9508	Free	Free	Free
135	675.691	-34.3302	12.8091	Free	Free	Free
136	689.921	-22.8886	12.6591	Free	Free	Free
137	703.599	-11.4179	12.5012	Free	Free	Free

138	13.098	-11.4188	18.7506	Free	Free	Free
139	26.7765	-22.8899	18.8296	Free	Free	Free
140	41.0063	-34.3313	18.9045	Free	Free	Free
141	55.7585	-45.6629	18.9754	Free	Free	Free
142	71.0041	-56.8069	19.0422	Free	Free	Free
143	86.714	-67.6877	19.105	Free	Free	Free
144	102.859	-78.2326	19.1638	Free	Free	Free
145	119.411	-88.3727	19.2184	Free	Free	Free
146	136.339	-98.041	19.269	Free	Free	Free
147	153.616	-107.176	19.3156	Free	Free	Free
148	171.213	-115.72	19.3581	Free	Free	Free
149	189.099	-123.619	19.3966	Free	Free	Free
150	207.247	-130.822	19.4311	Free	Free	Free
151	225.627	-137.286	19.4615	Free	Free	Free
152	244.21	-142.97	19.4878	Free	Free	Free
153	262.967	-147.839	19.51	Free	Free	Free
154	281.869	-151.864	19.5282	Free	Free	Free
155	300.887	-155.021	19.5424	Free	Free	Free
156	319.992	-157.289	19.5526	Free	Free	Free
157	339.156	-158.655	19.5586	Free	Free	Free
158	358.348	-159.112	19.5607	Free	Free	Free
159	377.541	-158.655	19.5586	Free	Free	Free
160	396.704	-157.289	19.5526	Free	Free	Free
161	415.809	-155.021	19.5424	Free	Free	Free
162	434.828	-151.864	19.5282	Free	Free	Free
163	453.73	-147.839	19.51	Free	Free	Free
164	472.487	-142.97	19.4878	Free	Free	Free
165	491.07	-137.286	19.4615	Free	Free	Free
166	509.45	-130.822	19.4311	Free	Free	Free
167	527.597	-123.619	19.3966	Free	Free	Free
168	545.484	-115.72	19.3581	Free	Free	Free
169	563.08	-107.176	19.3156	Free	Free	Free
170	580.357	-98.0409	19.269	Free	Free	Free
171	597.286	-88.3721	19.2184	Free	Free	Free
172	613.838	-78.2319	19.1638	Free	Free	Free
173	629.983	-67.6869	19.105	Free	Free	Free
174	645.693	-56.806	19.0422	Free	Free	Free
175	660.939	-45.6617	18.9754	Free	Free	Free
176	675.691	-34.3302	18.9045	Free	Free	Free
177	689.921	-22.8886	18.8296	Free	Free	Free
178	703.599	-11.4179	18.7506	Free	Free	Free
179	13.098	-11.4188	25	Free	Free	Free
180	26.7765	-22.8899	25	Free	Free	Free
181	41.0063	-34.3313	25	Free	Free	Free
182	55.7585	-45.6629	25	Free	Free	Free
183	71.0041	-56.8069	25	Free	Free	Free
184	86.714	-67.6877	25	Free	Free	Free
185	102.859	-78.2326	25	Free	Free	Free
186	119.411	-88.3727	25	Free	Free	Free
187	136.339	-98.041	25	Free	Free	Free
188	153.616	-107.176	25	Free	Free	Free
189	171.213	-115.72	25	Free	Free	Free
190	189.099	-123.619	25	Free	Free	Free
191	207.247	-130.822	25	Free	Free	Free
192	225.627	-137.286	25	Free	Free	Free
193	244.21	-142.97	25	Free	Free	Free
194	262.967	-147.839	25	Free	Free	Free
195	281.869	-151.864	25	Free	Free	Free
196	300.887	-155.021	25	Free	Free	Free
197	319.992	-157.289	25	Free	Free	Free
198	339.156	-158.655	25	Free	Free	Free
199	358.348	-159.112	25	Free	Free	Free
200	377.541	-158.655	25	Free	Free	Free
201	396.704	-157.289	25	Free	Free	Free
202	415.809	-155.021	25	Free	Free	Free
203	434.828	-151.864	25	Free	Free	Free
204	453.73	-147.839	25	Free	Free	Free
205	472.487	-142.97	25	Free	Free	Free
206	491.07	-137.286	25	Free	Free	Free
207	509.45	-130.822	25	Free	Free	Free
208	527.597	-123.619	25	Free	Free	Free
209	545.484	-115.72	25	Free	Free	Free
210	563.08	-107.176	25	Free	Free	Free
211	580.357	-98.0409	25	Free	Free	Free
212	597.286	-88.3721	25	Free	Free	Free
213	613.838	-78.2319	25	Free	Free	Free
214	629.983	-67.6869	25	Free	Free	Free
215	645.693	-56.806	25	Free	Free	Free
216	660.939	-45.6617	25	Free	Free	Free

217	675.691	-34.3302	25	Free	Free	Free
218	689.921	-22.8886	25	Free	Free	Free
219	703.599	-11.4179	25	Free	Free	Free
220	13.098	-11.4188	31.2494	Free	Free	Free
221	26.7765	-22.8899	31.1704	Free	Free	Free
222	41.0063	-34.3313	31.0955	Free	Free	Free
223	55.7585	-45.6629	31.0246	Free	Free	Free
224	71.0041	-56.8069	30.9578	Free	Free	Free
225	86.714	-67.6877	30.895	Free	Free	Free
226	102.859	-78.2326	30.8362	Free	Free	Free
227	119.411	-88.3727	30.7816	Free	Free	Free
228	136.339	-98.041	30.731	Free	Free	Free
229	153.616	-107.176	30.6844	Free	Free	Free
230	171.213	-115.72	30.6419	Free	Free	Free
231	189.099	-123.619	30.6034	Free	Free	Free
232	207.247	-130.822	30.5689	Free	Free	Free
233	225.627	-137.286	30.5385	Free	Free	Free
234	244.21	-142.97	30.5122	Free	Free	Free
235	262.967	-147.839	30.49	Free	Free	Free
236	281.869	-151.864	30.4718	Free	Free	Free
237	300.887	-155.021	30.4576	Free	Free	Free
238	319.992	-157.289	30.4474	Free	Free	Free
239	339.156	-158.655	30.4414	Free	Free	Free
240	358.348	-159.112	30.4393	Free	Free	Free
241	377.541	-158.655	30.4414	Free	Free	Free
242	396.704	-157.289	30.4474	Free	Free	Free
243	415.809	-155.021	30.4576	Free	Free	Free
244	434.828	-151.864	30.4718	Free	Free	Free
245	453.73	-147.839	30.49	Free	Free	Free
246	472.487	-142.97	30.5122	Free	Free	Free
247	491.07	-137.286	30.5385	Free	Free	Free
248	509.45	-130.822	30.5689	Free	Free	Free
249	527.597	-123.619	30.6034	Free	Free	Free
250	545.484	-115.72	30.6419	Free	Free	Free
251	563.08	-107.176	30.6844	Free	Free	Free
252	580.357	-98.0409	30.731	Free	Free	Free
253	597.286	-88.3721	30.7816	Free	Free	Free
254	613.838	-78.2319	30.8362	Free	Free	Free
255	629.983	-67.6869	30.895	Free	Free	Free
256	645.693	-56.806	30.9578	Free	Free	Free
257	660.939	-45.6617	31.0246	Free	Free	Free
258	675.691	-34.3302	31.0955	Free	Free	Free
259	689.921	-22.8886	31.1704	Free	Free	Free
260	703.599	-11.4179	31.2494	Free	Free	Free
261	13.098	-11.4188	37.4987	Free	Free	Free
262	26.7765	-22.8899	37.3408	Free	Free	Free
263	41.0063	-34.3313	37.1909	Free	Free	Free
264	55.7585	-45.6629	37.0492	Free	Free	Free
265	71.0041	-56.8069	36.9156	Free	Free	Free
266	86.714	-67.6877	36.7899	Free	Free	Free
267	102.859	-78.2326	36.6725	Free	Free	Free
268	119.411	-88.3727	36.5632	Free	Free	Free
269	136.339	-98.041	36.4619	Free	Free	Free
270	153.616	-107.176	36.3687	Free	Free	Free
271	171.213	-115.72	36.2836	Free	Free	Free
272	189.099	-123.619	36.2067	Free	Free	Free
273	207.247	-130.822	36.1379	Free	Free	Free
274	225.627	-137.286	36.0771	Free	Free	Free
275	244.21	-142.97	36.0245	Free	Free	Free
276	262.967	-147.839	35.9799	Free	Free	Free
277	281.869	-151.864	35.9435	Free	Free	Free
278	300.887	-155.021	35.9151	Free	Free	Free
279	319.992	-157.289	35.8948	Free	Free	Free
280	339.156	-158.655	35.8827	Free	Free	Free
281	358.348	-159.112	35.8787	Free	Free	Free
282	377.541	-158.655	35.8827	Free	Free	Free
283	396.704	-157.289	35.8948	Free	Free	Free
284	415.809	-155.021	35.9151	Free	Free	Free
285	434.828	-151.864	35.9435	Free	Free	Free
286	453.73	-147.839	35.9799	Free	Free	Free
287	472.487	-142.97	36.0245	Free	Free	Free
288	491.07	-137.286	36.0771	Free	Free	Free
289	509.45	-130.822	36.1379	Free	Free	Free
290	527.597	-123.619	36.2067	Free	Free	Free
291	545.484	-115.72	36.2837	Free	Free	Free
292	563.08	-107.176	36.3688	Free	Free	Free
293	580.357	-98.0409	36.4619	Free	Free	Free
294	597.286	-88.3721	36.5632	Free	Free	Free
295	613.838	-78.2319	36.6725	Free	Free	Free

296	629.983	-67.6869	36.7899	Free	Free	Free
297	645.693	-56.806	36.9156	Free	Free	Free
298	660.939	-45.6617	37.0492	Free	Free	Free
299	675.691	-34.3302	37.1909	Free	Free	Free
300	689.921	-22.8886	37.3408	Free	Free	Free
301	703.599	-11.4179	37.4987	Free	Free	Free

X/S Property Data

EPG	Num. of Layers
1	10
2	10
3	10
4	10
5	10
6	10
7	10
8	10
9	10
10	10
11	10

Layer Data

EPG	Layer	Thickness	Theta	MPG
1	1	3.53075	0	1
	2	3.53075	0	1
	3	3.53075	0	1
	4	3.53075	0	1
	5	3.53075	0	1
	6	3.53075	0	1
	7	3.53075	0	1
	8	3.53075	0	1
	9	3.53075	0	1
	10	3.53075	0	1
2	1	3.80209	0	1
	2	3.80209	0	1
	3	3.80209	0	1
	4	3.80209	0	1
	5	3.80209	0	1
	6	3.80209	0	1
	7	3.80209	0	1
	8	3.80209	0	1
	9	3.80209	0	1
	10	3.80209	0	1
3	1	4.05346	0	1
	2	4.05346	0	1
	3	4.05346	0	1
	4	4.05346	0	1
	5	4.05346	0	1
	6	4.05346	0	1
	7	4.05346	0	1
	8	4.05346	0	1
	9	4.05346	0	1
	10	4.05346	0	1
4	1	4.39723	0	1
	2	4.39723	0	1
	3	4.39723	0	1
	4	4.39723	0	1
	5	4.39723	0	1
	6	4.39723	0	1
	7	4.39723	0	1
	8	4.39723	0	1
	9	4.39723	0	1
	10	4.39723	0	1
5	1	4.39723	0	1
	2	4.39723	0	1
	3	4.39723	0	1
	4	4.39723	0	1
	5	4.39723	0	1
	6	4.39723	0	1
	7	4.39723	0	1
	8	4.39723	0	1
	9	4.39723	0	1
	10	4.39723	0	1

6	1	4.37544	0	1
	2	4.37544	0	1
	3	4.37544	0	1
	4	4.37544	0	1
	5	4.37544	0	1
	6	4.37544	0	1
	7	4.37544	0	1
	8	4.37544	0	1
	9	4.37544	0	1
	10	4.37544	0	1
7	1	3.94502	0	1
	2	3.94502	0	1
	3	3.94502	0	1
	4	3.94502	0	1
	5	3.94502	0	1
	6	3.94502	0	1
	7	3.94502	0	1
	8	3.94502	0	1
	9	3.94502	0	1
	10	3.94502	0	1
8	1	3.53075	0	1
	2	3.53075	0	1
	3	3.53075	0	1
	4	3.53075	0	1
	5	3.53075	0	1
	6	3.53075	0	1
	7	3.53075	0	1
	8	3.53075	0	1
	9	3.53075	0	1
	10	3.53075	0	1
9	1	3.53075	0	1
	2	3.53075	0	1
	3	3.53075	0	1
	4	3.53075	0	1
	5	3.53075	0	1
	6	3.53075	0	1
	7	3.53075	0	1
	8	3.53075	0	1
	9	3.53075	0	1
	10	3.53075	0	1
10	1	4.22979	0	1
	2	4.22979	0	1
	3	4.22979	0	1
	4	4.22979	0	1
	5	4.22979	0	1
	6	4.22979	0	1
	7	4.22979	0	1
	8	4.22979	0	1
	9	4.22979	0	1
	10	4.22979	0	1
11	1	4.77574	0	1
	2	4.77574	0	1
	3	4.77574	0	1
	4	4.77574	0	1
	5	4.77574	0	1
	6	4.77574	0	1
	7	4.77574	0	1
	8	4.77574	0	1
	9	4.77574	0	1
	10	4.77574	0	1

Material Properties

-----	
EPG	MPG
-----	
1	1
2	1
3	1
4	1
5	1
6	1
7	1
8	1
9	1
10	1
11	1

Max Element Stress Data

Stress	TS	EN	LAYER	MAX STRESS
SIGXX	31	21	10	-103.4
SIGYY	31	147	10	0.99245
SIGZZ	0	0	0	0
TAU MAX	31	21	10	51.7

Time Step 1

Nodal Displacement Data

NN	TS	X-Displacement	Y-Displacement	Z-Displacement
1	1	0	0	0
2	1	0	0	0
3	1	0	0	0
4	1	0	0	0
5	1	0	0	0
6	1	0	0	0
7	1	0	0	0
8	1	0	0	0
9	1	0	0	0
10	1	0	0	0
11	1	0	0	0
12	1	0	0	0
13	1	0	0	0
14	1	0	0	0
15	1	0	0	0
16	1	0	0	0
17	1	0	0	0
18	1	0	0	0
19	1	0	0	0
20	1	0	0	0
21	1	0	0	0
22	1	0	0	0
23	1	0	0	0
24	1	0	0	0
25	1	0	0	0
26	1	0	0	0
27	1	0	0	0
28	1	0	0	0
29	1	0	0	0
30	1	0	0	0
31	1	0	0	0
32	1	0	0	0
33	1	0	0	0
34	1	0	0	0
35	1	0	0	0
36	1	0	0	0
37	1	0	0	0
38	1	0	0	0
39	1	0	0	0
40	1	0	0	0
41	1	0	0	0
42	1	0	0	0
43	1	0	0	0
44	1	0	0	0
45	1	0	0	0
46	1	0	0	0
47	1	0	0	0
48	1	0	0	0
49	1	0	0	0
50	1	0	0	0
51	1	0	0	0
52	1	0	0	0
53	1	0	0	0
54	1	0	0	0
55	1	0	0	0
56	1	0	0	0
57	1	0	0	0
58	1	0	0	0
59	1	0	0	0
60	1	0	0	0
61	1	0	0	0
62	1	0	0	0

63	1	0	0	0
64	1	0	0	0
65	1	0	0	0
66	1	0	0	0
67	1	0	0	0
68	1	0	0	0
69	1	0	0	0
70	1	0	0	0
71	1	0	0	0
72	1	0	0	0
73	1	0	0	0
74	1	0	0	0
75	1	0	0	0
76	1	0	0	0
77	1	0	0	0
78	1	0	0	0
79	1	0	0	0
80	1	0	0	0
81	1	0	0	0
82	1	0	0	0
83	1	0	0	0
84	1	0	0	0
85	1	0	0	0
86	1	0	0	0
87	1	0	0	0
88	1	0	0	0
89	1	0	0	0
90	1	0	0	0
91	1	0	0	0
92	1	0	0	0
93	1	0	0	0
94	1	0	0	0
95	1	0	0	0
96	1	0	0	0
97	1	0	0	0
98	1	0	0	0
99	1	0	0	0
100	1	0	0	0
101	1	0	0	0
102	1	0	0	0
103	1	0	0	0
104	1	0	0	0
105	1	0	0	0
106	1	0	0	0
107	1	0	0	0
108	1	0	0	0
109	1	0	0	0
110	1	0	0	0
111	1	0	0	0
112	1	0	0	0
113	1	0	0	0
114	1	0	0	0
115	1	0	0	0
116	1	0	0	0
117	1	0	0	0
118	1	0	0	0
119	1	0	0	0
120	1	0	0	0
121	1	0	0	0
122	1	0	0	0
123	1	0	0	0
124	1	0	0	0
125	1	0	0	0
126	1	0	0	0
127	1	0	0	0
128	1	0	0	0
129	1	0	0	0
130	1	0	0	0
131	1	0	0	0
132	1	0	0	0
133	1	0	0	0
134	1	0	0	0
135	1	0	0	0
136	1	0	0	0
137	1	0	0	0
138	1	0	0	0
139	1	0	0	0
140	1	0	0	0
141	1	0	0	0

142	1	0	0	0
143	1	0	0	0
144	1	0	0	0
145	1	0	0	0
146	1	0	0	0
147	1	0	0	0
148	1	0	0	0
149	1	0	0	0
150	1	0	0	0
151	1	0	0	0
152	1	0	0	0
153	1	0	0	0
154	1	0	0	0
155	1	0	0	0
156	1	0	0	0
157	1	0	0	0
158	1	0	0	0
159	1	0	0	0
160	1	0	0	0
161	1	0	0	0
162	1	0	0	0
163	1	0	0	0
164	1	0	0	0
165	1	0	0	0
166	1	0	0	0
167	1	0	0	0
168	1	0	0	0
169	1	0	0	0
170	1	0	0	0
171	1	0	0	0
172	1	0	0	0
173	1	0	0	0
174	1	0	0	0
175	1	0	0	0
176	1	0	0	0
177	1	0	0	0
178	1	0	0	0
179	1	0	0	0
180	1	0	0	0
181	1	0	0	0
182	1	0	0	0
183	1	0	0	0
184	1	0	0	0
185	1	0	0	0
186	1	0	0	0
187	1	0	0	0
188	1	0	0	0
189	1	0	0	0
190	1	0	0	0
191	1	0	0	0
192	1	0	0	0
193	1	0	0	0
194	1	0	0	0
195	1	0	0	0
196	1	0	0	0
197	1	0	0	0
198	1	0	0	0
199	1	0	0	0
200	1	0	0	0
201	1	0	0	0
202	1	0	0	0
203	1	0	0	0
204	1	0	0	0
205	1	0	0	0
206	1	0	0	0
207	1	0	0	0
208	1	0	0	0
209	1	0	0	0
210	1	0	0	0
211	1	0	0	0
212	1	0	0	0
213	1	0	0	0
214	1	0	0	0
215	1	0	0	0
216	1	0	0	0
217	1	0	0	0
218	1	0	0	0
219	1	0	0	0
220	1	0	0	0

221	1	0	0	0
222	1	0	0	0
223	1	0	0	0
224	1	0	0	0
225	1	0	0	0
226	1	0	0	0
227	1	0	0	0
228	1	0	0	0
229	1	0	0	0
230	1	0	0	0
231	1	0	0	0
232	1	0	0	0
233	1	0	0	0
234	1	0	0	0
235	1	0	0	0
236	1	0	0	0
237	1	0	0	0
238	1	0	0	0
239	1	0	0	0
240	1	0	0	0
241	1	0	0	0
242	1	0	0	0
243	1	0	0	0
244	1	0	0	0
245	1	0	0	0
246	1	0	0	0
247	1	0	0	0
248	1	0	0	0
249	1	0	0	0
250	1	0	0	0
251	1	0	0	0
252	1	0	0	0
253	1	0	0	0
254	1	0	0	0
255	1	0	0	0
256	1	0	0	0
257	1	0	0	0
258	1	0	0	0
259	1	0	0	0
260	1	0	0	0
261	1	0	0	0
262	1	0	0	0
263	1	0	0	0
264	1	0	0	0
265	1	0	0	0
266	1	0	0	0
267	1	0	0	0
268	1	0	0	0
269	1	0	0	0
270	1	0	0	0
271	1	0	0	0
272	1	0	0	0
273	1	0	0	0
274	1	0	0	0
275	1	0	0	0
276	1	0	0	0
277	1	0	0	0
278	1	0	0	0
279	1	0	0	0
280	1	0	0	0
281	1	0	0	0
282	1	0	0	0
283	1	0	0	0
284	1	0	0	0
285	1	0	0	0
286	1	0	0	0
287	1	0	0	0
288	1	0	0	0
289	1	0	0	0
290	1	0	0	0
291	1	0	0	0
292	1	0	0	0
293	1	0	0	0
294	1	0	0	0
295	1	0	0	0
296	1	0	0	0
297	1	0	0	0
298	1	0	0	0
299	1	0	0	0

	300	1	0	0	0
	301	1	0	0	0
Max	0				
Node	1				
Min	0				
Node	1				